



BNXXXX-v0.0  
October 25, 2022

---

# Measurement of inclusive $B \rightarrow \Lambda_c$ branching fractions using Belle data and hadronic Full Event Interpretation

Leonardo Benjamin Rizzato<sup>1</sup>.

<sup>1</sup>*Institute Jožef Stefan, Ljubljana, Slovenia*

## Abstract

Inclusive  $B \rightarrow \Lambda_c$  branching fractions were measured most recently by BaBar collaboration. However, the measurement still presented a poor accuracy. A more precise measurement of inclusive  $B \rightarrow \Lambda_c$  branching fraction could be useful to gain a better confidence on B meson weak decays treatment. With help of the Full Event Interpretation algorithm, it is possible to perform a more precise measurement of inclusive  $B \rightarrow \Lambda_c$  branching fractions using Belle data set.



# Changelog

## Version 1.0

Version for first review

- moved figure 1
- introduced "misreconstructed signal" and "reconstructed signal" in 2.2
- added argumentation on using the FEI efficiencies ratios
- added Figures 14, 15 and 16 to compare the Mbc distributions of events with/without peaking  $\Lambda_c$ .
- added Fig. b for  $M(pK\pi)$  w/wo continuum suppression comparison
- description of continuum background modeling in Sec. 4.1 made more comprehensible
- moved toyMC plots on page 29 to Sec.4.2 with comment about the pulls.
- added some comments about Fig. 40 - Fig. 41
- added PID correction section in Chap. 4
- added Sec. 4.13 about the data sideband fit and quality of the shapes description.
- added Table 16
- Updated systematics (for all BR)
- Corrected the  $\epsilon_{\Lambda_c}$  in Sec. 6.10
- Added signal region/ sideband plots in Appendix .1
- use the 1 sigma discrepancy in Sec. 4.14 as systematic uncertainty to add to the overall systematics (which becomes then  $\pm 18\%$ ). OK? Then what to do...correct by this 1 sigma the result I will get on data?
- Added Sec. 5.12

# Contents

<b>1</b>	<b>Introduction</b>	<b>1</b>
1.1	Analysis Setup . . . . .	1
1.2	Datasets . . . . .	1
<b>2</b>	<b>Event selection and reconstruction</b>	<b>2</b>
2.1	$B_{tag}$ reconstruction . . . . .	2
2.2	$\Lambda_c$ reconstruction . . . . .	2
2.3	Wrongly reconstructed $B_{tag}$ candidates . . . . .	3
<b>3</b>	<b>Signal selection optimization</b>	<b>4</b>
<b>4</b>	<b><math>B^- \rightarrow \Lambda_c^+</math> decays</b>	<b>6</b>
4.1	Probability Density Functions (PDFs) for the two dimensional fit . . . . .	11
4.2	Two dimensional fit . . . . .	26
4.3	Probability Density Functions (PDFs) for the $B_{tag}$ . . . . .	31
4.4	$B_{tag}$ fit . . . . .	33
4.5	$\Lambda_c$ and FEI efficiency . . . . .	34
4.6	Studies of Systematic Effects . . . . .	36
4.7	Continuum background modeling . . . . .	36
4.8	Crossfeed background modeling . . . . .	38
4.9	Crossfeed ratio . . . . .	38
4.10	Efficiencies . . . . .	39
4.11	Fit biases . . . . .	39
4.12	PID efficiency correction . . . . .	39
4.13	Sideband fit on data . . . . .	40
4.14	Measured $B^+ \rightarrow \bar{\Lambda}_c^- X$ inclusive Branching Fraction . . . . .	41
<b>5</b>	<b><math>B^- \rightarrow D^0</math> control decay</b>	<b>43</b>
5.1	Dataset used . . . . .	43
5.2	Event selection and reconstruction . . . . .	43
5.3	Signal selection optimization . . . . .	43
5.4	Probability Density Functions (PDFs) for two dimensional fit . . . . .	44
5.5	2D Fit on Monte Carlo simulated data . . . . .	48
5.6	2D Fit on data . . . . .	49
5.7	Probability Density Functions (PDFs) for the $B_{tag}$ . . . . .	51
5.8	$B_{tag}$ Fit on Monte Carlo simulated data . . . . .	52
5.9	$B_{tag}$ Fit on data . . . . .	54
5.10	PID efficiency correction . . . . .	55
5.11	$D^0$ and FEI efficiency . . . . .	55
5.12	Studies of Systematic Effects . . . . .	56
5.13	Measured $B^+ \rightarrow \bar{D}^0 X$ inclusive Branching Fraction . . . . .	56

<b>6</b>	$B^- \rightarrow \bar{\Lambda}_c^-$ decays	<b>58</b>
6.1	Probability Density Functions (PDFs) for the two dimensional fit . . . . .	58
6.2	Two dimensional fit . . . . .	64
6.3	Probability Density Functions (PDFs) for the $B_{tag}$ . . . . .	68
6.4	$B_{tag}$ fit . . . . .	70
6.5	$\Lambda_c$ and FEI efficiency . . . . .	71
6.6	Studies of Systematic Effects . . . . .	72
6.7	Continuum background modeling . . . . .	72
6.8	Crossfeed background modeling . . . . .	74
6.9	Crossfeed ratio . . . . .	74
6.10	Efficiencies . . . . .	75
6.11	Fit biases . . . . .	75
6.12	Measured $B^+ \rightarrow \Lambda_c^+$ inclusive Branching Fraction . . . . .	75
<b>Appendix</b>		<b>77</b>
.1	$B^- \rightarrow \Lambda_c^+$ decays: additional plots . . . . .	79
.2	$B^- \rightarrow D^0$ decays: additional plots . . . . .	85
.3	$B^- \rightarrow \bar{\Lambda}_c^-$ decays: additional plots . . . . .	89

# <sup>1</sup> 1 Introduction

<sup>2</sup> Inclusive  $B$  meson baryonic decays with a  $\Lambda_c$  baryon in the final state are the most  
<sup>3</sup> abundant, due to a relatively large  $V_{cb}$  element of the CKM matrix. The *BaBar* experiment  
<sup>4</sup> measured their branching fractions to be around the percent level (see ref. [1]). However, the  
<sup>5</sup> branching fractions were determined with big uncertainties: nearly 50% on the measured  
<sup>6</sup> values or, in the case of the  $B^0 \rightarrow \Lambda_c^+$  decay, only an upper limit could be established.  
<sup>7</sup> A more precise measurement of inclusive  $B \rightarrow \Lambda_c$  branching fractions may shed light on  
<sup>8</sup> the appropriateness of  $B$  meson weak decays treatment, particularly of strong interaction  
<sup>9</sup> effects modelling. Predictions for inclusive branching fractions are given, for example, in  
<sup>10</sup> ref. [2].

<sup>11</sup> Exploiting the Full Event Interpretation (FEI) algorithm, developed for the Belle  
<sup>12</sup> II experiment, it may be possible to perform a more precise measurement of inclusive  
<sup>13</sup>  $B \rightarrow \Lambda_c$  branching fractions, using the full Belle data set. A more precise measurement  
<sup>14</sup> may also trigger further research on currently scarce theory predictions for  $B$  meson decays  
<sup>15</sup> to charm baryons.

## <sup>16</sup> 1.1 Analysis Setup

<sup>17</sup> The reconstruction is performed with BASF2 release 05-02-03 together with the `b2bii`  
<sup>18</sup> package in order to convert the *Belle* MDST files (BASF data format) to *Belle II* MDST files  
<sup>19</sup> (`BASF2` data format). The FEI version used is `FEI_B2BII_light-2012-minos`.

## <sup>20</sup> 1.2 Datasets

<sup>21</sup> The Belle detector acquired a dataset of about  $L_0 \approx 710 fb^{-1}$  of integrated luminosity in  
<sup>22</sup> its lifetime at the  $\Upsilon(4S)$  energy of 10.58 GeV, which corresponds to about  $771 \times 10^6 B\bar{B}$   
<sup>23</sup> meson pairs. Additionally, several streams of Monte-Carlo (MC) samples were produced,  
<sup>24</sup> where each stream of MC corresponds to the same amount of data that was taken with  
<sup>25</sup> the detector. No specific signal MC was used: instead of producing dedicated signal MC  
<sup>26</sup> samples, the samples were obtained by filtering the decays of interest from the generic  
<sup>27</sup> on-resonance MC samples. The following samples were used in this analysis:

- <sup>28</sup> • data
- <sup>29</sup> • MC - 10 streams of  $B^+B^-$  and  $B^0\bar{B}^0$  (denoted as `charged` and `mixed`) for signal  
<sup>30</sup> decays and backgrounds.
  - <sup>31</sup> - 6 streams of  $q\bar{q}$  produced at  $\Upsilon(4S)$  resonance energy
  - <sup>32</sup> - 6 streams of  $q\bar{q}$  produced at 60 MeV below  $\Upsilon(4S)$  resonance energy, where each  
<sup>33</sup> stream corresponds to  $1/10 \times L_0$ .

## 35    2 Event selection and reconstruction

36    In this chapter the procedure for reconstruction of the events where one  $B$  meson decays  
37    inclusively to a  $\Lambda_c$  baryon and the accompanying  $B$  meson decays hadronically.

### 38    2.1 $B_{tag}$ reconstruction

39    The FEI is an exclusive tagging algorithm that uses machine learning to reconstruct  
40     $B$  meson decay chains and calculates the probability that these decay chains correctly  
41    describe the true process. In this analysis only hadronically reconstructed decay chains  
42    are considered. The training called `FEI_B2BII_light-2012-minos` is used. Tag-side  $B$   
43    meson candidates are required to have a beam-constrained mass greater than  $5.22 \text{ GeV}/c^2$   
44    and  $-0.15 < \Delta E < 0.07 \text{ GeV}$ .

45    In the case of multiple candidates in the same event, the candidate with the highest  
46    SignalProbability (the signal probability calculated by FEI using FastBDT) is chosen. To  
47    suppress the background consisting of  $B^0$  events misreconstructed as  $B^+$  (and vice-versa)  
48    from neutral (charged) decays also a  $B^0$  ( $B^+$ ) candidate is reconstructed with FEI and if  
49    its SignalProbability is higher than the charged (neutral) reconstructed  $B$  meson, the event  
50    is discarded. This constitutes a sort of crossfeed-veto, rejecting part of events belonging  
51    to the other typology of decays of interest: for example in the case one is interested  
52    in reconstructing  $B^{+/-}$  decays and the event actually contains  $B^0/\bar{B}^0$  decays, the FEI  
53    reconstructed neutral  $B$  meson candidate most likely presents a higher SignalProbability  
54    than the charged FEI reconstructed candidate.

### 55    2.2 $\Lambda_c$ reconstruction

56    In the *rest of event* (ROE) of the reconstructed  $B_{tag}$  meson, to select  $\Lambda_c \rightarrow pK\pi$  signal  
57    candidates, the following event selection criteria are applied. Charged tracks with the  
58    impact parameters perpendicular to and along the nominal interaction point (IP) are  
59    required to be less than 2 cm and 4 cm respectively ( $dr < 2 \text{ cm}$  and  $|dz| < 4 \text{ cm}$ ).

60    The pion tracks are required to be identified with  $\frac{\mathcal{L}_\pi}{\mathcal{L}_K + \mathcal{L}_\pi} > 0.6$ . The kaon tracks are  
61    required to be identified with  $\frac{\mathcal{L}_K}{\mathcal{L}_K + \mathcal{L}_\pi} > 0.6$ , and the proton/anti-proton tracks are  
62    required to be identified with  $\frac{\mathcal{L}_{p/\bar{p}}}{\mathcal{L}_K + \mathcal{L}_{p/\bar{p}}} > 0.6$  and  $\frac{\mathcal{L}_{p/\bar{p}}}{\mathcal{L}_\pi + \mathcal{L}_{p/\bar{p}}} > 0.6$ , where the  $\mathcal{L}_{\pi,K,p/\bar{p}}$  are the  
63    likelihoods for pion, kaon, proton/anti-proton, respectively, determined using the ratio of  
64    the energy deposit in the ECL to the momentum measured in the SVD and CDC, the  
65    shower shape in the ECL, the matching between the position of charged track trajectory  
66    and the cluster position in the ECL, the hit information from the ACC and the dE/dx  
67    information in the CDC.

68    For the  $\Lambda_c$  candidates a vertex fit is performed with `TreeFitter`, requiring it to converge.  
69    If there are more than one  $\Lambda_c$  combination, then the best candidate based on the  $\chi^2$   
70    probability is chosen. The  $\Lambda_c$  signal region is defined to be  $|M_{\Lambda_c} - m_{\Lambda_c}| < 20 \text{ MeV}/c^2$  ( $\sim$   
71     $3\sigma$ ), here  $m_{\Lambda_c}$  is the nominal mass of  $m_{\Lambda_c}$ .

72

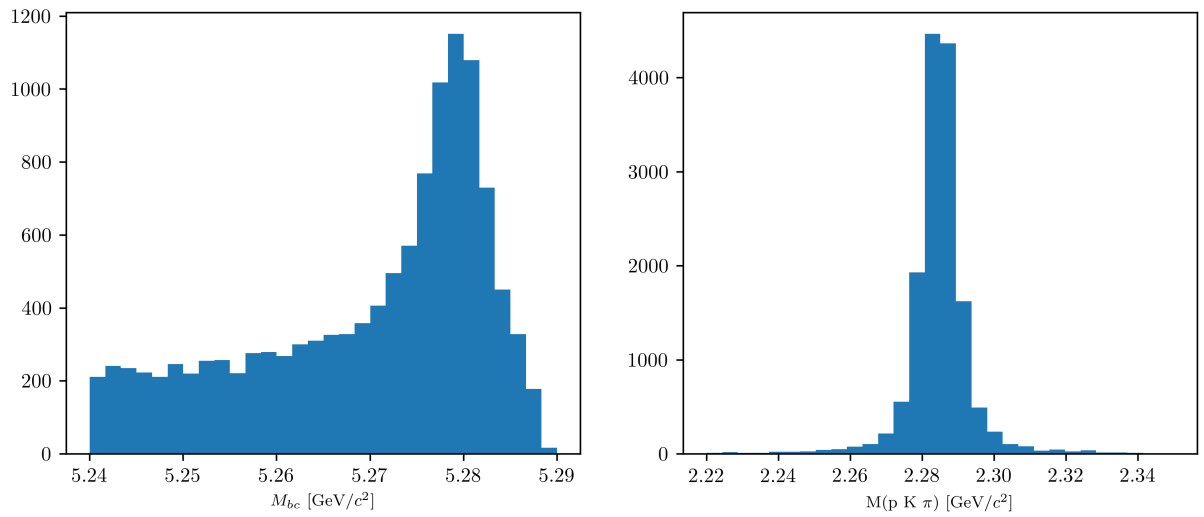


Figure (1)  $M_{bc}$  and  $M(pK\pi)$  distributions of  $B_{tag}$  and  $\Lambda_c$  candidates reconstructed in the signal sample.

### **73 2.3 Wrongly reconstructed $B_{tag}$ candidates**

**74** In the case of the signal sample the distributions for the beam-constrained mass  $M_{bc}$  and  
**75** for the correctly reconstructed  $\Lambda_c$  candidates, look like in Fig. 1. If one then investigates  
**76** the  $M_{bc}$  distribution of the  $B_{tag}$  candidates reconstructed with FEI, it can be seen that  
**77** there is a peaking structure for wrongly reconstructed  $B$  mesons (as in Fig. 2), according  
**78** to the BASF2 internal truth matching variable **isSignal**. It is obvious from this that the  
**79** BASF2 internal truth matching variable cannot be used to separate properly the signal  
**80** events in correctly and wrongly reconstructed  $B$  mesons. In the study BELLE2-NOTE-TE-  
**81** 2021-026 <https://docs.belle2.org/record/2711/files/BELLE2-NOTE-TE-2021-026.pdf> a possible solution was found developing new variables that can be used for an  
**82** improved truth matching for the FEI (those variables were added to a newer BASF2  
**83** release than the one used for this study). In the present study instead a more "traditional"  
**84** approach was adopted: fitting the  $M_{bc}$  distribution with a sum of PDFs that account for the  
**85** flat (background) component and the peaking (signal) component. The first component  
**86** represents the combinatorial background, i.e.  $B$  mesons that were mis-reconstructed,  
**87** and therefore those events are denoted from now on as "**misreconstructed signal**".  
**88** The peaking component represents the correctly reconstructed signal events in  $M_{bc}$  and  
**89** therefore denoted from now on as "**reconstructed signal**". Only the second one is then  
**90** considered for the signal yield, while the first is counted as a background. To validate this  
**91** method a control decay study was performed on the flavor correlated  $B^+ \rightarrow \bar{D}^0$  channel.  
**92**

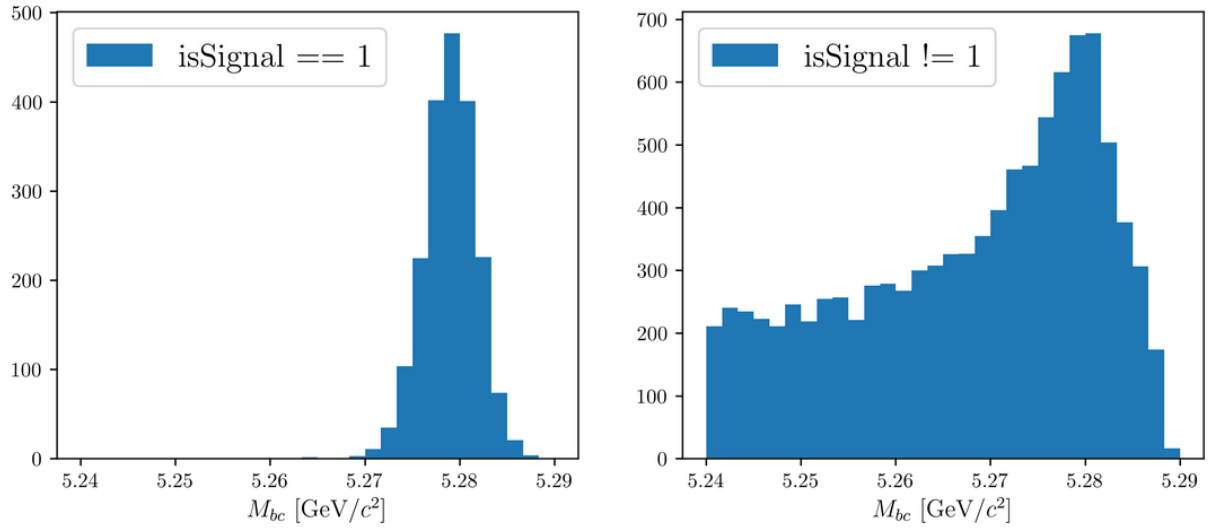


Figure (2)  $M_{bc}$  distribution of  $B_{tag}$  candidates reconstructed in the signal sample, truth-matched (on the left) and not (on the right).

### 93 3 Signal selection optimization

94 To further enhance the purity of the signal decays, an optimization procedure is adopted  
 95 to determine optimal cuts for a set of variables for each decay mode under investigation  
 96 by this study. The cuts on the following variables are optimized:

- 97 • *foxWolframR2*: the event based ratio of the 2-nd to the 0-th order Fox-Wolfram  
 98 moments
- 99 • SignalProbability: the already mentioned signal probability calculated by FEI using  
 100 FastBDT
- 101 •  $p_{CMS}^{\Lambda_c}$ : momentum of the  $\Lambda_c$  candidates in the center of mass system

102 The optimization is based on the Figure Of Merit (FOM):  $FOM = \frac{S}{\sqrt{S+B}}$   
 103 Where S and B are respectively signal and background events in the signal region:  
 104  $M_{bc} > 5.27 \text{ GeV}/c^2$ ,  $2.2665 < M(pK\pi) < 2.3065 \text{ GeV}/c^2$ .

105 Due to the issue reported in Sec. 2.3, to separate signal events that peak in  $M_{bc}$  from  
 106 the ones that are not (which are then categorized as background events), the events  
 107 reconstructed in the signal sample are fitted with a sum of Crystal Ball function and  
 108 Argus for each cut value on the corresponding variable to optimize (as in Fig. 3).

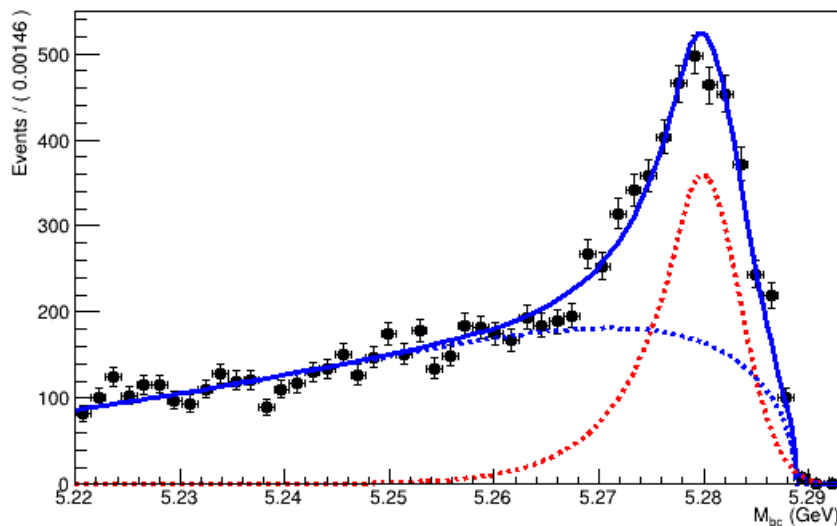


Figure (3) Example of a fit used to separate the correctly reconstructed  $B$  mesons (described by the red dotted Crystal Ball function) from the wrongly reconstructed ones (described by the blue dotted Argus function).

<sup>109</sup> **4  $B^- \rightarrow \Lambda_c^+ \text{ decays}$**

<sup>110</sup> First, in order to suppress the continuum background the cut on *foxWolframR2* is  
<sup>111</sup> optimized. Fig. 4 shows the *foxWolframR2* distributions for signal and continuum  
events.

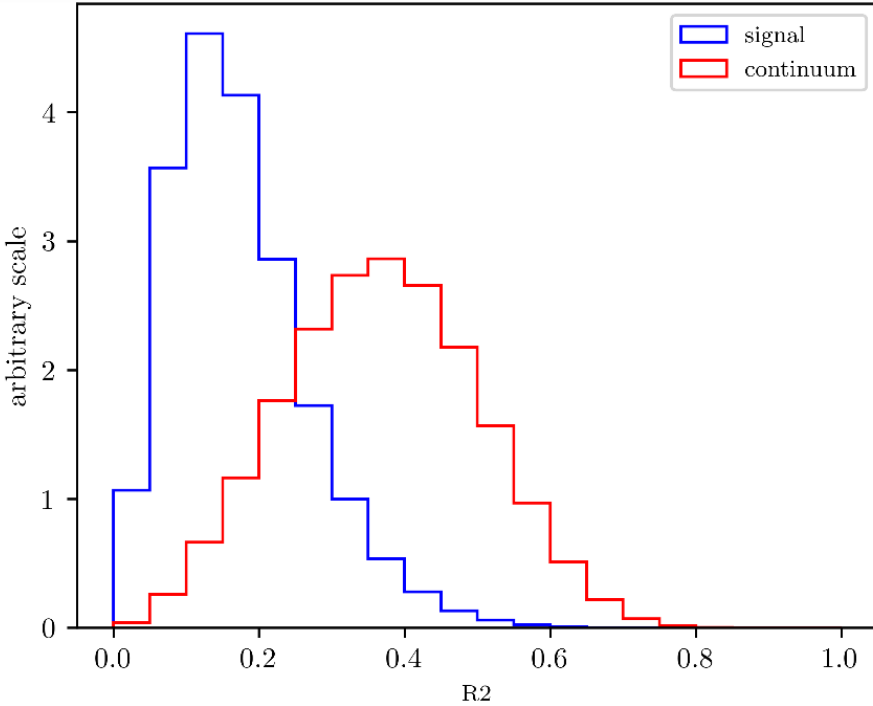


Figure (4) Distribution of the *foxWolframR2* variable for signal and continuum back-ground events.

<sup>112</sup>  
<sup>113</sup> With the optimized cut  $\text{foxWolframR2} < 0.27$ , the cut on SignalProbability is  
<sup>114</sup> optimized in the same way (see Fig. 7).

<sup>115</sup>  
<sup>116</sup> With the optimized cut SignalProbability  $> 0.01$ , the cut on *foxWolframR2* variable is  
<sup>117</sup> rechecked (Fig. 8). Being the maximum values fluctuating around  $\text{foxWolframR2} < 0.3$ ,  
this cut is the one finally chosen for this variable.

<sup>118</sup>  
<sup>119</sup> With the optimized cuts on SignalProbability and *foxWolframR2* variable, the cut  
on  $p_{CMS}^{\Lambda_c}$  is optimized

<sup>120</sup>

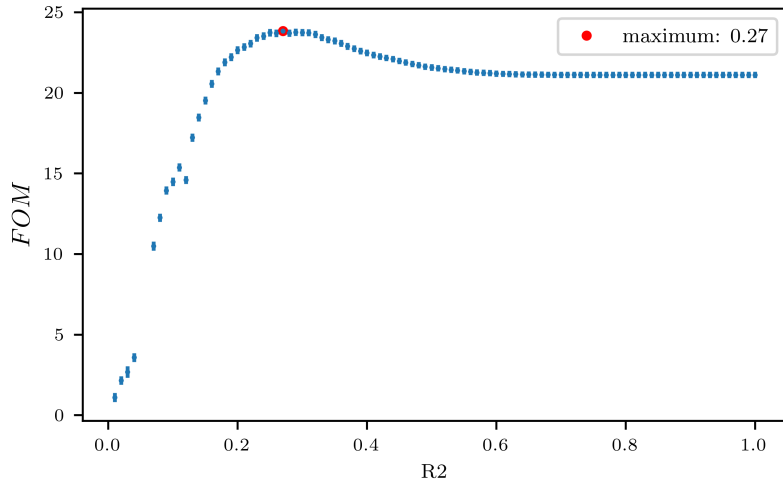


Figure (5) Figure of Merit values calculated at several cuts on the *foxWolframR2* variable

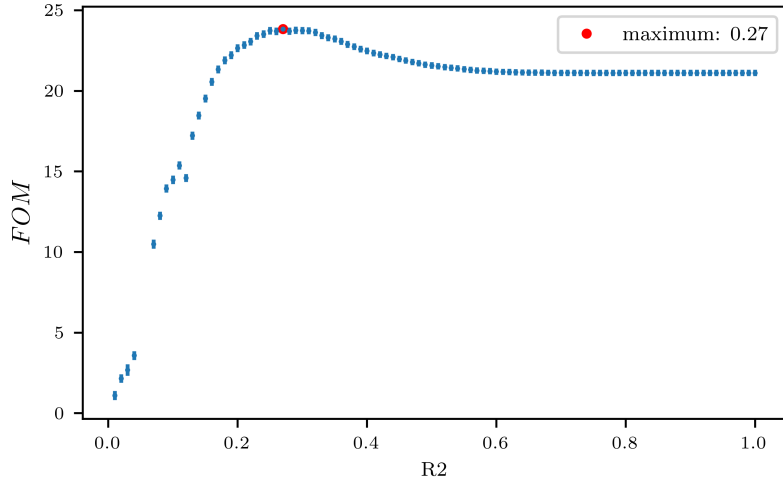


Figure (6) Figure of Merit values calculated at several cuts on the *foxWolframR2* variable

121 From Fig. 9 one can see that with values of the cut above  $p_{CMS}^{\Lambda_c} < 1.8 \text{ GeV}/c^2$  a  
 122 plateau of maximum FOM values is reached. But such a cut would still be useful to reject  
 123 some background events as one can see from Fig. 10.

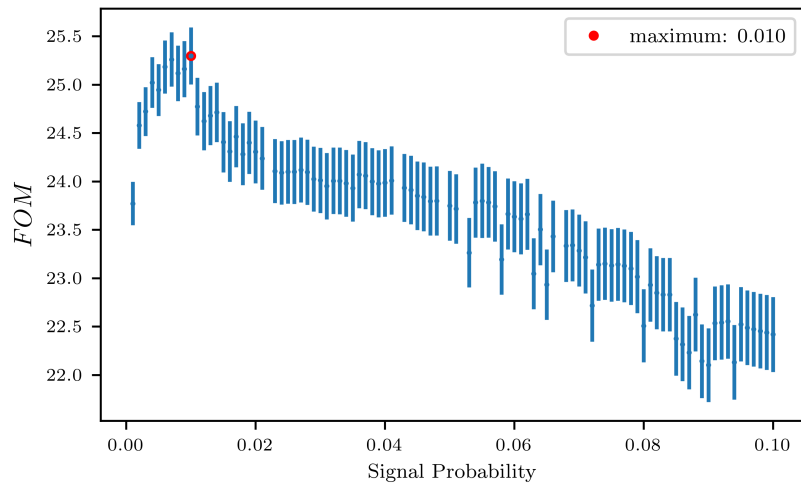


Figure (7) Figure of Merit values calculated at several cuts on the SignalProbability variable

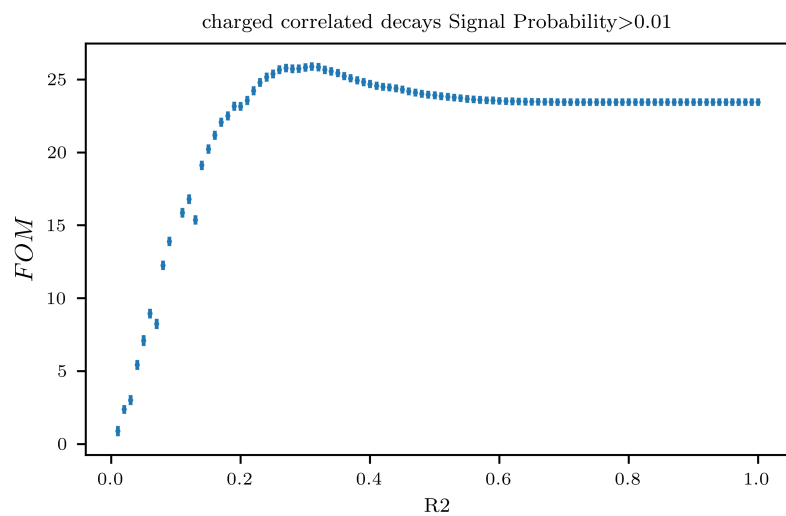


Figure (8) Figure of Merit values calculated at several cuts on the *foxWolframR2* variable

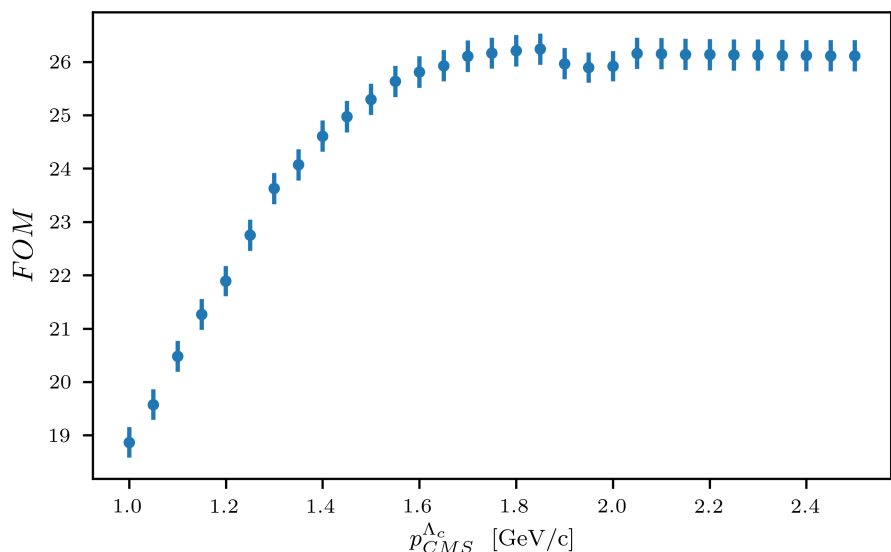


Figure (9) Figure of Merit values calculated at several cuts on the momentum of the  $\Lambda_c$  candidates in the center of mass system

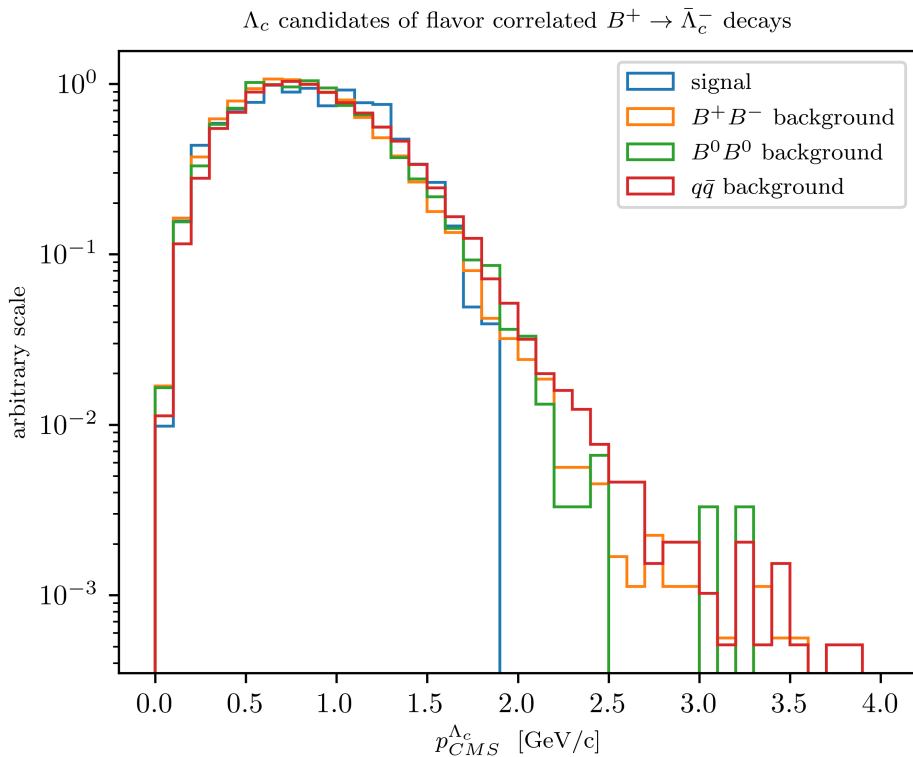


Figure (10) Distribution of  $\Lambda_c$  candidates momenta in the center of mass system

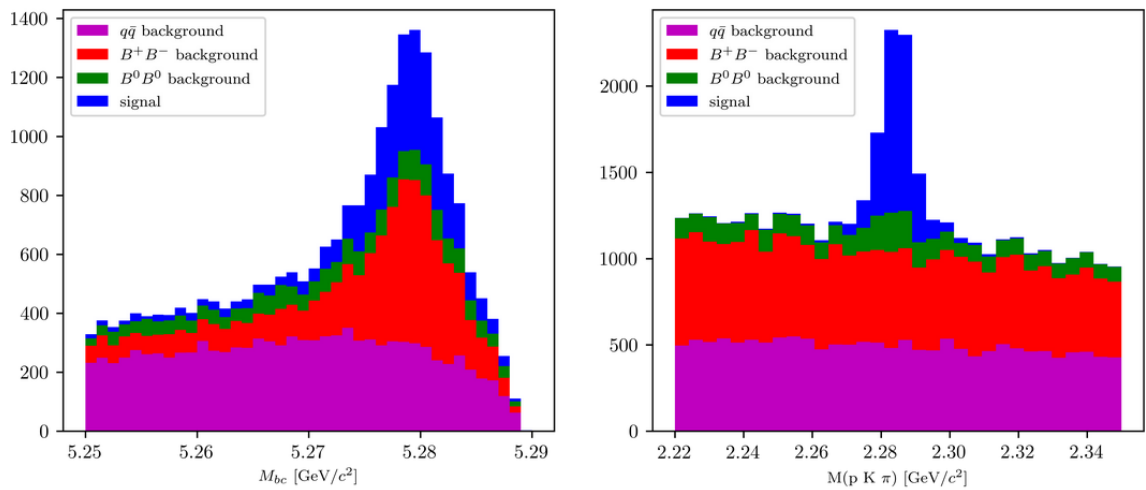


Figure (11) Distribution of  $M_{bc}$  (left) and invariant mass of charged correlated  $\Lambda_c$  candidates (right), in the signal region after the above mentioned selection cuts.

128 To measure the inclusive branching fraction of  $B^- \rightarrow \Lambda_c^+ X$  the following quantities  
 129 need to be known:

$$Br(B^- \rightarrow \Lambda_c^+ X) = \frac{N_{tag,\Lambda_c} \cdot \epsilon_{FEI}^+}{N_{tag} \cdot Br(\Lambda_c^+ \rightarrow pK^-\pi^+) \epsilon_{\Lambda_c} \epsilon_{FEI,sig}^+} \quad (1)$$

130

131 Where

- 132 •  $N_{tag,\Lambda_c}$  is the reconstructed signal yield obtained from a two dimensional fit of  $M_{bc}$   
 133 and  $M(pK\pi)$  in the final sample.
- 134 •  $N_{tag}$  is the reconstructed signal yield obtained from the  $M_{bc}$  fit of all the tagged  $B$   
 135 mesons in the final sample.
- 136 •  $\epsilon_{\Lambda_c}$  is the  $\Lambda_c$  reconstruction efficiency.
- 137 •  $\epsilon_{FEI}^+$  represents the hadronic tag-side efficiency for generic  $B^+B^-$  events.
- 138 •  $\epsilon_{FEI,sig}^+$  represents the hadronic tag-side efficiency for  $B^+B^-$  events where the tagged  
 139  $B$  meson decays hadronically and the accompanying meson decays inclusively into  
 140 the studied signal channel.
- 141 •  $Br(\Lambda_c^+ \rightarrow pK^-\pi^+)$ : the branching fraction of the decay mode used to reconstruct  
 142 the  $\Lambda_c$  baryon.

143 Here a decision was made not to rely on the estimated number of  $B$  meson pair, as it is  
 144 usually done, and the absolute FEI efficiency, since the latter shows large discrepancy  
 145 between MC and data (see i.e. the results reported in the PhD Thesis by M. Gelb [3] and  
 146 also by J. Schwab [4] ) and also it depends strongly on the signal-side (i.e.  $\epsilon_{FEI}^+ \neq \epsilon_{FEI,sig}^+$ ).  
 147 Instead, to limit the systematics, the branching ratio normalization is obtained using the  
 148 fitted tagged  $B$  mesons and the ratio  $\epsilon_{FEI,sig}^+/\epsilon_{FEI}^+$  measured on MC, which is expected to  
 149 be described much better rather than the absolute FEI efficiency.

150 The final samples contain both signal and background candidates from various sources  
 151 and in order to extract  $N_{tag,\Lambda_c}$  and  $N_{tag}$  unbinned extended maximum-likelihood fits are  
 152 performed.

153 In the next sections the methods used to determine the above mentioned quantities are  
 154 described. First the fit model that accurately describes the distributions in the  $B_{tag} + \Lambda_c$   
 155 final sample will be described.

## 156 4.1 Probability Density Functions (PDFs) for the two dimensional 157 fit

158 The PDFs used to describe the signal distributions are discussed first. The final sample of  
 159 total signal events presents a peak around the expected  $B$  meson mass and a tail at low  
 160  $M_{bc}$  values.

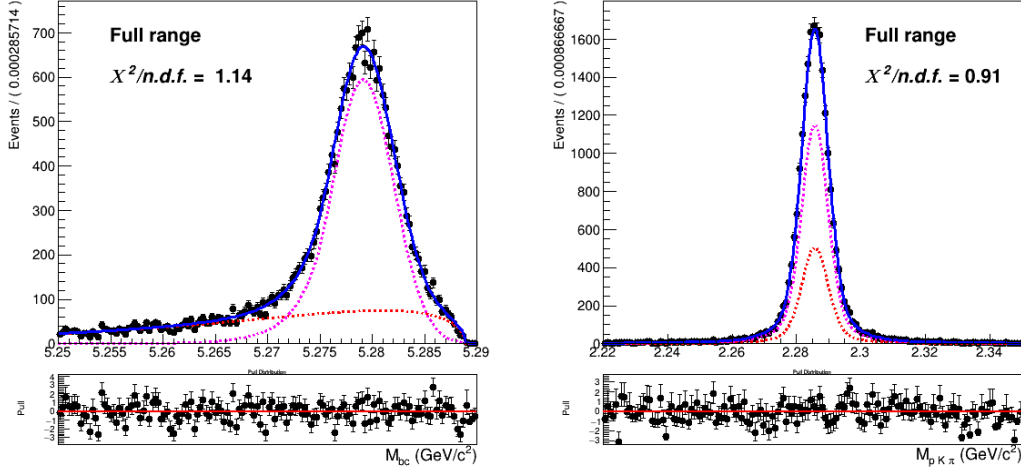


Figure (12) Two dimensional fit of total signal events in  $M_{bc}$  and  $M(pK\pi)$

161 The 2D fit shown in Fig. 12 is performed on five streams of signal MC with a sum of  
 162 the following probability density functions:

$$P_{B,\Lambda_c}^{recSig}(M_{bc}, M(pK\pi)) = \Gamma_{CB}(M_{bc}) \times \rho_G(M(pK\pi)) \quad (2)$$

$$P_{B,\Lambda_c}^{misSig}(M_{bc}, M(pK\pi)) = \Gamma_{ARG}(M_{bc}) \times \rho_G(M(pK\pi)) \quad (3)$$

164  
 165 The first is used to fit the reconstructed signal and  $\Gamma_{CB}(M_{bc})$  is a Crystal Ball function.  
 166 The second is used to model the misreconstructed signal and  $\Gamma_{ARG}(M_{bc})$  is an Argus  
 167 function. In both cases a sum of three Gaussian functions  $\rho_G(M(pK\pi))$  describes the  
 168 mass of the  $\Lambda_c$  baryon.

169 As already said in Sec. 2.3, only the reconstructed signal considered for the signal  
 170 yield, while the misreconstructed signal is considered as background. Other background  
 171 components that will be discussed in the next pages are:

- 172 • **generic** (charged  $B$ ) background
- 173 • **crossfeed** (neutral  $B$ ) background
- 174 • **continuum** background

175 **Generic background**

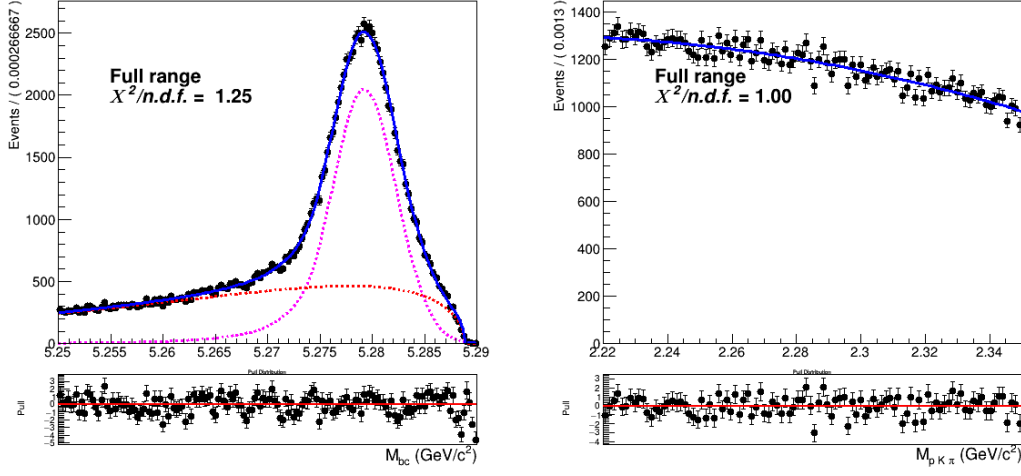


Figure (13) Two dimensional fit of generic ( $B^+B^-$ ) events in  $M_{bc}$  and  $M(pK\pi)$ .

176 The generic background deriving from other  $B^+B^-$  events presents a similar shape of the  
 177 distribution in  $M_{bc}$  (see Fig. 13): the probability density functions used for it are again a  
 178 Crystal Ball and an Argus. For both functions the parameters differ from the ones used in  
 179 Eq. 2-4.1. Instead, the flat background in  $M(pK\pi)$  can be described with a second order  
 180 Chebychev polynomial function. The two dimensional PDF in this case is given by:

$$P_{B,\Lambda_c}^{GenBkg}(M_{bc}, M(pK\pi)) = [\Gamma_{CB}(M_{bc}) + \Gamma_{ARG}(M_{bc})] \times \rho_{Cheb2}(M(pK\pi)) \quad (4)$$

181 **Crossfeed background**

182 The contamination of misreconstructed  $B^0$  events in the  $B^+$  signal (and vice-versa) induces  
 183 a background which peaks near the  $B$  meson mass, as one can see in Fig. 14, independently  
 184 from the category of events in the  $\Lambda_c$  mass (see Figures 15- 16). Since among the  
 185 misreconstructed  $B^0$  events there are also  $B^0 \rightarrow \Lambda_c$  decays (peaking at the  $\Lambda_c$  mass, see  
 186 e.g. Fig. 15), this background contribution is also named "crossfeed background".

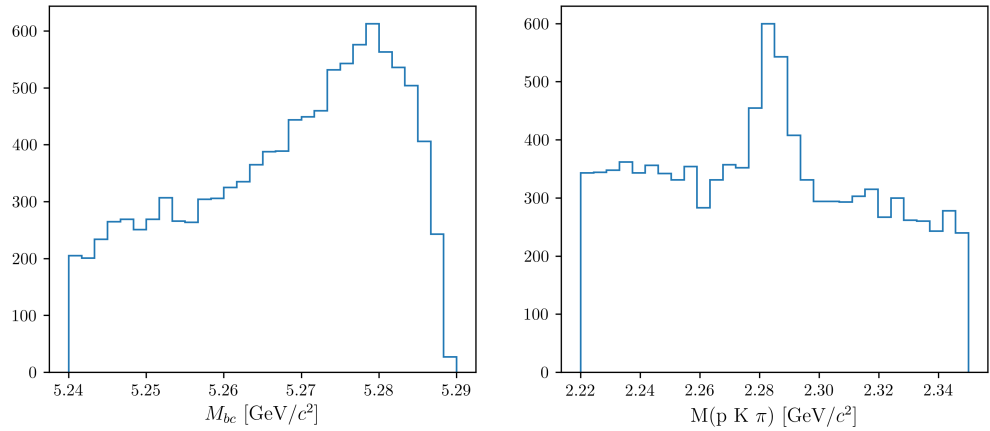


Figure (14)  $M_{bc}$  and  $M(pK\pi)$  distributions of crossfeed background events.

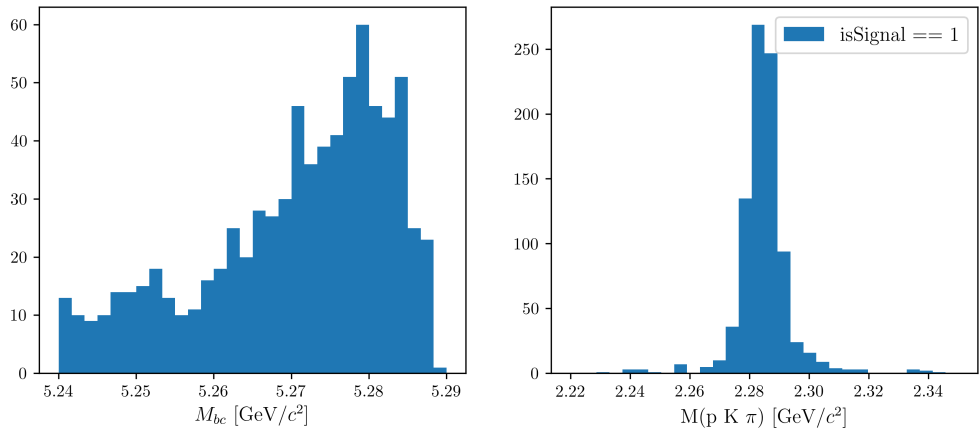


Figure (15)  $M_{bc}$  and  $M(pK\pi)$  of crossfeed events peaking at the  $\Lambda_c$  mass, i.e.: where true  $\Lambda_c$  baryons were correctly reconstructed.

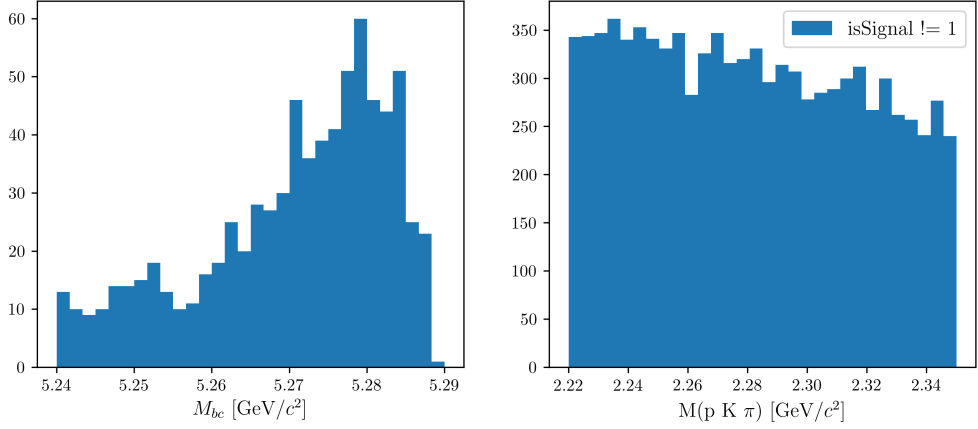


Figure (16)  $M_{bc}$  and  $M(pK\pi)$  of crossfeed events without  $\Lambda_c$  peak, i.e.: where  $\Lambda_c$  baryons were not present or not correctly reconstructed.

Fig. 17 shows the projections in  $M_{bc}$  and  $M(pK\pi)$  of the two dimensional fit of this type of background. The  $M_{bc}$  is modelled with a sum of Novosibirsk (colored in magenta) and Argus function (colored in red). Whereas the  $M(pK\pi)$  distribution is described by the sum of a first order Chebychev polynomial and the peak by the same sum of three Gaussian functions used to describe the signal peak. In fact the latter is the result of the reconstruction of crossfeed events  $B^0 \rightarrow \Lambda_c$ . Therefore the 2D PDF can be written as:

193

$$P_{B,\Lambda_c}^{CrossBkg}(M_{bc}, M(pK\pi)) = [\Gamma_{Nov}(M_{bc}) + \Gamma_{ARG}(M_{bc})] \times [\rho_{Cheb1}(M(pK\pi)) + \rho_G(M(pK\pi))] \quad (5)$$

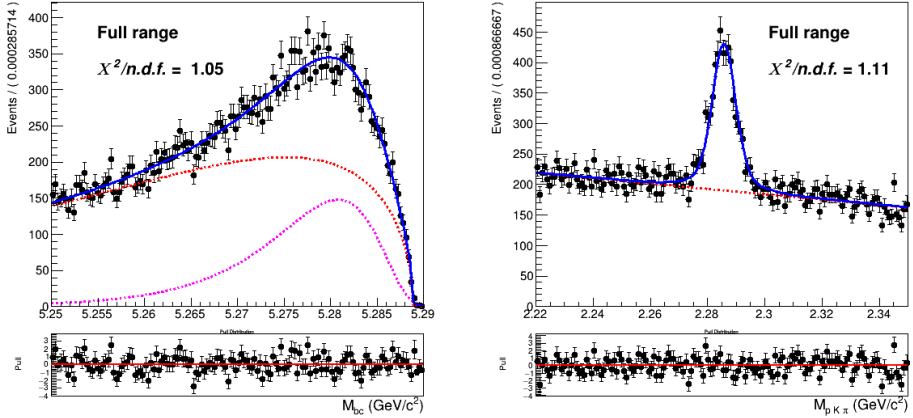


Figure (17) Two dimensional fit of crossfeed ( $B^0 \bar{B}^0$ ) events in  $M_{bc}$  and  $M(pK\pi)$ .

From the projections plotted in Fig. 17 the distributions appear to be well described by the PDF discussed above. Though the agreement in the  $\Lambda_c$  invariant mass is not fully

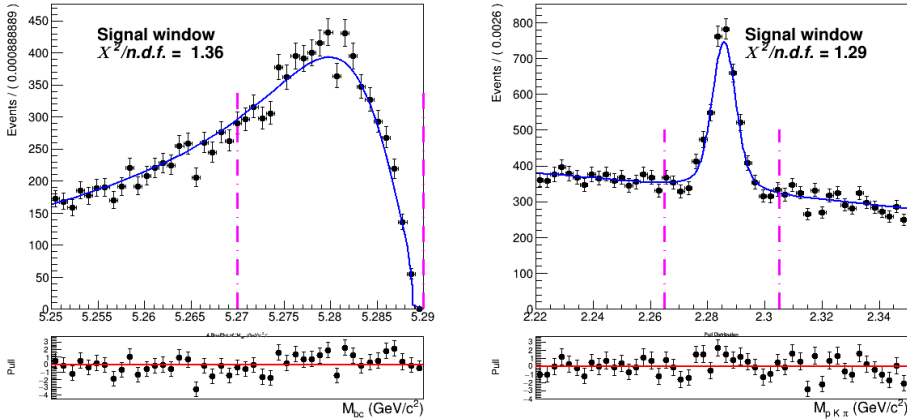


Figure (18) Signal region projections in  $M_{bc}$  and  $M(pK\pi)$ .

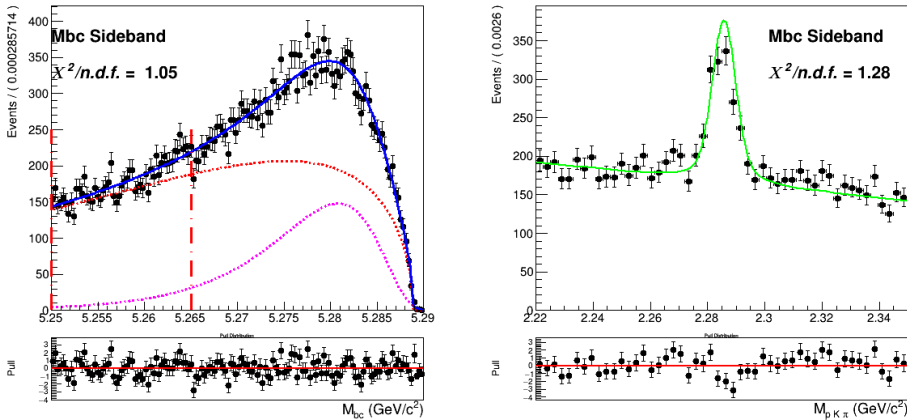


Figure (19)  $M_{bc}$  sideband region projection.

respected when different regions of  $M_{bc}$  are considered, as one can see from Fig. 18 and Fig. 19. The fraction of the amount of peaking events is not uniform among different  $M_{bc}$  regions. Since this background typology is peaking in both the observables of the fit, the potential correlation between them could have an impact on the signal yield extraction in the total fit.

To minimize this effect, and to avoid possible biases deriving from this feature, a correction is attempted. The  $M_{bc}$  is divided in 5 different regions. As shown in Figures ??-21e, for each of these regions a fit on the projected  $\Lambda_c$  invariant mass is performed to extract 5 values of the fraction of peaking events in those regions (all other parameters are fixed). Those values are then used for a parametrization of this parameter as a function of  $M_{bc}$ . From the plot shown in Fig. 20 one can see that it is possible to describe the trend with a linear dependence with a good approximation.

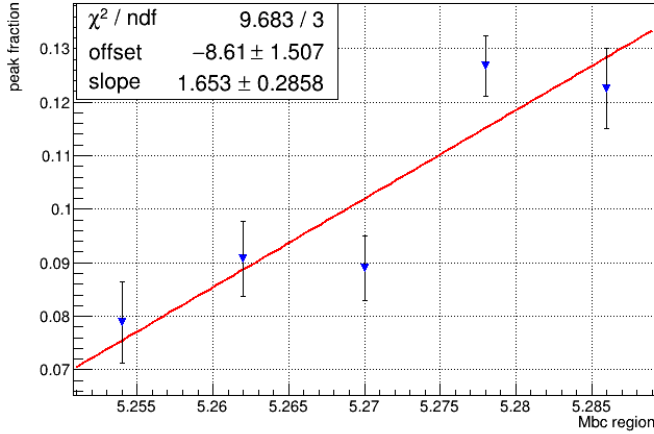
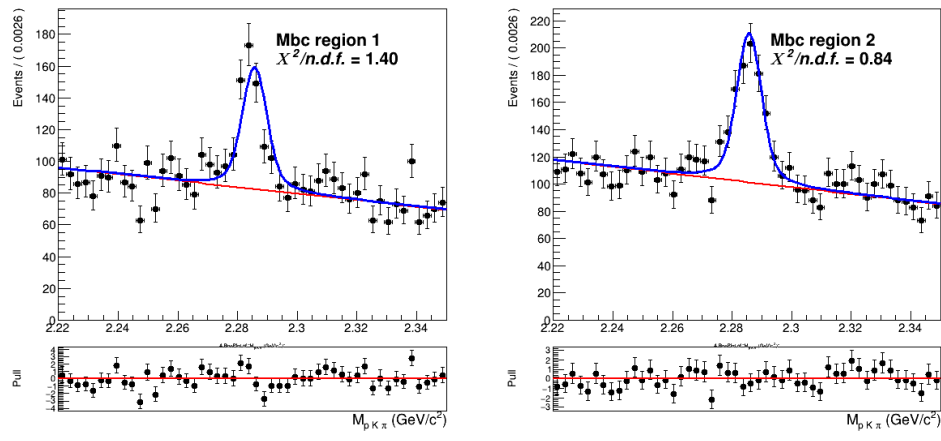
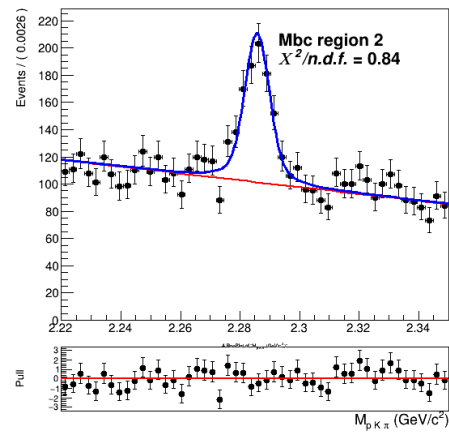


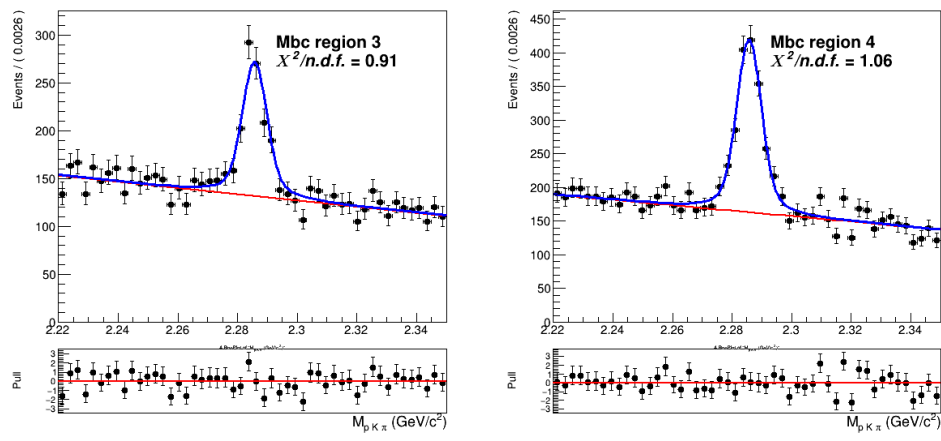
Figure (20) Invariant mass peak fraction as a function of  $M_{bc}$ .



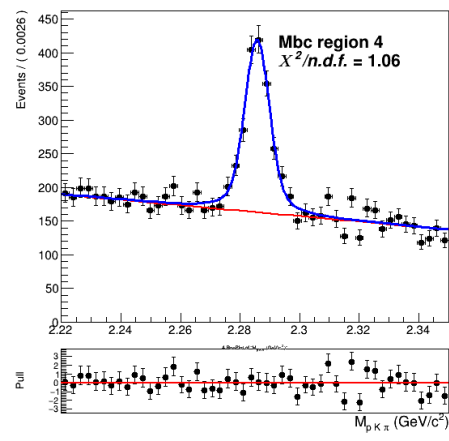
(a)



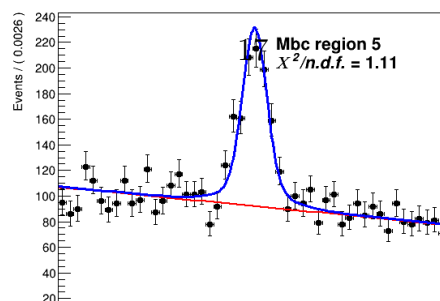
(b)



(c)



(d)



208     The 2D PDF describing the crossfeed background is consequently modified:

209      $P_{B,\Lambda_c}^{CrossBkg}(M_{bc}, M(pK\pi)) = [\Gamma_{Nov}(M_{bc}) + \Gamma_{ARG}(M_{bc})] \times [F(M(pK\pi)|M_{bc})]$

210     where the conditional PDF  $F(M(pK\pi)|M_{bc})$  describing the invariant mass is still a  
 211     sum of  $\rho_{Cheb1}(M(pK\pi))$  and  $\rho_G(M(pK\pi))$ , but their fraction is now parametrized as a  
 212     function of  $M_{bc}$ .

213     In Figures 22- 23 one can appreciate the improvement obtained with this correction.

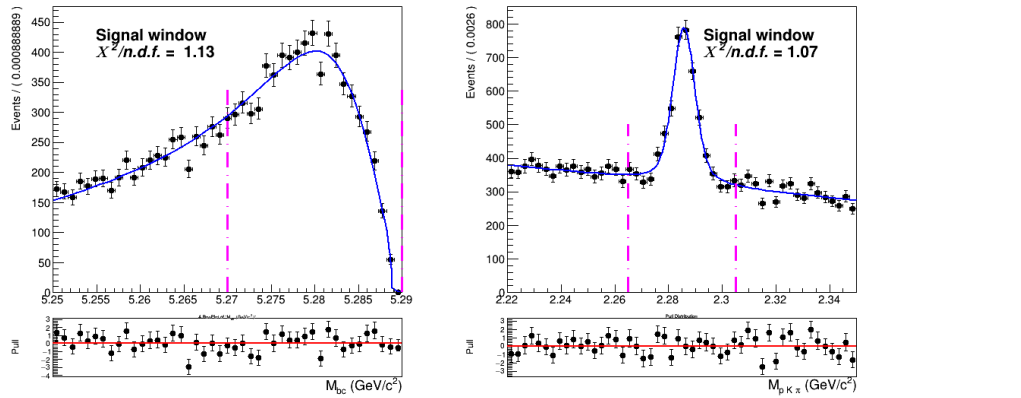


Figure (22) Signal region projections in  $M_{bc}$  and  $M(pK\pi)$  after the parametrization.

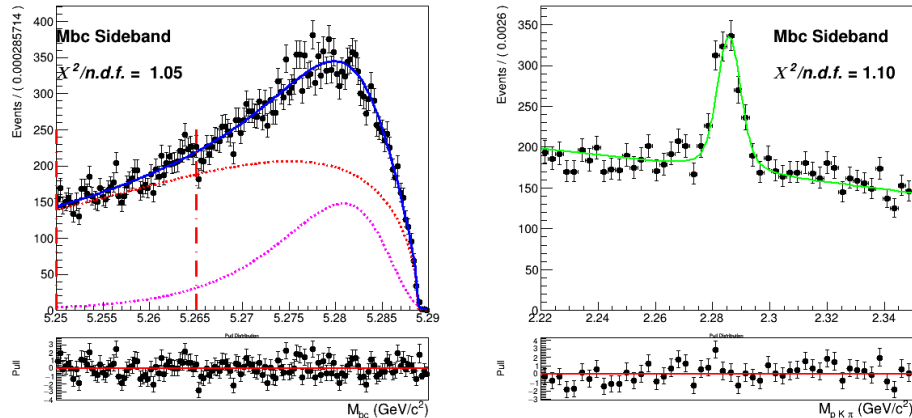


Figure (23)  $M_{bc}$  sideband region projection after the parametrization.

## 216     Continuum background

217     Besides the dataset recorded at the energy of the  $\Upsilon(4S)$  resonance ( $E_{CMS}^{on-res} = 10.58$  GeV),  
 218     the *Belle* experiment recorded a sample of  $89.4 \text{ fb}^{-1}$  at an energy 60 MeV below the  
 219     nominal  $\Upsilon(4S)$  resonance ( $E_{CMS}^{off-res} = 10.52$  GeV). The dataset allows to check for an

appropriate modeling of the continuum MC simulation. Using the official tables (<https://belle.kek.jp/secured/nbb/nbb.html>) the off-resonance sample is scaled by

$$\frac{\mathcal{L}^{on-res}}{\mathcal{L}^{off-res}} \left( \frac{E_{CMS}^{off-res}}{E_{CMS}^{on-res}} \right)^2 \quad (6)$$

taking into account the difference in luminosity and in  $E_{CMS}$  (Energy in center of mass system).

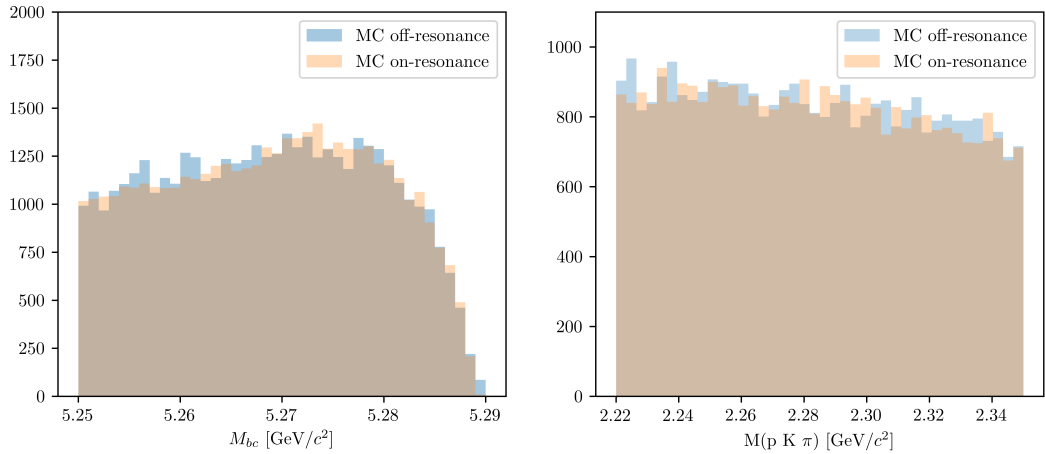


Figure (24)  $M_{bc}$  and  $M(pK\pi)$  comparison between on-/off-resonance (scaled) Monte Carlo simulated continuum. The scaling is applied according to Eq. (6) and shifting the  $M_{bc}$  distribution by  $E_{CMS}^{on-res} - E_{CMS}^{off-res}$ .

The plot in Fig.24 shows the  $M_{bc}$  and  $M(pK\pi)$  distributions in the MC on-/off-resonance continuum after the scaling<sup>1</sup>.

Ideally, provided that there's a good agreement between MC and data for the off-resonance sample and also between the MC on-/off-resonance continuum after the scaling, one could directly use the scaled off-resonance data to describe the continuum background in the fit on data. There are two reasons that prevent this very straightforward approach:

- First, since the off-resonance MC (and data) present very low statistics (Fig. 26a shows the  $\Lambda_c$  invariant mass in off-resonance data), scaling them with all the applied selection cuts would cause the PDF describing the continuum to be very much affected by statistical fluctuations.
- Secondly, the  $B$  meson candidates are reconstructed in both on-resonance and off-resonance events for values of  $M_{bc} \geq 5.22 \text{ GeV}/c^2$ , but the  $E_{CMS}$  differs: there can be effects of correlations between the applied *SignalProbability* cut and the  $M_{bc}$  variable that one needs to take into account.

<sup>1</sup>it is obtained with the MC off-resonance sample being composed of 6 streams: the total amount is normalized

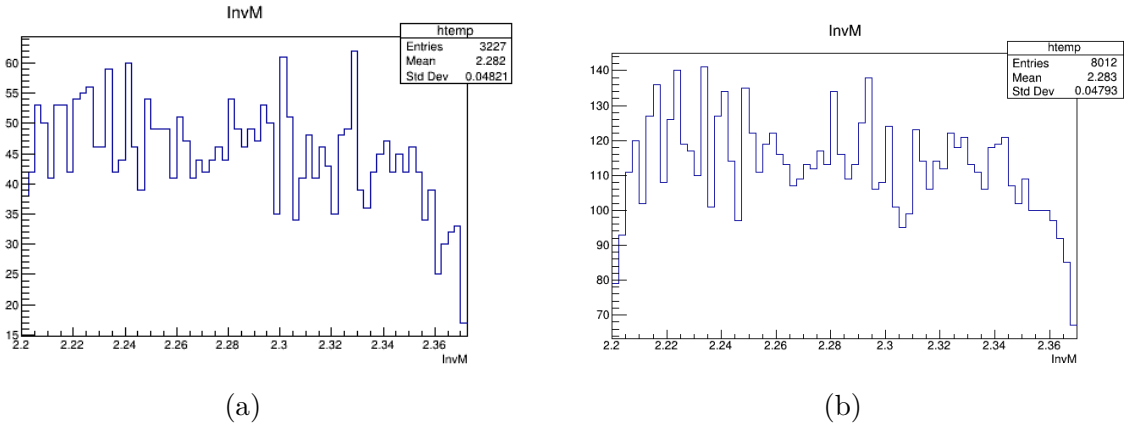


Figure (26) On the left:  $\Lambda_c$  invariant mass in off-resonance data (all nominal cuts applied). On the right:  $\Lambda_c$  invariant mass in off-resonance data after the continuum suppression cut removal.

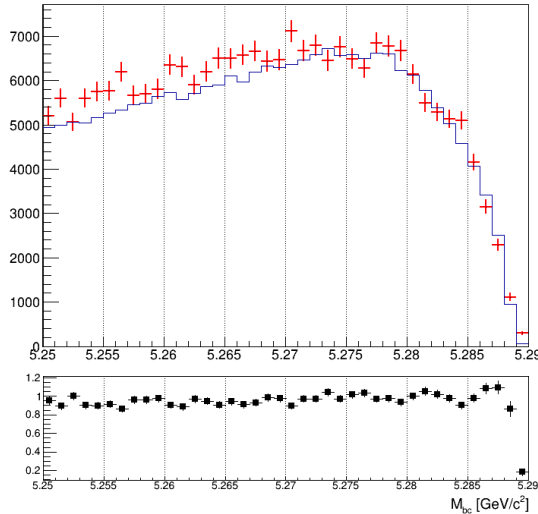


Figure (25)  $M_{bc}$  distributions of the MC (scaled) off-resonance sample (in red) and on-resonance (in blue) using 5 streams statistics and all nominal selection cuts applied.

In Fig. 25 one can notice some discrepancy in the shapes, apart from the not negligible statistical fluctuations in the (scaled) off-resonance distribution. In the  $\Lambda_c$  invariant mass one doesn't expect correlation effects, but nevertheless there can be differences due to the limited statistics of the off-resonance sample. In fact, in the case of on-resonance MC some events in which  $\Lambda_c$  candidates survive nominal selection cuts are visible and can be described with a small Gaussian on the top of the flat background (Fig.31a). On the contrary the off-resonance sample doesn't show anything else beside the flat background (the Fig.31b shows a 5 streams statistics).

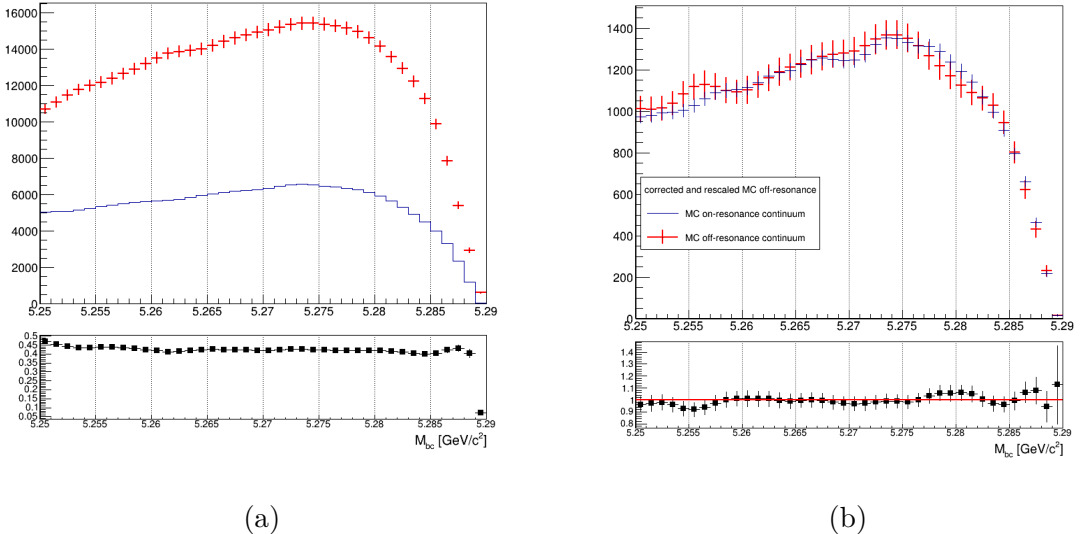


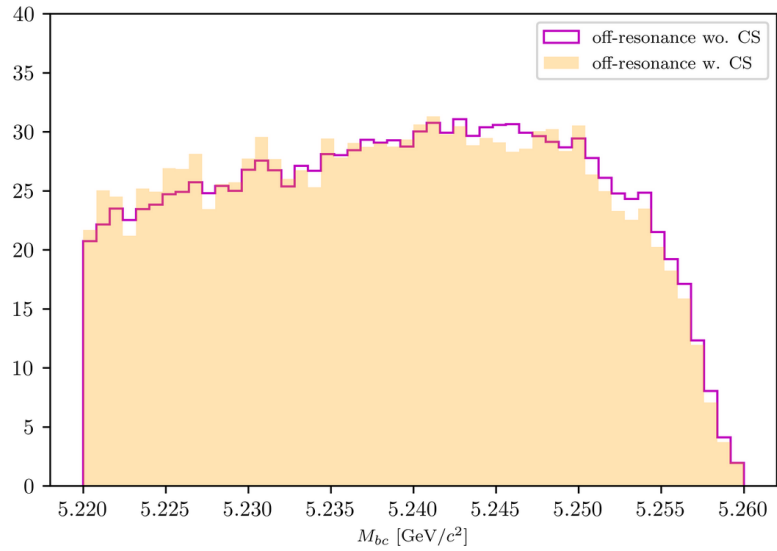
Figure (27) On the left:  $M_{bc}$  distributions of the MC off-resonance sample without continuum suppression and the MC continuum sample with applied continuum suppression. On the right:  $M_{bc}$  distributions of the corrected scaled MC off-resonance and on-resonance MC continuum.

246 The procedure adopted to obtain the PDF describing the continuum background  $M_{bc}$   
247 distribution is the following:

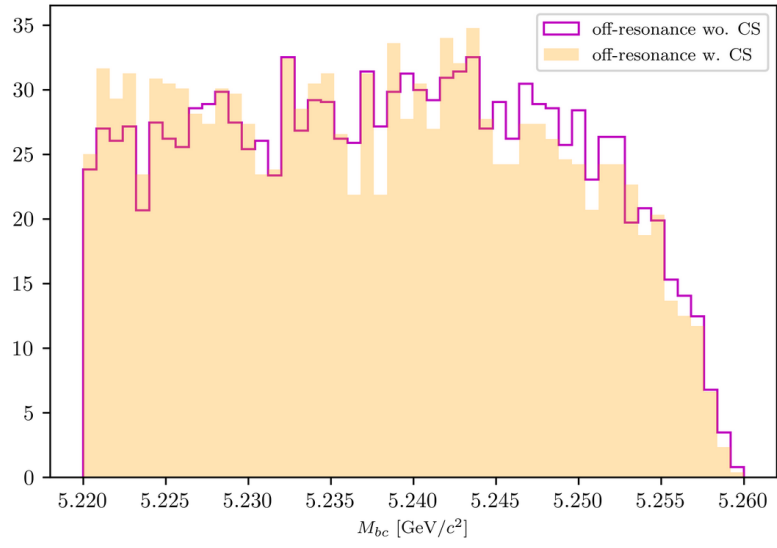
- 248
- 5 streams of off-resonance MC were scaled according to Eq. (6) without continuum  
249 suppression being applied and compared to the distribution of 5 streams of on-  
250 resonance continuum
  - From a ratio plot, like the one in Fig. 27a, the bin-correction is obtained to correct  
251 the off-resonance data in the scaling procedure. To obtain the shape that can describe  
252 the continuum background  $M_{bc}$  distribution on data the continuum suppression is not  
253 applied on the off-resonance continuum sample, in order to acquire more statistics.  
254

255 This procedure is first tested on an independent MC sample (see Fig. 27b ) to check the  
256 result on simulated data before applying it on data.

257 The validity of the method relies on the fact that on-/off-resonance continuum events are  
258 well modeled in MC and that the shape of the  $M_{bc}$  distribution doesn't change significantly  
259 when removing the continuum suppression cut both on MC and data (as one can see  
260 from Figures 28a - 28b). Additionally, the continuum suppression cut efficiency should  
261 be the same in data and MC in order to have the correct scaling on data with the above  
262 mentioned method. Fig. 29 shows the distribution of the *foxWolframR2* variable in  
263 off-resonance MC and data. The slight shift visible in data can cause a different impact on  
264 data in terms of rejected continuum background when applying the *foxWolframR2* < 0.3  
265 cut. It is found to reject about 60% of the continuum background in data, whereas it



(a)



(b)

Figure (28) Above:  $M_{bc}$  distributions of the MC off-resonance sample (5 streams) with and without continuum suppression. Below:  $M_{bc}$  distributions on data with and without continuum suppression.

rejects 55% of the continuum background in MC ( 56% in on-resonance MC). Therefore in data one can expect about 2.25% less continuum background events. This discrepancy is not statistical significant (the statistical uncertainty for the continuum background events is of the level of  $\sim 1\%$ ), a simple correction to the number of events can be applied on data and its possible systematics can be then taken into account.

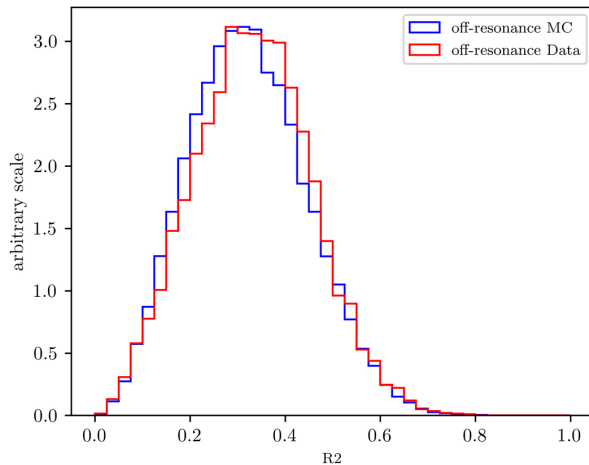


Figure (29) Distributions of variable  $foxWolframR2$  in off-resonance MC and data.

<sup>271</sup> The obtained distribution can be then fitted (see Fig. 30), i.e. with a Novosibirsk function.  
<sup>272</sup> This is the procedure which can be then applied on the off-resonance data to obtain the  $M_{bc}$  shape describing the continuum background in data.

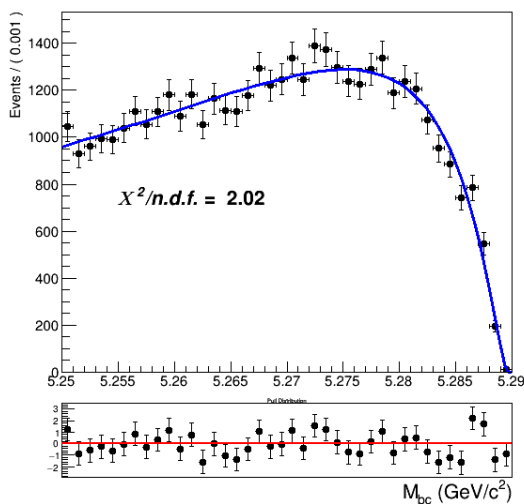


Figure (30) Fit of the  $M_{bc}$  distribution MC (scaled) off-resonance continuum (one stream).

<sup>273</sup>

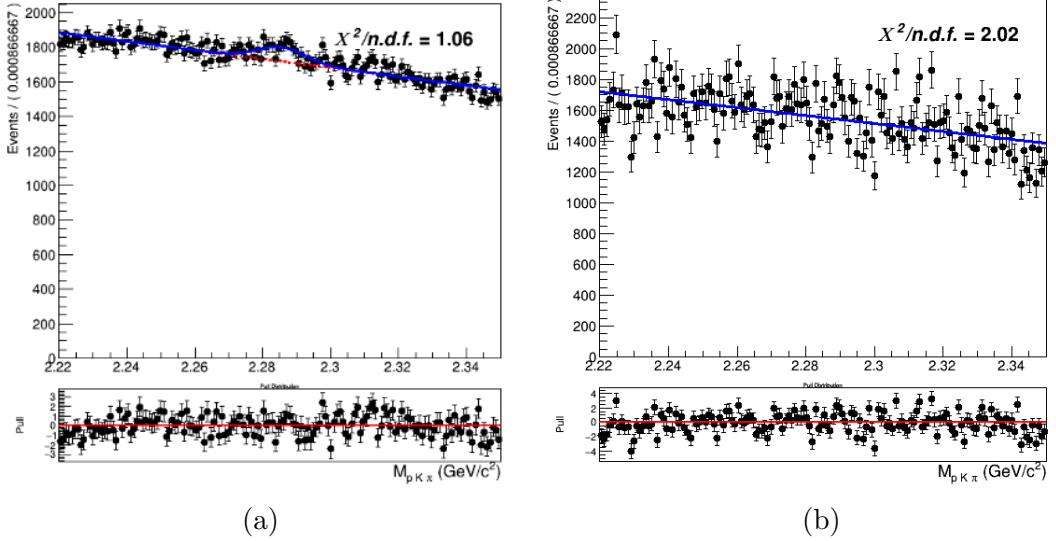


Figure (31) Comparison between 5 streams of MC on-resonance continuum 31a) and off-resonance (scaled) continuum in  $M(pK\pi)$  (31b).

274     The shape describing the  $\Lambda_c$  invariant mass is obtained from the simulated on-resonance  
 275     continuum, again using 5 streams statistics (see Fig. ?? ).

276     Finally, it is possible to examine the validity of the whole procedure on the independent  
 277     stream. Fig. 33 shows the  $M_{bc}$ ,  $M(pK\pi)$  projections of the two dimensional fit with the  
 278     one-dimesional PDFs obtained with the above described procedure. The 2D PDF used  
 279     can be written as:

280

$$281 \quad P_{B,\Lambda_c}^{Continuum}(M_{bc}, M(pK\pi)) = \Gamma_{Nov}(M_{bc}) \times [\rho_{Cheb1}(M(pK\pi)) + \rho_{G1}(M(pK\pi))]$$

282

283     where, as already anticipated, the invariant mass is described by a sum of a first order  
 284     Chebychev polynomial and the peak by a single Gaussian function.

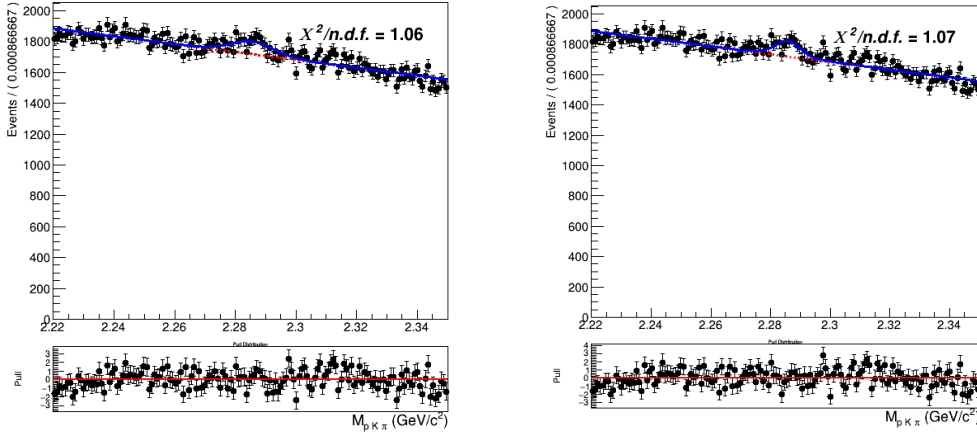


Figure (32)  $\Lambda_c$  invariant mass fits using five streams. On the left: fit of the  $\Lambda_c$  invariant mass of on-resonance continuum using the one Gaussian description (all nominal cuts applied). On the right: fit of the  $\Lambda_c$  invariant mass of on-resonance continuum using the same three gaussian PDF to describe the peak in the signal invariant mass (all nominal cuts applied).

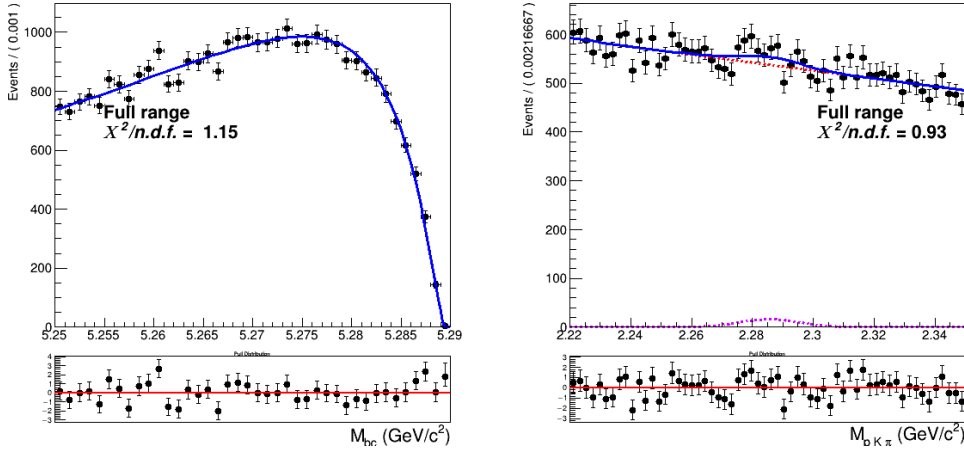


Figure (33) Two dimensional fit of continuum events (one stream).

285 It was then also investigated to alternatively use the same triple Gaussian PDF (used  
 286 in Eq. 2 for the signal peak) to describe the peak, as it is shown in Fig. 32 . The two  
 287 descriptions seem to be equivalent. The final fits described in Sec. 4.2 were performed  
 288 with the one Gaussian description (keeping all parameters fixed), but it was also tried  
 289 with the alternative three Gaussian description (with main Gaussian having the width as  
 290 free parameter): no significant difference was noticed and the signal yields differ by only  
 291 about 10% of the statistical uncertainties. Though, for consistency reasons, on data the  
 292 second description will be applied.

## 293 4.2 Two dimensional fit

294 All the already discussed PDFs describing the various categories of events were constructed  
 295 using five streams. Then an independent stream is used to test if the total PDF enables  
 296 to extract the signal yield in an unbiased way. In order to test this a total of six fits are  
 297 performed on six different streams of generic MC. Exemplary, the distributions of stream  
 298 0 overlaid by the fitted PDF are depicted in Fig. 34 (see Appendix .1 for the projections  
 299 in signal and sideband regions). In all six fits all the shaping parameters are kept fixed,  
 300 except:

- 301 •  $\sigma_{G1}$ : the width of the wider of the three Gaussian functions in  $\rho_G(M(pK\pi))$
- 302 •  $\sigma_{CB}$  parameter for the Crystal Ball describing the signal peak in  $M_{bc}$

303 In the  $M_{bc}$  distribution the  $\sigma_{CB}$  parameter for the Crystal Ball describing the generic  
 304 background is expressed as function of the signal  $\sigma_{CB}$  with a ratio fixed from the MC. For  
 305 the crossfeed background the ratio between its contribution and misreconstructed signal is  
 306 fixed from the MC.

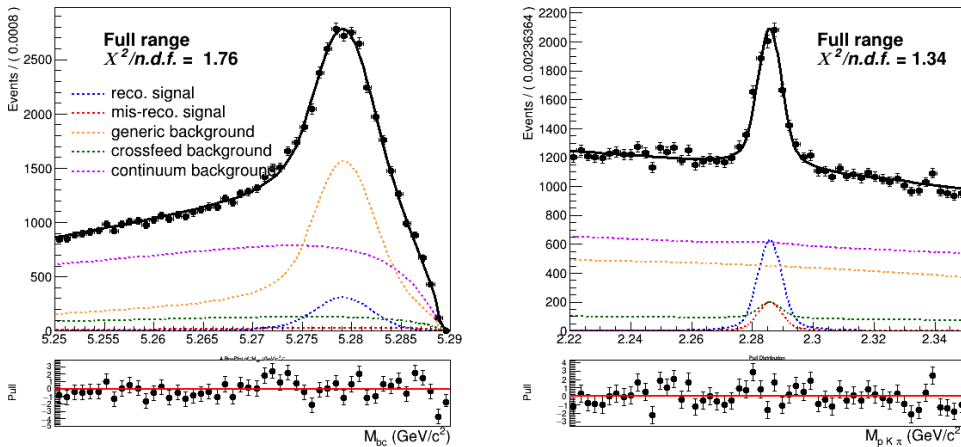


Figure (34) Two dimensional fit on stream 0 Monte Carlo simulated data.

307 The normalizations of mis-/reconstructed signal events and generic background events are  
 308 floated in the two dimensional unbinned maximum likelihood fits.

309 In Table 1 the signal yields of the fits (**Reconstructed Signal**) to the two dimensional  
 310 distributions for the six streams of  $B^- \rightarrow \Lambda_c^+$  flavor-correlated decays are listed and  
 311 compared to the yields obtained from fits of signal distributions of each individual stream.  
 312 The latter are the "expected" yields of reconstructed signal from a fit to the total signal  
 313 events in the individual stream as the one plotted on Fig. 35 where all the parameters of  
 314 the PDFs described in Eq. (2) are kept fixed and the corresponding yields are extracted  
 315 from the fit.

316 Except for stream 3, the fits present slightly higher values of reconstructed signal than  
 317 expected ones, although always within the  $1\sigma$  uncertainties (as shown in Fig. 36). The

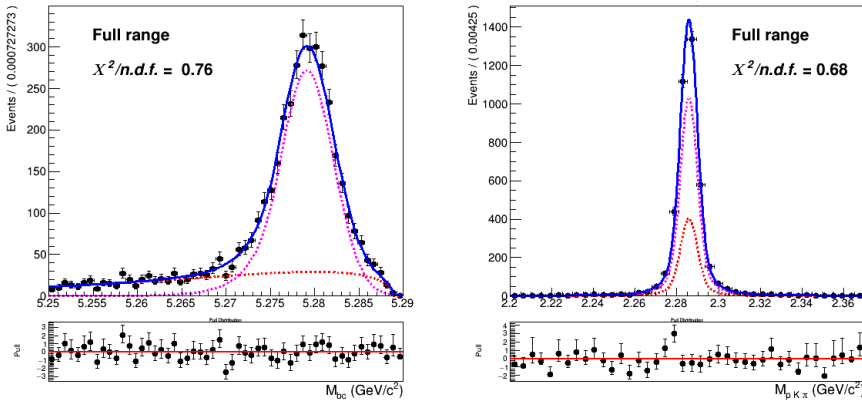


Figure (35) Two dimensional fit of Total Signal of stream 0 used to extract the expected reconstructed (corresponding to the PDF colored in magenta) and expected misreconstructed yields (corresponding to the PDF colored in red).

	Reconstructed Signal		Total Signal			
	fit	expected	fit	MC truth	fit - MC truth	
stream 0	$3058 \pm 123$	$2928 \pm 66$	$4037 \pm 121$	4061	-24	-0.6%
stream 1	$3047 \pm 127$	$2956 \pm 66$	$4098 \pm 126$	4084	14	0.3%
stream 2	$3100 \pm 126$	$3038 \pm 68$	$4189 \pm 125$	4267	-78	-1.8%
stream 3	$3124 \pm 126$	$3156 \pm 68$	$4377 \pm 125$	4337	40	0.9%
stream 4	$3125 \pm 128$	$3048 \pm 67$	$4054 \pm 125$	4169	-115	-2.8%
stream 5	$2909 \pm 127$	$2816 \pm 65$	$4080 \pm 129$	4001	79	2.0%
sum	18363	17942	24844	24919	-75	-0.3%

Table (1) Comparison of fitted and expected signal yields, fitted and truth-matched total signal for six streams of Belle generic MC when fitting the two dimensional distributions of  $M_{bc}$  and  $M(pK\pi)$ .

318 table also reports the fitted and truth-matched number of total signal (sum of reconstructed  
 319 and misreconstructed signal) events. The values show that deviations are within statistical  
 320 expectations, which indicates that this sum doesn't present biases. Nevertheless the fact  
 321 that the reconstructed signal is not fluctuating around zero can be seen as an evidence  
 322 of a small bias. Fig. 37 shows the differences between fitted and expected values of  
 323 reconstructed signal with associated uncertainties (calculated as sum of quadrature of both  
 324 uncertainties on the results from the fits and the expected values). The performed linear  
 325 fit shows that, taken together, the six fits present an overall, small but not negligible, bias,  
 326 which has to be taken into account while fitting the data.

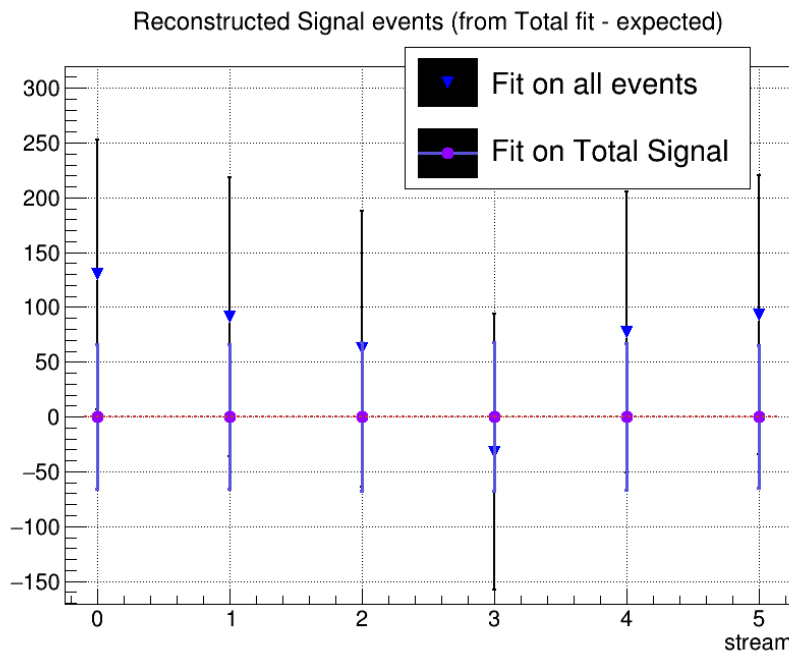


Figure (36) Differences between results from the fits and "expected" values for signal yields as reported in the first columns on Table1 .

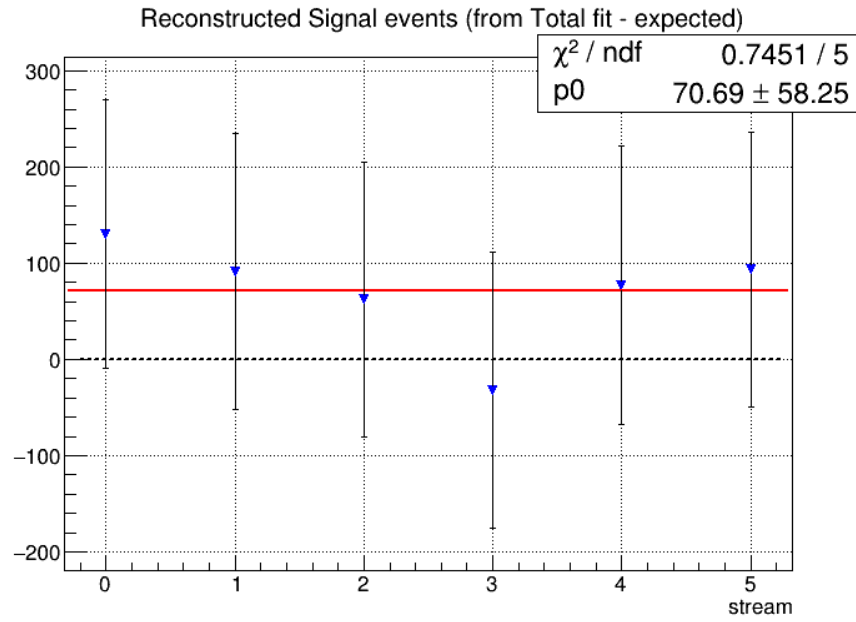


Figure (37) Fitted-expectation subtracted values for reconstructed signal yields with associated uncertainties summed in quadrature.

<sup>327</sup> Additionally, one can investigate the behaviour for different signal-to-background ratio.

328 Thus, a second test of the fit model is performed. Using four independent streams the  
 329 amount of total signal is varied between 25% and 100% of the nominal values. The  
 330 amount of background varies according to poissonian fluctuations, as it is taken from  
 331 four independent streams. The plot in Fig. 38 shows the values of reconstructed signal  
 332 obtained in the total fits versus those expected by the fits on total signal events. One can  
 333 see that the values distribute according to a linear dependence. The linear fit suggests  
 334 a compatibility with a 1:1 relation: the red and the blue dotted lines don't overlap, but  
 335 the values of the fitted line are compatible within the uncertainties with the identity line.  
 336 Though also in this second test we see a slight tendency of overshooting the expected  
 337 values.

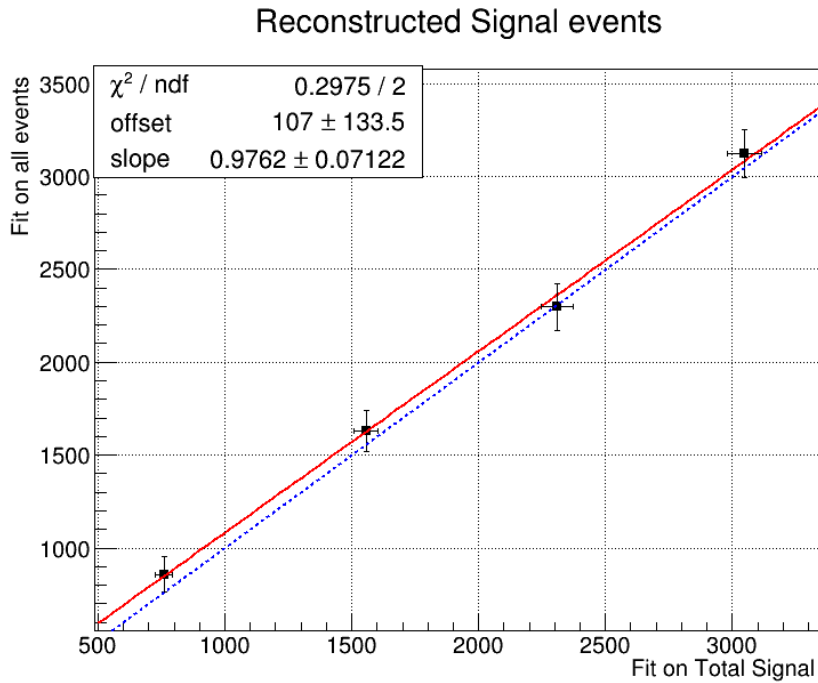


Figure (38) Linearity test: on the x-axis the obtained reconstructed signal yields from fits on different amounts of total signal; on y-axis the yields of reconstructed signal obtained fitting all events (as in Fig. 34). The values are fitted with a red continuous line, whereas the blue dotted line corresponds to a 1:1 linear dependence.

338 For the fit model also toy MC pseudo-experiments were performed in order to confirm the  
 339 behavior of the fit setup. With toy MC experiments the yields, errors and the pulls of the  
 340 fit are studied by generating our own pseudo-datasets, according to the MC (see plots in  
 341 the next page).  $3 \times 10^3$  pseudo-datasets are constructed, where each dataset was generated  
 342 with the expected amount of events, distributed according to the Poisson distribution.  
 343 Then the composition of each toy pseudo-experiment is fitted as if they were data, and  
 344 the pull-value distributions of the fit results are calculated. The pulls distributions are  
 345 centered at zero, indicating there's no significant bias in the fitted yields/parameters.

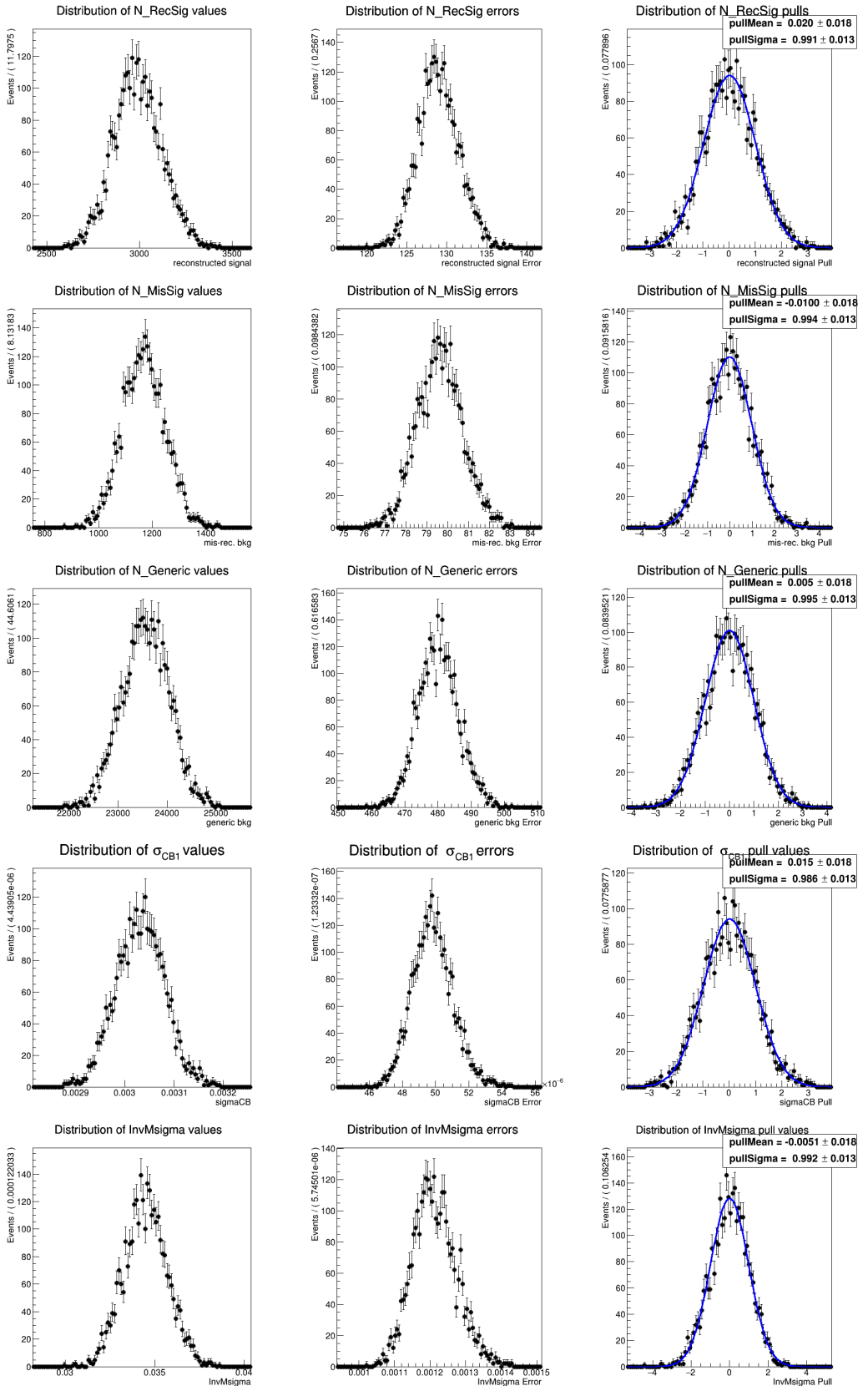


Figure (39) Toy MC study plots for the two dimensional fit model

### 346 4.3 Probability Density Functions (PDFs) for the $B_{tag}$

347 The  $M_{bc}$  distribution of the tagged  $B$  mesons is fitted with a Crystal Ball as for the  
 348 "peaking" component and the "flat" component is fitted with a Novosibirsk function (Fig.  
 349 40). The crossfeed background, consisting of neutral  $B$  mesons tagged as charged  $B$ , is  
 350 fitted instead with a sum of a Novosibirsk and an asymmetric Gaussian PDF (Fig. 41).  
 351 Both fits shows a  $\chi^2/n.d.f.$  considerably higher than one and pulls exceeding  $3\sigma$  deviation  
 352 in some regions, but the systematics represented by this is negligible compared to other  
 353 sources of systematic uncertainties and statistical uncertainties in the two dimensional fit.

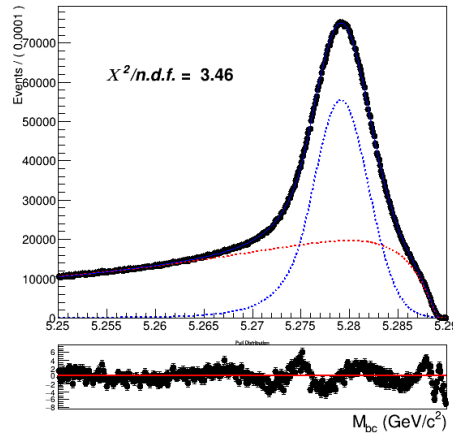


Figure (40) Fitted distribution of tagged charged  $B$  mesons: reconstructed signal events are described by the blue dotted PDF, the misreconstructed with a Novosibirsk function (red dotted).

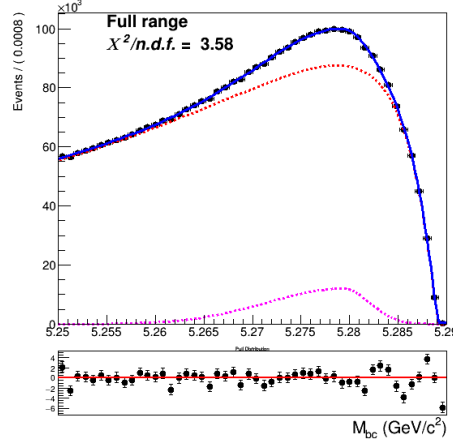


Figure (41) Crossfeed distribution fitted with a sum of Novosibirsk (red) and asymmetric Gaussian PDF (magenta)

354 As for the continuum background, a similar procedure as the one described already for the  
 355 two dimensional fit was adopted:

- 356 • first the off-resonance sample is scaled accordingly  
 357 • the ratio between the scaled off-resonance and the on-resonance in MC is calculated  
 358 in each bin (see Fig.42a)  
 359 • the bin-correction is applied on an independent stream and the scaled and bin-  
 360 corrected  $M_{bc}$  distribution is compared with the on-resonance distribution as shown  
 361 in Fig.42b

362 As for the  $B_{tag}$  continuum background the statistics is much larger than in the 2D sample,  
 363 there's no need to remove the continuum suppression cut on the off-resonance sample.

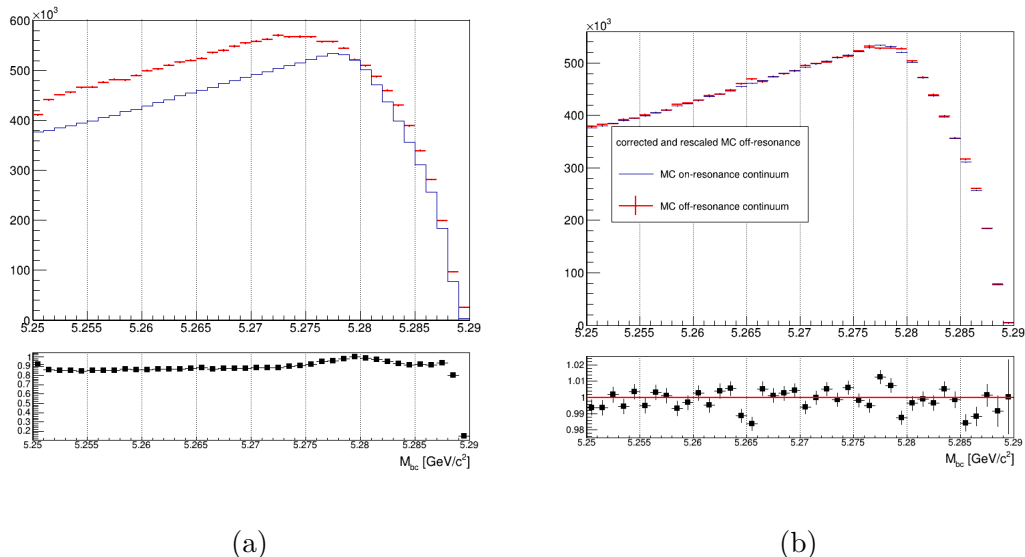


Figure (42) On the left:  $M_{bc}$  distributions of the MC off-resonance sample and the MC continuum sample with applied continuum suppression. On the right:  $M_{bc}$  distributions of the corrected scaled MC off-resonance and on-resonance MC continuum.

364    **4.4  $B_{tag}$  fit**

365    An independent Monte Carlo stream was used to test the total fit model on tagged  $B$  meson  
 366    candidates. As in the 2D fit, the parameter for the width,  $\sigma_{CB}$ , of the Crystal Ball is floated  
 367    and the ratio between expected crossfeed background events and misreconstructed signal  
 368    events is fixed from the MC. The Novosibirsk function describing the misreconstructed  
 369    signal is also not fully constrained: the parameter describing the tail is free. To avoid  
 370    introducing significant systematic uncertainties in the fit deriving from the  $M_{bc}$  endpoint  
 371    region, where one has a smearing effect due to variations of the beam energy at the MeV  
 372    level, the range for the fit is restricted to values between 5.250 and 5.287 GeV/c<sup>2</sup>. Yields  
 373    for the reconstructed and misreconstructed signal are obtained from the fit:

374

375

NrecSig	$4.2681 \cdot 10^6 \pm 5871$
NmisSig	$5.8787 \cdot 10^6 \pm 5128$

376    The Total Signal (the sum NrecSig+NmisSig) is  $10146748 \pm 4380$  (to be compared with  
 377    10158571 from the Monte Carlo). This reflects a  $\sim 2.5\sigma$  discrepancy between the true MC  
 378    value and the result from the fit. This can produce some systematic effect, but the relative  
 379    error is at the  $\sim \%$  level. This is still negligible compared to the systematic uncertainty  
 380    corresponding to the the  $N_{tag}$  determination, and furthermore in the branching fraction  
 381    calculation it is also negligible compared to the statistical uncertainty on the extracted  
 382    yields from the two dimensional fit.

383    To check the stability of the fit model a toy MC study was performed with  $3 \times 10^3$   
 384    pseudo-datasets (as it was done for the two-dimensional fit model). No evidence for  
 385    possible biases in the reconstructed signal yields was found (see Fig. 44).

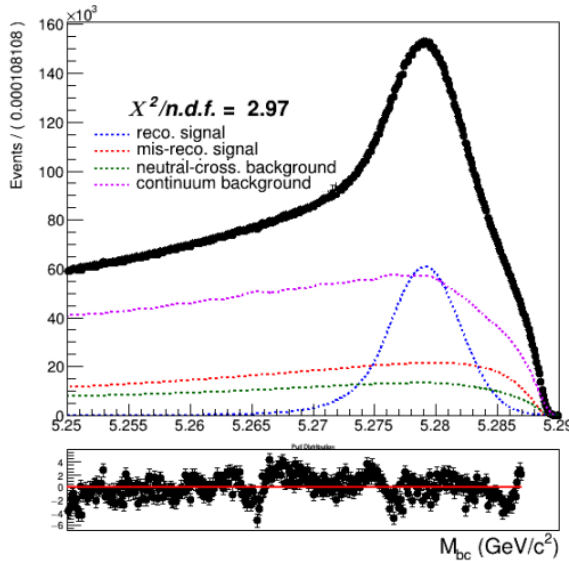


Figure (43)    Total fit of tagged  $B$  mesons on Monte Carlo simulated data.

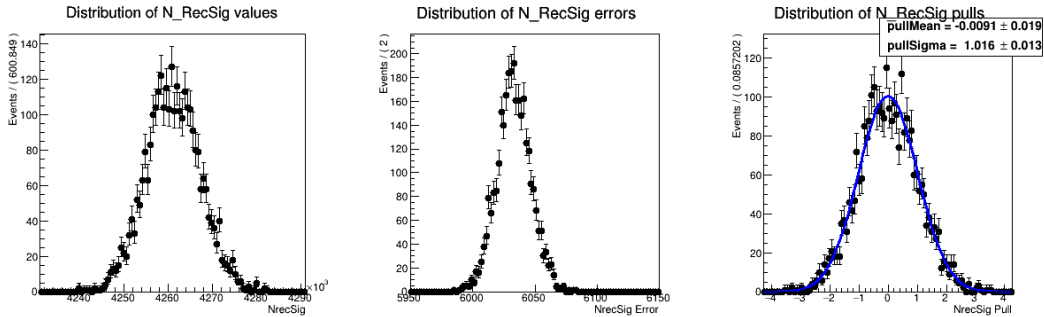


Figure (44) Plots showing distributions of the fitted signal yields, errors and the pull distribution of all pseudo-fits. (see Appendix .1 for the other free parameters' results)

#### 386 4.5 $\Lambda_c$ and FEI efficiency

387 The efficiency in reconstructing the  $\Lambda_c$  baryon after correctly tagging the charged  $B$   
 388 meson, can be estimated from Monte Carlo simulated data as the fraction of correctly  
 389 reconstructed signal events that have a correctly reconstructed  $B_{tag}$  companion, i.e.:

$$\frac{N_{recSig}(B_{tag}, \Lambda_c)}{N_{recSig}(B_{tag}^{sig})} \quad (7)$$

390 where  $N_{recSig}(B_{tag}, \Lambda_c)$  are the yields of reconstructed signal from the two dimensional  
 391 fits (reported in Table 1 ) and  $N_{recSig}(B_{tag}^{sig})$  are the yields of correctly reconstructed signal  
 392 in a fit of  $B$  mesons tagged in events where one of the two mesons decayed hadronically  
 393 and inclusively into a  $\Lambda_c$  baryon (see Fig 45). To minimize statistical uncertainties, in  
 394 the efficiency calculation the results from all the two dimensional fits were used and six  
 395 streams of  $B_{tag}$  candidates reconstructed in signal events were used for the  $M_{bc}$  shown  
 396 below.

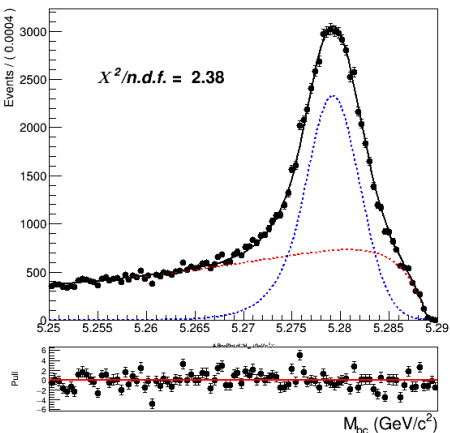


Figure (45) Fit of tagged  $B$  mesons in the "signal events" sample

397 From this and the results listed in sec. 4.2 the efficiency to reconstruct  $\Lambda_c$  is obtained :

398

$$399 \quad \epsilon_{\Lambda_c} = \frac{N_{recSig}(B_{tag}, \Lambda_c)}{N_{recSig}(B_{tag})} = 44.83 \pm 0.32\%$$

400 The yields from the fit shown in (Fig. 45) can be used also to calculate the FEI tag-side  
401 efficiency for signal events, i.e. the efficiency to tag the  $B$  meson accompanying a  $B_{sig}$   
402 decaying into a  $\Lambda_c$  on the signal side. Whereas results from the fit of charged  $B_{tag}$  shown  
403 in Fig. 40 can be used to calculate the hadronic tag-side efficiency in the generic  $B^+B^-$   
404 events case.

405 The ratio between the two efficiencies is calculated:  $\frac{\epsilon_{FEI,sig}^+}{\epsilon_{FEI}^+} = 0.908 \pm 0.017$   
406

407 **4.6 Studies of Systematic Effects**

408 In Table 2 the systematic uncertainties of the various considered sources are summarized.  
409 The full estimate of the systematic uncertainty is summed up in quadrature and applied  
410 to the result in Section 4.14 Their individual calculation is outlined in the subsequent  
411 subsections.

source	%
Continuum modeling	0.07
Crossfeed PDFs	0.02
Crossfeed fraction	0.04
$\epsilon_{FEI,sig}^+/\epsilon_{FEI}^+$	0.06
$\epsilon_{\Lambda_c}$	0.02
Fit bias	0.06
PID	0.05
Total	0.13

Table (2) Systematic uncertainties in the determination of the  $B^+ \rightarrow \bar{\Lambda}_c^- X$  branching fraction in %.

412 **4.7 Continuum background modeling**

413 Regarding this source of systematics, one has to take into account two different types.  
414 First of all the statistical uncertainties, which are reflected in the uncertainties on the  
415 PDF parameters. To estimate this type of uncertainty two-dimensional fits with varied  
416 parameters' values by their uncertainties (a fit with +err and -err) were performed.  
417 Whereas, the estimation of statistical uncertainty in the case of the  $B_{tag}$  should be  
418 estimated in principle varying each bin content of its error. On first approximation this is  
419 equivalent to vary the nominal number of events described with the histogram PDF by  
420 Poissonian variation. Exemplary, fits used to estimate the impact of these uncertainties  
421 are shown here in Figures 46 - 47. The yields obtained from those fits for benchmark  
422 stream5 results are then compared with the ones already reported previously and a mean  
423 deviation value is obtained for both the two-dimensional fit and the  $B_{tag}$  fit.

Fit	$-\sigma$	$+\sigma$	$\pm\bar{\sigma}$
2D	87	53	70
$B_{tag}$	10218	10620	10419

Table (3) Offsets on the signal yields obtained in the two dimensional and  $B_{tag}$  fit and mean deviations reported in the last column.

424 The estimated systematic uncertainty on Br value from this source is 0.07%.

425 The other type of systematic uncertainty in modeling the continuum is originated by the  
426 continuum suppression cut having a slightly different efficiency on data (as a consequence  
427 of the shift in off-resonance MC and data visible in the the *foxWolframR2* distribution

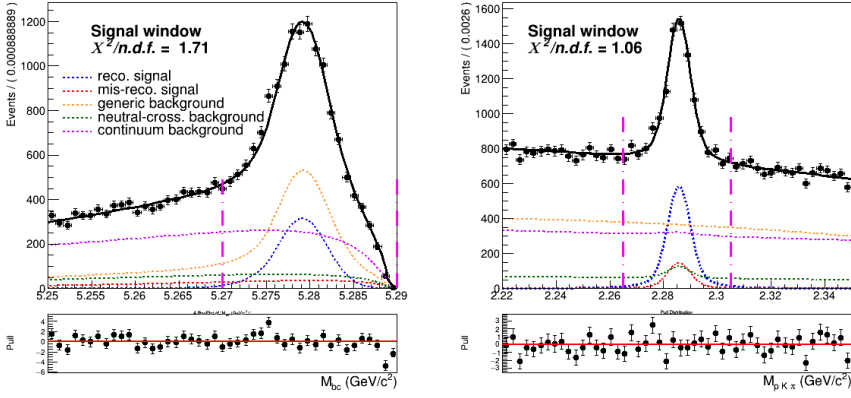


Figure (46) Signal window projections of a two dimensional fit on Monte Carlo simulated data where the shaping parameters were varied of their uncertainties.

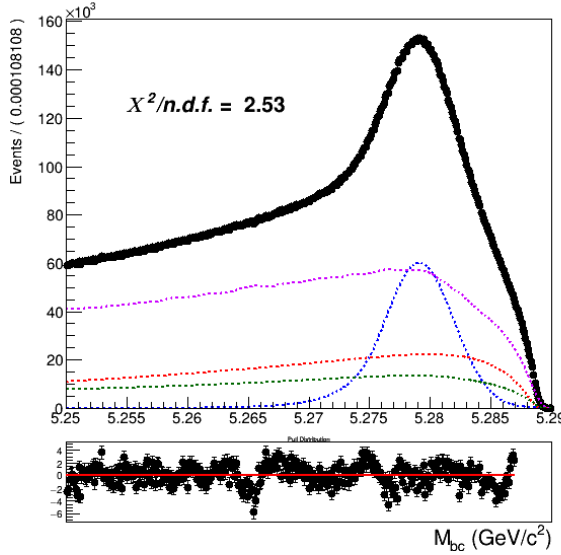


Figure (47) Fit of tagged  $B$  meson candidates on Monte Carlo simulated data where the amount of continuum was varied according to poissonian fluctuations.

in Fig. 29). As already discussed, it originates a possible discrepancy of about 2.25% in continuum background events in the two dimensional fit (and only 1.25% in the  $B_{tag}$  fit). The statistical uncertainty on this fraction of events can also be taken into account as systematics. Being the number of events in the off-resonance data sample without the continuum suppression applied is very small (less than  $10^4$  in the two dimensional fit and about 18500 in the  $B_{tag}$  fit), the uncertainty in the mentioned fraction of events is negligible compared to the statistical uncertainty on the on-resonance continuum background events in MC: it would account for 0.002% on the BR value. Therefore, this second source of uncertainty is not taken into account. There would be also a third of systematic uncertainty

437 given by potential difference in the on-/off-resonance correction between data and MC,  
438 but there's no way one can estimate it properly.

## 439 4.8 Crossfeed background modeling

440 Since also the shapes of the PDFs describing the crossfeed background are fully fixed to the  
441 ones determined with the limited Monte Carlo statistics, also their statistical uncertainties  
442 need to be taken into account as possible source of systematics. The procedure to estimate  
443 this source of systematic uncertainty is the same described in the previous section regarding  
444 the continuum background. In the table below the signal yields' offsets are listed changing  
445 the parameters within their uncertainties, and the mean offsets value used to calculate the  
446 expected uncertainty on the BR value. The resulting absolute systematic uncertainty is  
447 about 0.02% on the BR value.

Fit	$-\sigma$	$+\sigma$	$\pm\bar{\sigma}$
2D	27	8	18
$B_{tag}$	5400	5700	5550

Table (4) Offsets on the signal yields obtained varying the parameters of crossfeed background PDFs within their uncertainties in the two dimensional and  $B_{tag}$  fit and mean deviations reported in the last column.

## 448 4.9 Crossfeed ratio

449 The crossfeed/misreconstructed events' ratio is kept fixed both in the two-dimensional fit  
450 and the  $B_{tag}$  fit to the values found in MC. This choice was made according to the fact  
451 that the two categories of events are similar: in both cases the  $B$  mesons were not correctly  
452 reconstructed, either because of missing or wrongly added partilces (misreconstructed  
453 signal events) or, in the case of crossfeed events because the tagged  $B$  meson was not the  
454 required one ( $B^0$  meson instead of a  $B^{+/-}$  meson). The ratio between these two categories  
455 of events is therefore expected to be very similar in MC and data, though there's no  
456 guarantee that it is the same value in data. Unfortunately there's no direct way to have  
457 an estimate of the possible discrepancy of this value.

458 In [3] (and previously in [4]) it was found that there's a substantial difference in terms of  
459 tagging efficiency for FEI applied on Monte Carlo and on Belle data, being the discrepancy  
460 around  $\sim 20\%$ . We can assume that the efficiency for the two categories of events on data  
461 will both differ of that value and the ratio of the events being the same MC value, but in  
462 absence of any other method to estimate the uncertainty on it one can consider a maximal  
463 discrepancy of to 20% between Monte Carlo and data to study the impact on the yields<sup>2</sup>.

---

<sup>2</sup>This method was also validated with the control decay sample and the originated uncertainty is well within the PDG reported ones.

464 For the two-dimensional fit the ratio was artificially set to consider scenarios of  $\pm 20\%$   
 465 difference in the ratio, whereas in the case of the  $B_{tag}$  fit the number of crossfeed events  
 466 were varied artificially in order to have  $\pm 20\%$  different ratio, keeping the previously  
 467 determined Monte Carlo ratio fixed.

Fit	$-\sigma$	$+\sigma$	$\pm\bar{\sigma}$
2D	24	48	36
$B_{tag}$	2807	3940	3374

Table (5) Offsets on the signal yields obtained varying of  $\pm 20\%$  the cross-feed/misreconstructed in the two dimensional and  $B_{tag}$  fit and mean deviations reported in the last column.

468 The estimated systematic uncertainty on Br value from this source is 0.04%.

## 469 4.10 Efficiencies

470 The ratio between the two FEI efficiencies is:  $\frac{\epsilon_{FEI,sig}^+}{\epsilon_{FEI}^+} = 0.908 \pm 0.017$

471 The uncertainty on this value originates a systematic uncertainty of 0.06% on the Br  
 472 value. The  $\Lambda_c$  reconstruction efficiency is determined to be  $\epsilon_{\Lambda_c} = 44.83 \pm 0.32\%$ . The  
 473 systematic uncertainty originated by its uncertainty is 0.02% on the Br value.

## 474 4.11 Fit biases

475 The small bias on the reconstructed signal seen in the two-dimensional fit model (see Fig.  
 476 37) has to be corrected when fitting data, but the uncertainty on it has to be taken into  
 477 account in the systematics. Also the discrepancy in the total signal fit result observed in  
 478 the  $B_{tag}$  (Sec. 4.4) needs to be included in the systematic effects. Propagating the two  
 479 sources of systematics in the branching fraction calculation results in an additional 0.06%  
 480 uncertainty on the branching fraction value.

## 481 4.12 PID efficiency correction

482 The PID selection efficiency for the three charged particles in the signal decay needs to  
 483 be corrected on MC due to various differences, when comparing to data. The Belle PID  
 484 group has prepared a set of correction factors and tables of systematic uncertainties for  
 485 PID efficiencies for all charged particles. The proton identification efficiency was studied  
 486 in [5]. The inclusive  $\Lambda^0$  decay  $\Lambda^0 \rightarrow p\pi^-$  was used to examine the proton identification  
 487 efficiency difference between data and MC in *Belle*. The datasets for the SVD1 and SVD2  
 488 periods are treated separately, and the efficiency ratio dependence on proton charge,

489 momentum and polar angle is considered. The study is done for the proton ID cut values  
 490 0.6, 0.7, 0.8 and 0.9<sup>3</sup>. The binning on the momentum starts at 0.2 GeV. The proton ID  
 491 efficiency is defined as

492

493  $\epsilon_{PID} = \frac{\text{number of } p\text{ tracks identified as } p}{\text{number of } p\text{ tracks}}$

494

495 and the comparison between MC efficiency and data efficiency by a double ratio  
 496 defined as

497

498  $R_p = \epsilon^{data}/\epsilon^{MC}$

499

500 The average proton ID correction is estimated to be:  $R_p = 0.969 \pm 0.003$ .

501 The kaon identification efficiency was studied in detail in Belle Note 779 [6] ([http://belle.kek.jp/secured/belle\\_note/gn779/bn779.ps.gz](http://belle.kek.jp/secured/belle_note/gn779/bn779.ps.gz)). The decay  $D^{*+} \rightarrow D^0\pi^+$   
 502 followed by  $D^0 \rightarrow K^-\pi^+$ , was used to examine it. As for the proton identification efficiency  
 503 it considers the dependence on Kaon charge, momentum and polar angle and same ID cut  
 504 values<sup>4</sup>.

505 For Kaons and Pions the average ID correction is estimated to be  $R_K = 0.853 \pm 0.010$   
 506 and  $R_\pi = 0.983 \pm 0.008$  respectivley.

507 The final PID efficiency systematic error is determined to be 0.01% on the branching  
 508 fraction value.

### 510 4.13 Sideband fit on data

511 As a preliminary check of the quality of the shapes modeling, a fit of the sideband  
 512 region  $2.225 < M(pK\pi) < 2.245$  GeV/c<sup>2</sup> projection in  $M_{bc}$  was performed. The only  
 513 events present in this sideband region are: the generic, the crossfeed and the continuum  
 514 backgrounds. Therefore the only free parameters in the fit are:

- 515 • the width of the generic background Crystal Ball  $\sigma_{CB2}$   
 516 • the normalization of the generic background  
 517 • the normalization of the crossfeed background

---

<sup>3</sup>Here, proton ID cut value  $X$  means  $\mathcal{L}_{p/K} > X$  and  $\mathcal{L}_{p/\pi} > X$

<sup>4</sup>Here, Kaon ID cut value  $X$  means  $\mathcal{L}_{K/\pi} > X$ , so for values below  $X$  the tracks are identified as pions

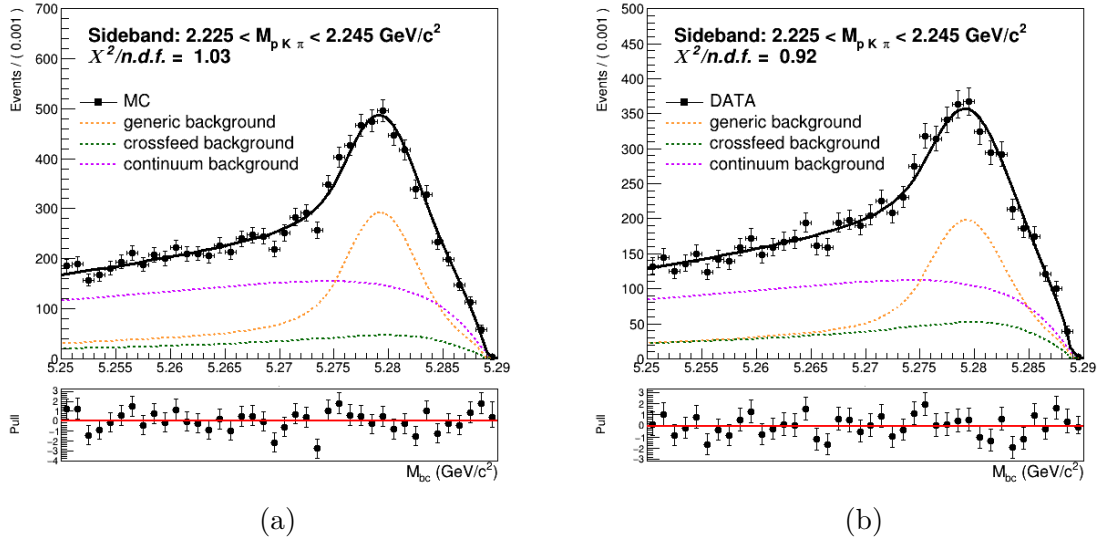


Figure (48) Fitted  $M_{bc}$  distributions corresponding to the projection in the sideband region of  $\Lambda_c$  invariant mass distribution in Monte Carlo and in data.

518 The fit shows a really good agreement with data points, from which one can assume that  
 519 the shapes of the three main background contributions are describing at a good level the  
 520 data. Moreover the fitted fractions of the background components present a quite good  
 521 MC-data agreement:

522

523

Background	MC	Data
Crossfeed	$12.22 \pm 2.69 \%$	$17.76 \pm 3.21 \%$
Generic	$37.11 \pm 2.55 \%$	$34.64 \pm 3.04 \%$

524

## 525 4.14 Measured $B^+ \rightarrow \bar{\Lambda}_c^- X$ inclusive Branching Fraction

526 Now that all ingredients are available, it's possible by mean of the formula in Eq. 4 (at  
 527 the beginning of this Chapter) , to calculate the branching ratio for the charged correlated  
 528 decays into  $\Lambda_c$  baryons.

529 As the measurement is performed considering only the  $\Lambda_c \rightarrow pK\pi$  decays, to evaluate the  
 530 inclusive  $B^+ \rightarrow \bar{\Lambda}_c^- X$  Branching Ratio on Monte Carlo simulated data one needs to take  
 531 into account the value set for that particular final state: the total  $Br(\Lambda_c^+ \rightarrow pK^-\pi^+) =$   
 532  $5.53\%$  in Belle Generic MC (including resonant decays). Using the results from the two

dimensional fits, the  $B_{tag}$  fit (with/without background included) and with all the needed factors known, one can calculate  $\mathcal{B}(B^+ \rightarrow \bar{\Lambda}_c^- X)$  on the six independent streams as displayed in Table 16. From the reported values one can notice first of all the effect of the bias encountered in Sec. 4.2, pushing the branching fraction to higher values (first column) compared to the expected ones and the branching ratio set in Belle MC. The discrepancy is of the order of  $1\sigma$  statistical uncertainty. After inspecting all the signal and sideband regions of the various background components that populate the samples (exemplary plots can be found in Appendix .1), a decision was made to add this value to the systematic uncertainties. The total systematic uncertainties would then sum up to 0.18% on the branching fraction value.

	total fit	signal fit	BELLE MC VALUE
stream 0	(3.03 $\pm$ 0.12)%	(2.96 $\pm$ 0.07)%	(2.95 $\pm$ 0.03)%
stream 1	(3.17 $\pm$ 0.13)%	(2.99 $\pm$ 0.07)%	(2.91 $\pm$ 0.03)%
stream 2	(3.23 $\pm$ 0.13)%	(3.07 $\pm$ 0.07)%	(2.98 $\pm$ 0.03)%
stream 3	(3.25 $\pm$ 0.13)%	(3.19 $\pm$ 0.07)%	(3.05 $\pm$ 0.03)%
stream 4	(3.25 $\pm$ 0.13)%	(3.08 $\pm$ 0.07)%	(2.99 $\pm$ 0.03)%
stream 5	(3.03 $\pm$ 0.13)%	(2.85 $\pm$ 0.07)%	(2.92 $\pm$ 0.03)%
average	(3.16 $\pm$ 0.05)%	(3.02 $\pm$ 0.03)%	(2.98 $\pm$ 0.01)%

Table (6) Measured branching fraction values obtained using the results listed in Table 1 for the six different streams (only statistical uncertainties are displayed) and its average.

Comparing the obtained values with the branching fraction measured by BaBar experiment (see results reported by *BaBar* [1]), the uncertainties appear substantially reduced (statistical uncertainties almost by factor four).

546    **5     $B^- \rightarrow D^0$  control decay**

547    To monitor the analysis steps, which are applied to both measured and simulated data, a  
548    control decay of the form

549

550                          
$$B^+ \rightarrow D^0 X, D^0 \rightarrow K^+ \pi^-$$

551    is used. The statistics is much more abundant for this channel.

552    **5.1    Dataset used**

553    For this analysis the amount of data and Monte Carlo simulated data used was restricted  
554    to the SVD2 period: experiments ranging from 31 to 65. This choice was made to save  
555    processing time, anyway most of the  $B\bar{B}$  meson pairs were produced in this range of  
556    experiments ( $620 \times 10^6$  out of almost  $800 \times 10^6$  ).

557    **5.2    Event selection and reconstruction**

558    The approach used for the inclusive decays reconstruction is the same as for the  $B \rightarrow \Lambda_c$   
559    analysis. The same FEI training was used, though excluding the signal decay  $D^0 \rightarrow K^+ \pi^-$   
560    from the decay chains used by the FEI to reconstruct the  $B_{tag}$ . Same preliminary selection  
561    criteria were applied to the tag-side  $B$  meson candidates as well.

562    In the *rest of event* (ROE) of the reconstructed  $B_{tag}$  meson, to select  $D^0 \rightarrow K^+ \pi^-$  signal  
563    candidates, the following event selection criteria are applied:

- 564        •  $dr < 2$  cm and  $|dz| < 4$  cm  
565        •  $\frac{\mathcal{L}_K}{\mathcal{L}_K + \mathcal{L}_\pi} > 0.6$

566    For the  $D^0$  candidates a vertex fit is performed with `TreeFitter`, requiring it to converge.  
567    If there are more than one  $D^0$  combination, then the best candidate based on the  $\chi^2$   
568    probability is chosen. The  $D^0$  signal region is defined to be  $|M_{D^0} - m_{D^0}| < 30$  MeV/ $c^2$   
569    ( $\sim 3\sigma$ ), where  $m_{D^0}$  is the nominal mass of  $D^0$ .

570

571    **5.3    Signal selection optimization**

572    Following the same procedure as for the  $B \rightarrow \Lambda_c$  analysis, the optimized selection cuts  
573    obtained for the event based ratio of the 2-nd to the 0-th order Fox-Wolfram moments,  
574    the  $B_{tag}$  signal probability and the momentum of the  $D^0$  candidates in the center of mass  
575    system are:

- 576        •  $foxWolframR2 < 0.3$   
577        •  $SignalProbability > 0.004$

- 578        •  $p_{CMS}^{D^0} > 1 \text{ GeV}/c^2$

579        Figure 49 shows the distributions of  $M_{bc}$  and invariant mass in the signal region<sup>5</sup> for the  
 580         $B^- \rightarrow D^0 X$  reconstructed events after the selection cuts were applied.

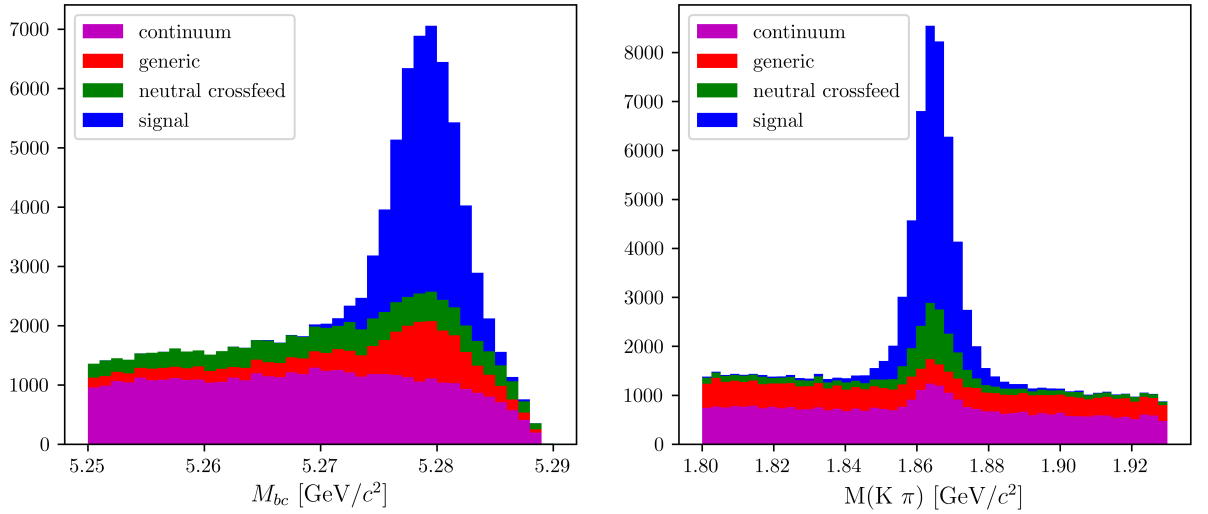


Figure (49) Distribution of  $M_{bc}$  (left) and invariant mass of charged correlated  $D^0$  candidates (right), in the signal region after the above mentioned selection cuts.

581        **5.4 Probability Density Functions (PDFs) for two dimensional  
 582        fit**

583        As already said the main goal of the control sample analysis is to ensure that the method  
 584        used to extract the signal yields discriminating the correctly reconstructed from the  
 585        misreconstructed signal events by fitting is valid. The reconstructed events in  $M_{bc}$  are  
 586        fitted with a Crystal Ball, the misreconstructed signal with a Novosibirsk function. As in  
 587        the  $B \rightarrow \Lambda_c$  analysis both components have a correspondent peak in the  $D^0$  mass which is  
 588        fitted with a sum of three gaussians with a common mean. The fitted distribution of  $M_{bc}$   
 589        and  $M(\pi K)$  are shown in Fig. 50 with signal MC sample.

---

<sup>5</sup>signal region:  $M_{bc} > 5.27 \text{ GeV}/c^2$  and  $|M_{D^0} - m_{D^0}| < 30 \text{ MeV}/c^2$

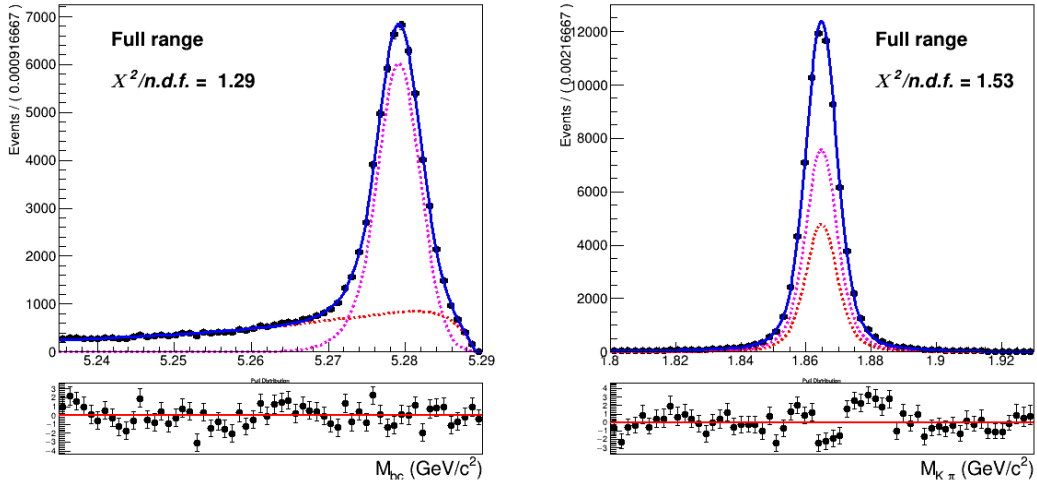


Figure (50) Two dimensional fit of total signal events in  $M_{bc}$  and  $M(pK\pi)$  (in magenta reconstructed signal PDF, misreconstructed signal PDF in red)

590 As already seen in the  $B \rightarrow \Lambda_c$  analysis besides the misreconstructed signal the other  
 591 background components are:

- 592 • **generic** (charged  $B$ ) background  
 593 • **crossfeed** (neutral  $B$ ) background  
 594 • **continuum** background

595 **Generic background**

596 The generic background deriving from other  $B^+B^-$  events presents a similar shape in  
 597  $M_{bc}$ : it is fitted again with a sum of Crystal Ball and Novosibirsk function. Instead the  
 598 distribution in the  $D^0$  mass is fitted with a sum of first order Polynomial function and a  
 599 small gaussian peak, which is due to the small amount of flavor anti-correlated  $B^+ \rightarrow D^0$   
 600 reconstructed events (see Fig. 51). The total two-dimensional PDF is a product of the  
 601 one-dimensional PDFs in  $M_{bc}$  and  $D^0$  mass:

$$P_{B,D^0}^{GenBkg}(M_{bc}, M(K\pi)) = [\Gamma_{CB}(M_{bc}) + \Gamma_{Nov}(M_{bc})] \times [\rho_{pol1}(M(K\pi)) + \rho_G(M(K\pi))] \quad (8)$$

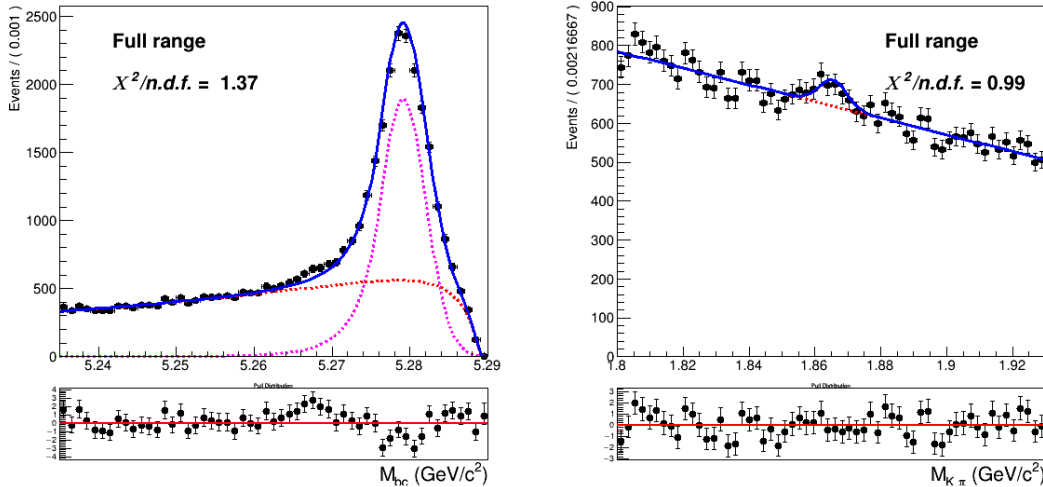


Figure (51) Two dimensional fit of generic ( $B^+ B^-$ ) background events in  $M_{bc}$  and  $M(K\pi)$ .

602 **Crossfeed background** The crossfeed background deriving from  $B^0 \bar{B}^0$  events is shown  
 603 in Fig. 52. The  $M_{bc}$  distribution is fitted with a sum of Novosibirsk and Argus functions.  
 604 The distribution in the  $D^0$  mass is fitted with a first order Chebyshev polynomial and the  
 605  $D^0$  mass peak is fitted with the same sum of three gaussians used to describe the signal  
 606 peak (same parametrization used already in  $B \rightarrow \Lambda_c$  analysis).

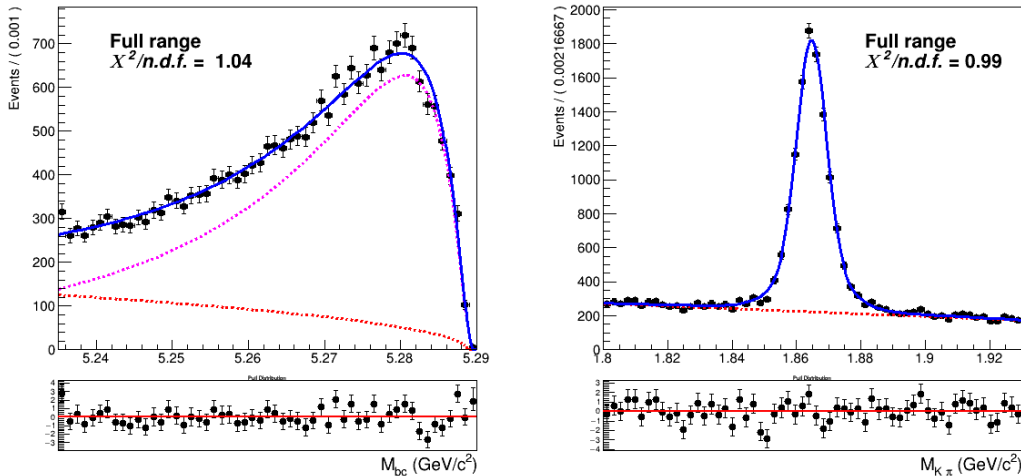


Figure (52) Two dimensional fit of crossfeed ( $B^0 \bar{B}^0$ ) events in  $M_{bc}$  and  $M(K\pi)$ .

### 607 Continuum background

608 The procedure adopted to model the continuum background is the same used for the  
 609  $B \rightarrow \Lambda_c$  decays, but in this case the available statistics is enough to perform the scaling  
 610 with all the selection cuts also in the case of the two-dimensional fit (not removing the  
 611 continuum suppression).

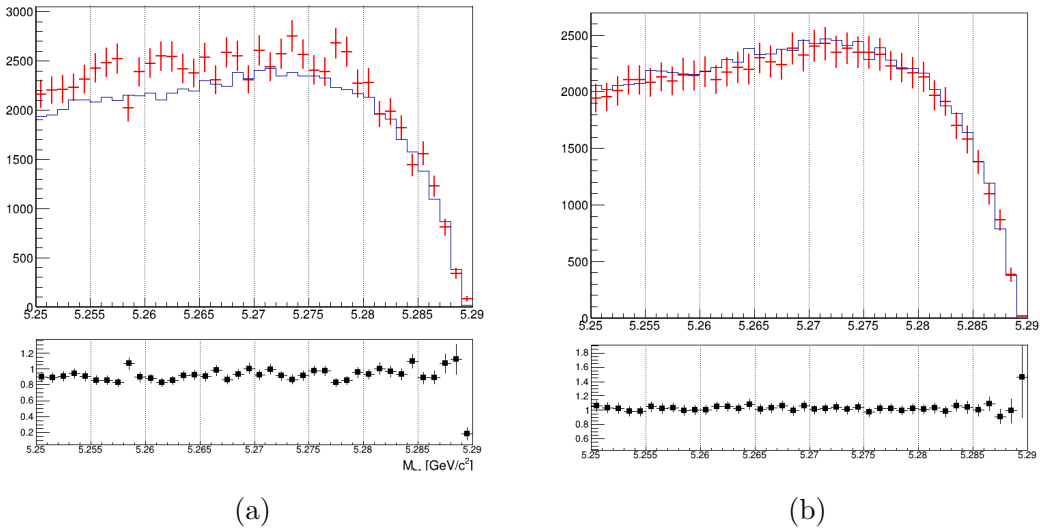


Figure (53) In Fig. 53a  $M_{bc}$  distributions of the MC (scaled) off-resonance sample (in red) and on-resonance (in blue). In Fig. 53b  $M_{bc}$  distributions of the corrected scaled off-resonance and on-resonance MC continuum.

612 For each bin a correction factor is calculated, in order to have a reasonable match with the  
 613 expected continuum background. Fig. 53b shows the applied correction on an independent  
 614 MC sample. As in the case of  $B \rightarrow \Lambda_c$  analysis, then the resulting  $M_{bc}$  distribution is  
 615 fitted with a Novosibirsk function , whereas the  $D^0$  mass distribution is fitted with a sum  
 616 of first order Chebyshev polynomial and the sum of three gaussians used to describe the  
 617 signal peak (as shown in Fig. 54). The fraction of events in the peak is the same in on-  
 618 and off-resonance MC. This method is applied also to scale the off-resonance data.

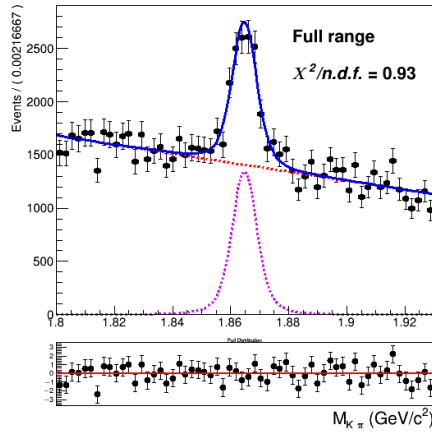


Figure (54)  $D^0$  mass fit of scaled off-resonance Monte Carlo

619 **5.5 2D Fit on Monte Carlo simulated data**

620 As in the  $B \rightarrow \Lambda_c$  study, five streams of Monte Carlo simulated data have been used to  
 621 get values for the shaping parameters for the individual components described in the  
 622 previous section and the fit model is tested on an independent stream.

623 For the six fits, the exact same conditions (floated parameters and fixed width ratios)  
 624 were applied as to the two dimensional fit in the case of the  $B \rightarrow \Lambda_c$  study. Exemplary, the  
 625 distributions of stream 0 overlaid by the fitted PDF are depicted in Fig. 55 (see Appendix  
 626 .2 for the projections of signal regions and sidebands).

627 In Table 7 the yields for reconstructed and misreconstructed signal are listed for each  
 628 stream.

629

stream	0	1	2	3	4	5
NrecSig	$56986 \pm 400$	$57766 \pm 437$	$55607 \pm 426$	$57068 \pm 372$	$58385 \pm 369$	$57501 \pm 437$
NmisSig	$31453 \pm 321$	$30513 \pm 350$	$32580 \pm 350$	$33340 \pm 399$	$29966 \pm 390$	$32012 \pm 355$

Table (7) reconstructed and misreconstructed signal yields obtained fitting 6 independent streams

630 To be sure that the PDFs enables us to extract the signal yield in an unbiased way, the  
 631 sum of reconstructed and misreconstructed signal yields, i.e. total signal, from the fits are  
 632 compared to the true values of each stream (Table 8). There are quite some differences  
 633 between the fitted signal yield and the true values in individual streams. However, all  
 634 these deviations are within statistical expectations.

635

streams	fit	MC truth	fit - MC truth	
stream 0	$88439 \pm 340$	88144	+ 295	(+0.33%)
stream 1	$88279 \pm 361$	88551	-272	(- 0.31%)
stream 2	$88187 \pm 360$	88487	-300	(- 0.34%)
stream 3	$90408 \pm 372$	90149	+ 259	(+ 0.29%)
stream 4	$88351 \pm 383$	87981	+ 370	(+ 0.42%)
stream 5	$89513 \pm 366$	89710	-197	(- 0.22%)
sum	533177	533022	+155	(+0.03%)

Table (8) Comparison of fitted and truth-matched total signal events in each stream.

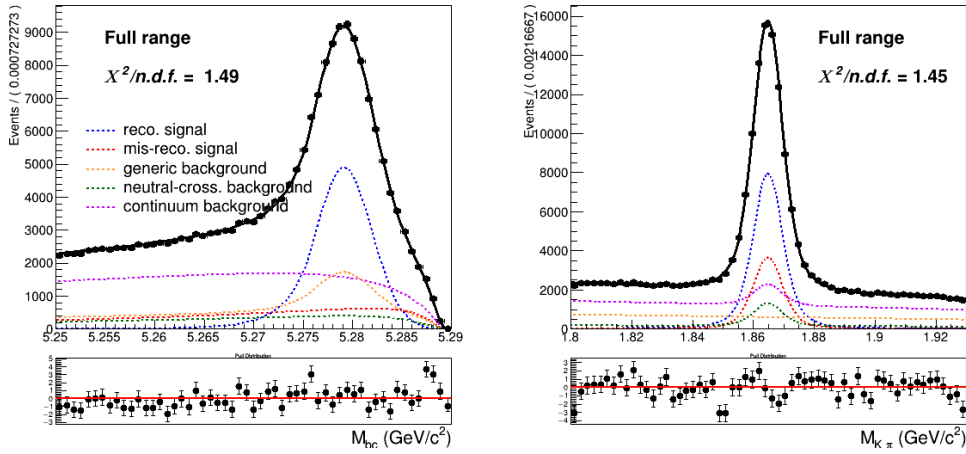


Figure (55) Two dimensional fit on stream 0 Monte Carlo simulated data.

## 636 5.6 2D Fit on data

637 After obtaining the model for the continuum background scaling and correcting the  $M_{bc}$   
 638 distribution of the off-resonance data, the model tested on Monte Carlo simulated data is  
 639 applied on data with same free parameters and yields. Fig. 56 shows the projections of the  
 two dimensional fit (see Appendix .2 for the projections of signal regions and sidebands).

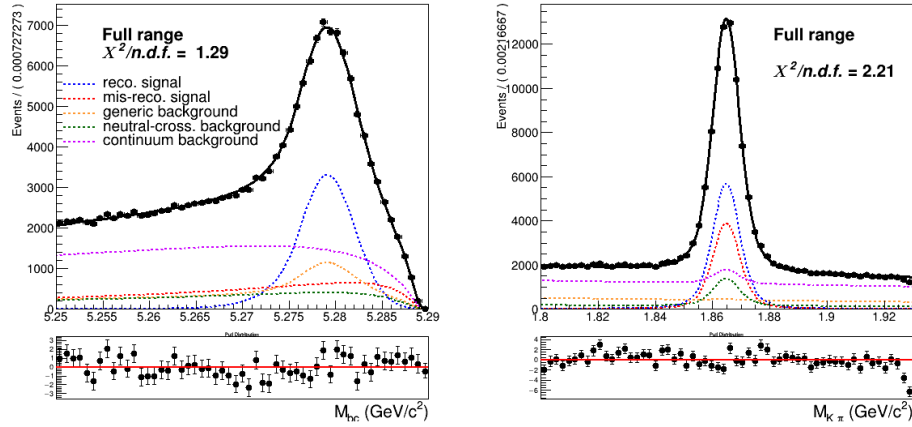


Figure (56) Two dimensional fit on Data

640  
 641 Yields for the reconstructed and misreconstructed signal and for generic background are  
 642 obtained from the fit:

NrecSig	$35629 \pm 368$
NmisSig	$24425 \pm 311$
Generic	$24596 \pm 407$

ratio	MC	DATA
NmisSig/NrecSig	$0.56 \pm 0.01$	$0.68 \pm 0.01$
NmisSig/Generic	$0.90 \pm 0.02$	$0.99 \pm 0.02$
Generic/NrecSig	$0.62 \pm 0.01$	$0.69 \pm 0.02$

Table (9) Comparison of ratios of yields from the two dimensional fits on Monte Carlo simulated data and on Data.

<sup>646</sup> The total normalization from the fit is  $174230 \pm 407$  (to be compared with the total  
<sup>647</sup> data events: 173964).

<sup>648</sup>

649 **5.7 Probability Density Functions (PDFs) for the  $B_{tag}$**

650 Like for the signal model in the 2D fit the  $M_{bc}$  distribution of the tagged charged  $B$   
 651 mesons is fitted with a Crystal Ball as for the reconstructed signal component, whereas  
 652 the misreconstructed signal component is fitted with a Novosibirsk function (Fig. 57a).

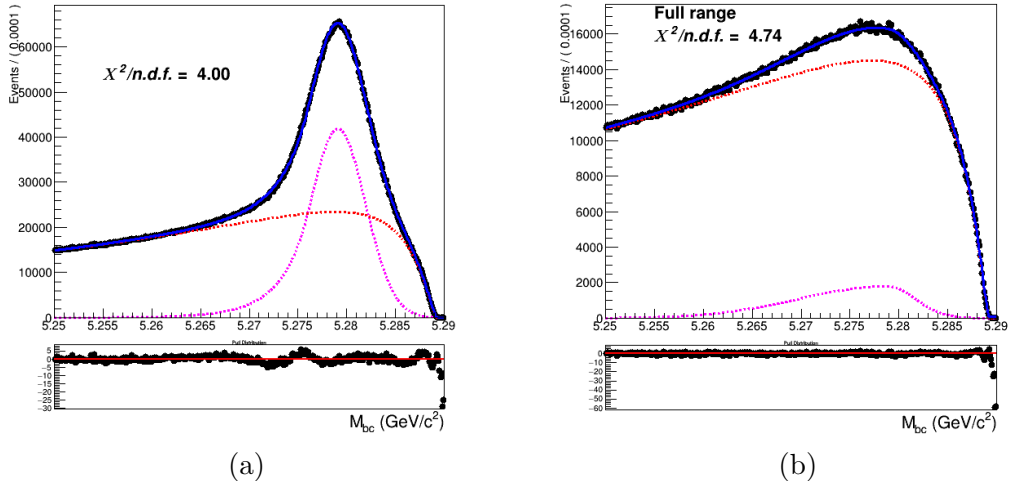


Figure (57) On the left: fitted distribution of tagged charged  $B$  mesons, reconstructed signal events (magenta) are described by a Crystal Ball whereas the misreconstructed signal events (red) are described by a Novosibirsk function. On the right: Crossfeed distribution fitted with a sum of Novosibirsk (red) and asymmetric Gaussian PDF (magenta)

653 The crossfeed background is fitted instead with a sum of a Novosibirsk and an asymmetric  
 654 Gaussian PDF (Fig. 57b).

655  
 656 Regarding the continuum background component, same procedure used for the 2D fit was  
 657 applied to the  $M_{bc}$  distribution of the continuum background in this case (see Fig. ?? for  
 658 the result).

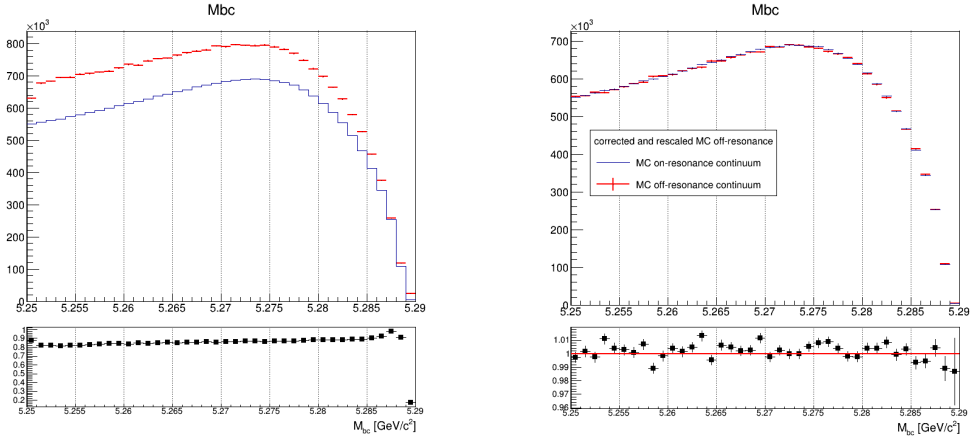


Figure (58) On the left:  $M_{bc}$  distributions of the MC off-resonance sample and the MC continuum sample. On the right:  $M_{bc}$  distributions of the corrected scaled MC off-resonance and on-resonance MC continuum.

## 659 5.8 $B_{tag}$ Fit on Monte Carlo simulated data

660 An independent Monte Carlo stream was used to test the total fit model on tagged  $B$   
 661 mesons candidates. The usual condition is applied to the crossfeed background events:  
 662 the ratio between its contribution and misreconstructed signal events is fixed from the  
 663 other Monte Carlo stream.  
 664 In this fit the shaping parameters that are not kept fixed are the Crystal Ball width ( $\sigma_{CB}$ )  
 665 and the width of the Novosibirsk function describing the misreconstructed signal events.  
 666 As in the case of  $B_{tag}$  fit in Sec. 4.4 the range for the fit is restricted to values between  
 667 5.250 and 5.287  $\text{GeV}/c^2$ .

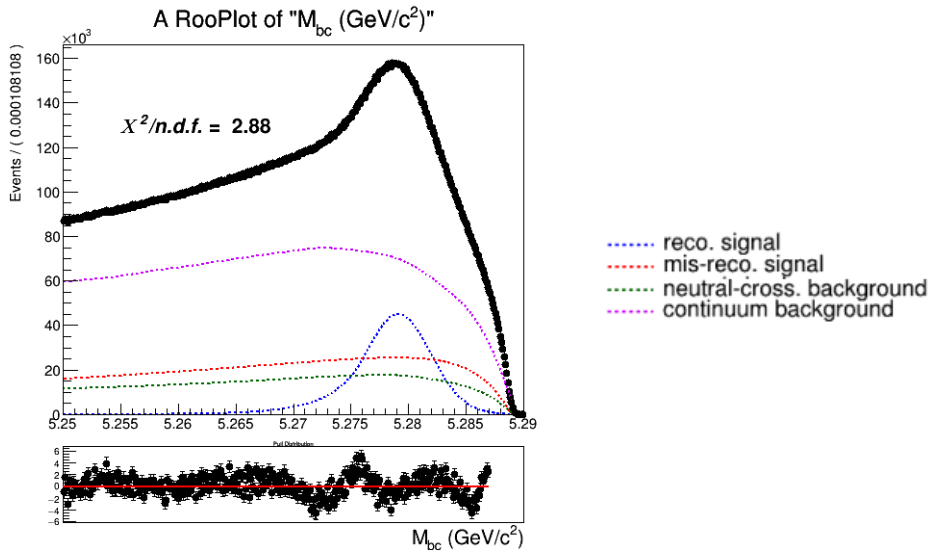


Figure (59) Total fit of tagged  $B$  mesons

668 Yields for the reconstructed and misreconstructed signal are obtained from the fit:

NrecSig	$3.25110 \cdot 10^6 \pm 6759$
NmisSig	$7.41107 \cdot 10^6 \pm 5341$

670 One can then compare the sum NrecSig+NmisSig (the so called total signal) with the true  
 671 value known from the Monte Carlo and the same for the total number of events in this  
 672 particular stream:

	fit	MC value
Total Signal	$10.662 \cdot 10^6 \pm 5249$	$10.671 \cdot 10^6$
Total events	$38.601 \cdot 10^6 \pm 6886$	$38.610 \cdot 10^6$

673 The discrepancy in the total signal events from the fit and the MC here is about  $1.7\sigma$ , but  
 674 the relative error is an order of magnitude smaller than the one found in  $B_{tag}$  fit in 4.4  
 677 (below the %level), therefore it's negligible.

## 678 5.9 $B_{tag}$ Fit on data

679 The fit model tested on Monte Carlo simulated data is then applied with the same method  
 680 on data Fig. 60.

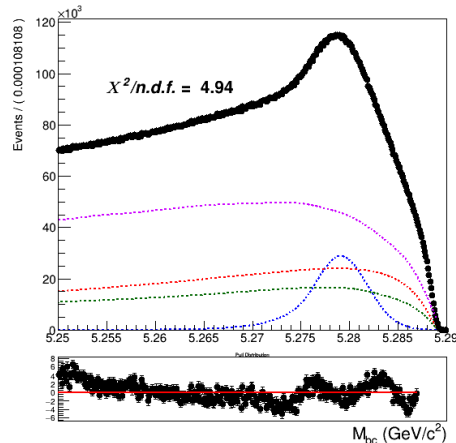


Figure (60) Total fit of tagged  $B^+$  mesons candidates on data

681 Yields for the reconstructed and misreconstructed signal are obtained from the fit:

NrecSig	$2.011 \cdot 10^6 \pm 5858$
NmisSig	$6.975 \cdot 10^6 \pm 4667$
Total Signal	$8.982 \cdot 10^6 \pm 4587$

ratio	MC	DATA
NmisSig/NrecSig	$2.28 \pm 0.01$	$3.47 \pm 0.01$

Table (10) Comparison of ratios of yields from the tagged  $B$  mesons fits on Monte Carlo simulated data and on Data.

## 683 5.10 PID efficiency correction

684 The PID selection is applied only to Kaons:  $\frac{\mathcal{L}_K}{\mathcal{L}_K + \mathcal{L}_\pi} > 0.6$

685 Using the values provided in the global tag **BellePID** (as done in the  $B \rightarrow \Lambda_c$  study),  
686 the average Kaon ID correction for this analysis is estimated to be  $R = 0.976 \pm 0.008$ .

## 687 5.11 $D^0$ and FEI efficiency

688 The efficiency in reconstructing the  $D^0$  after correctly tagging the charged  $B$  meson, can  
689 be estimated from the 2D fit on Monte Carlo simulated data, using the reconstructed  
690 signal yield and from a sample of  $B_{tag}$  candidates reconstructed in signal events in the  
691 Monte Carlo: where from  $B^+B^-$  at least a  $D^0$  decaying into  $\pi K$  is produced.

692 For the latter a fit is performed to extract the yield of correctly tagged  $B$  mesons (Fig.  
693 61)

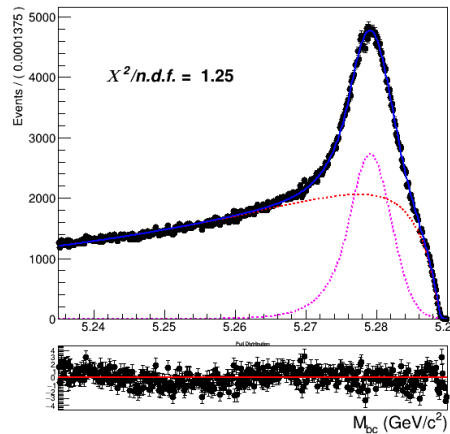


Figure (61) Fit of tagged  $B$  mesons in the "signal events" sample

694 Yields for the reconstructed and misreconstructed signal :

NrecSig	$1.46779 \cdot 10^{-5} \pm 767$
NmisSig	$6.16717 \cdot 10^{-5} \pm 1028$

696 From this and the results listed in Sec. 5.5 the efficiency to reconstruct  $D^0$  is obtained :

697

$$698 \epsilon_{D^0} = \frac{N_{recSig}(2D)}{N_{recSig}((B_{tag}^{sig})} = 39.1 \pm 0.4\%^6 \quad (\text{KID efficiency corrected value for data: } 38.2 \%)$$

699

700 The results from the fit shown in (Fig. 61) can be used also to calculate the FEI tag-side  
701 efficiency for signal events, i.e. the efficiency to tag the  $B$  meson accompanying a  $B_{sig}$   
702 decaying into a  $D^0$  on the signal side. Whereas results from the fit of charged  $B_{tag}$  shown

---

<sup>6</sup>the error reflects the limited Monte Carlo statistics

703 in Fig. 57a can be used to calculate the hadronic tag-side efficiency in the generic  $B^+B^-$   
 704 events case.

705 The ratio of the two efficiencies is found to be:  $\frac{\epsilon_{FEI,sig}^+}{\epsilon_{FEI}^+} = 1.50 \pm 0.01$   
 706

## 707 5.12 Studies of Systematic Effects

708 The systematic uncertainties are studied the same way as in the case of the  $B^+ \rightarrow \bar{\Lambda}_c^- X$   
 709 branching fraction. The values are reported in the next section. Again, the dominant  
 710 systematic uncertainty is the one originated by the continuum background modeling and  
 711 its incidence in terms of relative error on the branching fraction value is same as for the  
 712  $B^+ \rightarrow \bar{\Lambda}_c^- X$  study.

## 713 5.13 Measured $B^+ \rightarrow \bar{D}^0 X$ inclusive Branching Fraction

714 The inclusive branching fraction of  $B^+ \rightarrow \bar{D}^0 X$  can be determined by:

$$Br(B^+ \rightarrow \bar{D}^0) = \frac{r}{Br(D^0 \rightarrow K^+\pi^-)\epsilon_{D^0}} \cdot \frac{\epsilon_{FEI}^+}{\epsilon_{FEI,sig}^+} \quad (9)$$

715 Where

- 716 •  $r = \frac{N_{tag,D^0}}{N_{tag}}$  is the ratio of reconstructed signal yield in the two dimensional fit and in  
 717 the  $M_{bc}$  fit of the tagged  $B$  mesons.
- 718 •  $\epsilon_{D^0}$  is the  $D^0$  reconstruction efficiency calculated as fraction of reconstructed signal  
 719 events with correct tag of which then also a correctly reconstructed  $D^0$  is recon-  
 720 structed in the signal side.
- 721 •  $\frac{\epsilon_{FEI}^+}{\epsilon_{FEI,sig}^+}$  is the ratio of the FEI efficiencies: the hadronic tag-side efficiency for generic  
 722  $B^+B^-$  events ( $\epsilon_{FEI}^+$ ) and signal-side dependent one ( $\epsilon_{FEI,sig}^+$ ) where one of the two  $B$   
 723 mesons decays inclusively into the signal channel ( $D^0 \rightarrow K^+\pi^-$ )
- 724 •  $Br(D^0 \rightarrow K^+\pi^-) = 3.8\%$  in Belle DECAY.DEC table,  $Br(D^0 \rightarrow K^+\pi^-) = 3.95\%$   
 725 in PDG.

726 In Monte Carlo:  $Br(B^+ \rightarrow \bar{D}^0) = 79.4 \pm 0.6^{(stat.)}\%$  (true MC value: 79.1%)  
 727

728 In Data:  $Br(B^+ \rightarrow \bar{D}^0) = 78.3 \pm 0.8^{(stat.)}\%$  (PDG value:  $79 \pm 4\%$ )  
 729

730 The systematic uncertainties are dominating as one can see from the Table below, listing  
 731 the contribution of the various sources of systematics in terms of Branching Fraction in

<sup>732</sup> percentage.

<sup>733</sup>

continuum modelling	1.8 %
Crossfeed PFDs	0.4 %
Crossfeed fraction	0.8 %
FEI efficiency	0.5 %
$\epsilon_{D^0}$	0.8 %
PID	0.6 %
Total	2.3 %

Table (11) Sources of systematic uncertainties and their contributions.

734    **6     $B^- \rightarrow \bar{\Lambda}_c^-$  decays**

735    Applying the same procedure already illustrated in Sec. 4, the optimized selection cuts for  
 736    the charged flavor-anticorrelated decays are:

- 737       •  $\text{foxWolframR2} < 0.3$   
 738       •  $\text{SignalProbability} > 0.1$   
 739       •  $p_{CM\text{S}}^{\Lambda_c} < 1.5 \text{ GeV}/c$

740    **6.1 Probability Density Functions (PDFs) for the two dimensional fit**  
 741

742    The PDFs used to describe the signal distributions are the same already used in Sec. 4.1  
 743    (only the shaping parameters differ) and an example of the 2D fit is shown in Fig. 62.  
 744    Also the generic background deriving from other  $B^+B^-$  events presents similar shapes of  
 745    the distributions as shown already in Sec. 4.1, therefore the probability density functions  
 746    used are the same (fit is shown in Fig. 63).

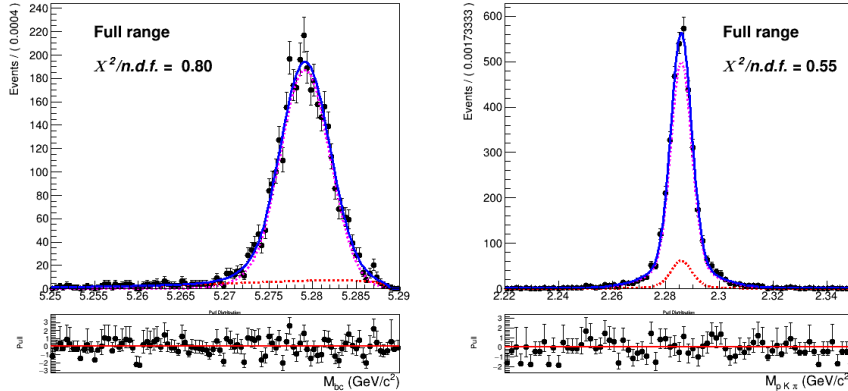


Figure (62) Two dimensional fit of total signal events in  $M_{bc}$  and  $M(pK\pi)$ .

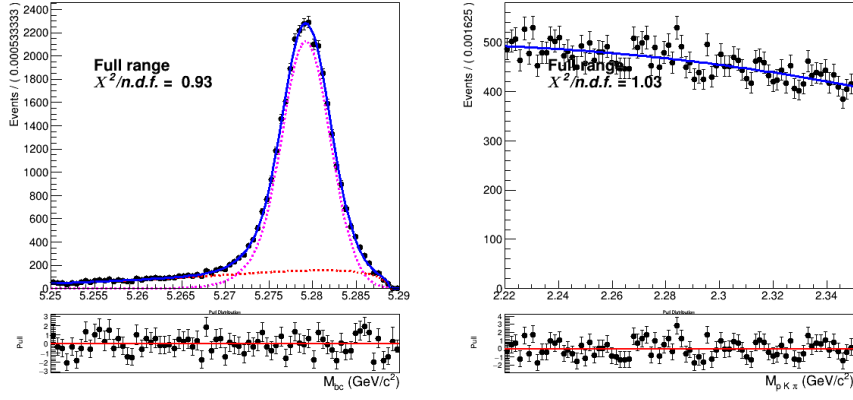


Figure (63) Two dimensional fit of generic ( $B^+B^-$ ) events in  $M_{bc}$  and  $M(pK\pi)$ .

747 The same can be said about the misreconstructed  $B^0$  events (Fig. 64)

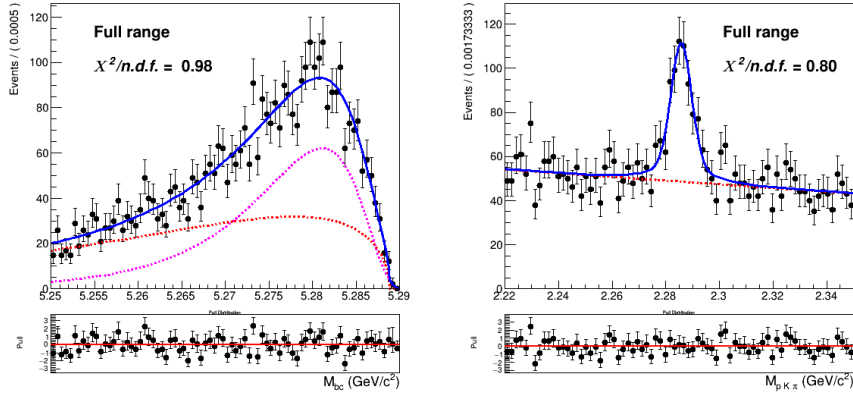


Figure (64) Two dimensional fit of crossfeed ( $B^0\bar{B}^0$ ) events in  $M_{bc}$  and  $M(pK\pi)$ .

748 To check that the shapes determined using 5 streams of Monte Carlo are describing with  
 749 reasonable accuracy the 2D distribution, the projections of the fit of the two-dimensional  
 750 distributions in the signal and sideband regions are plotted (Fig. 66 - Fig. 68). One can see  
 751 the same tendencies of undershooting/overshooting the  $\Lambda_c$  invariant mass peak, as in the  
 752 case of charged correlated decays (Figures 18 - 19). But when examining the independent  
 753 Monte Carlo stream distribution overlaid by the determined PDF in the very same regions  
 754 (see Figures 69 - 71) those effects are so much diminished, according to the statistics, that  
 755 the effects are within statistical fluctuations and therefore negligible, contrary to the case  
 756 of charged flavor-correlated decays.

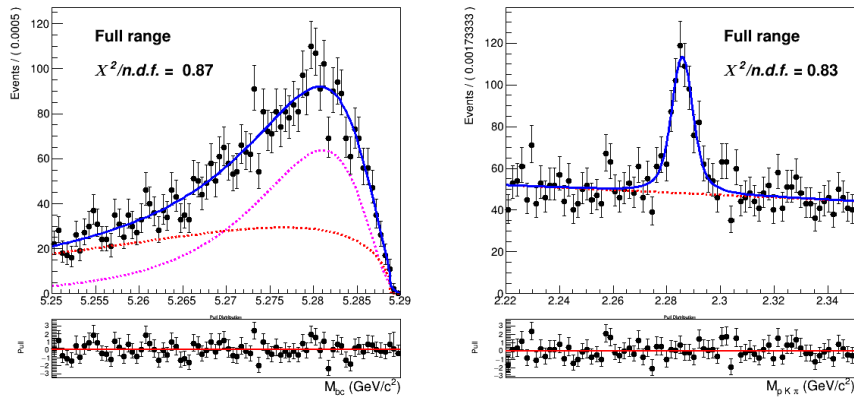


Figure (65) Two dimensional fit of crossfeed  $(B^0 \bar{B}^0)$  events in  $M_{bc}$  and  $M(pK\pi)$ .

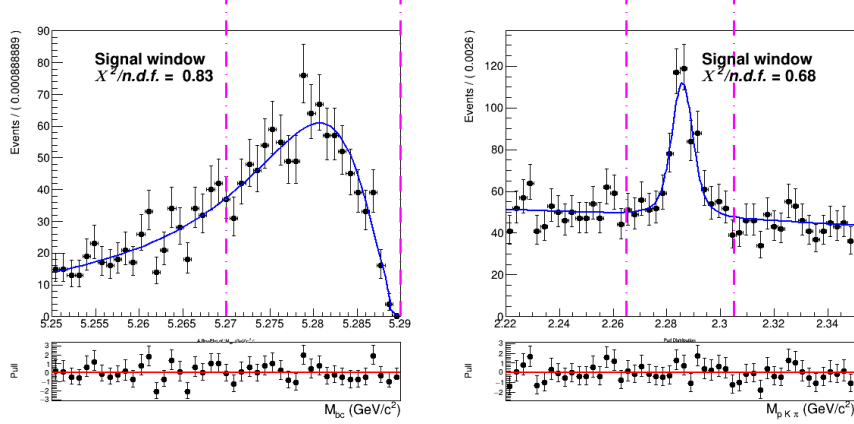


Figure (66) Signal region projections in  $M_{bc}$  and  $M(pK\pi)$  of the fit of crossfeed events.

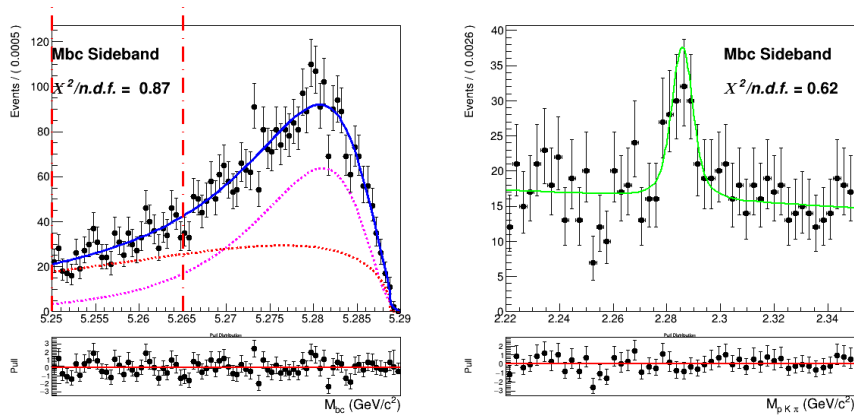


Figure (67)  $M_{bc}$  sideband region projection of the fit of crossfeed events in  $M(pK\pi)$ .

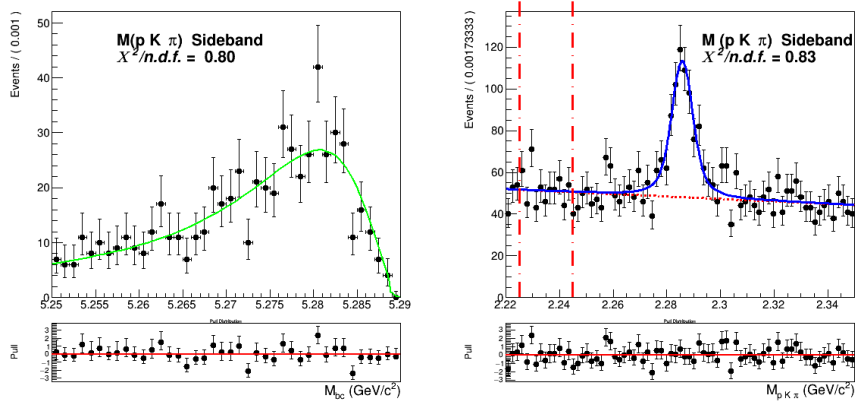


Figure (68)  $M(pK\pi)$  sideband region projection of the fit of crossfeed events in  $M_{bc}$ .

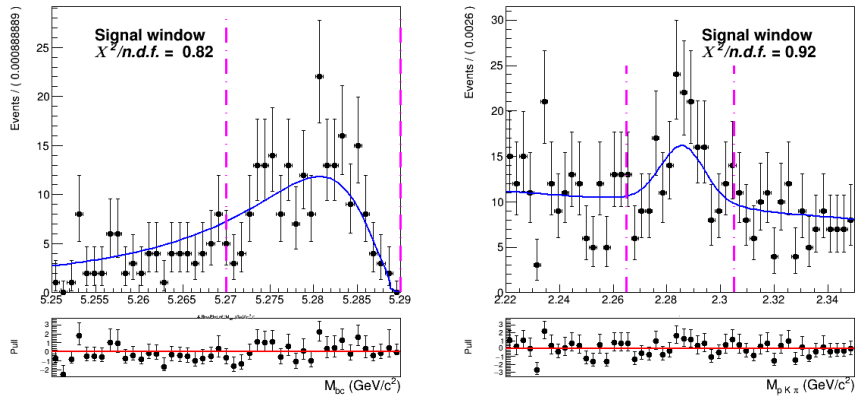


Figure (69) Signal region projections in  $M_{bc}$  and  $M(pK\pi)$  of the fit of crossfeed events.

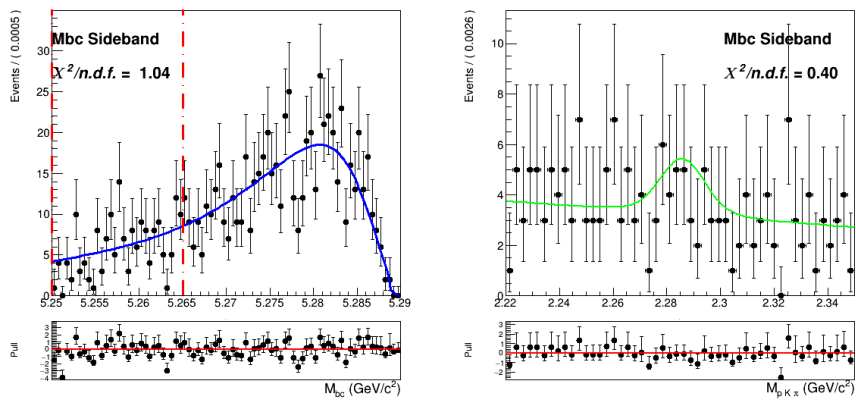


Figure (70) Two dimensional fit of crossfeed ( $B^0\bar{B}^0$ ) events in  $M_{bc}$  and  $M(pK\pi)$ .

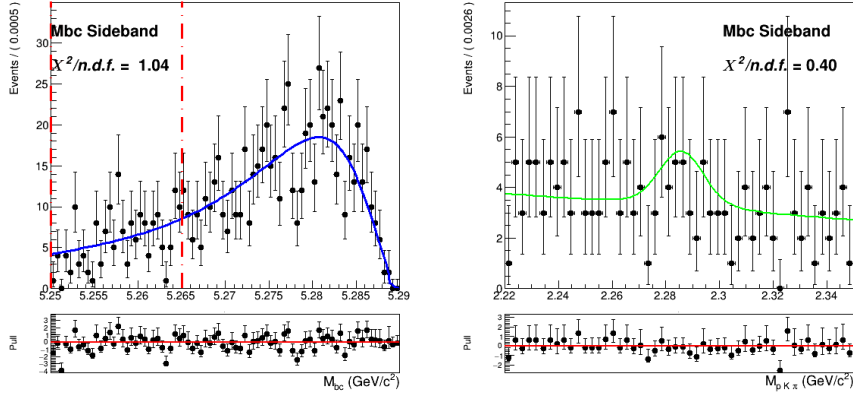


Figure (71) Two dimensional fit of crossfeed ( $B^0 \bar{B}^0$ ) events in  $M_{bc}$  and  $M(pK\pi)$ .

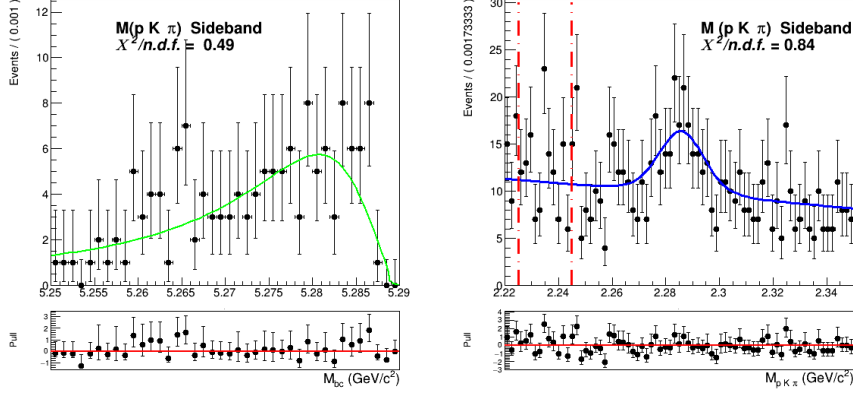


Figure (72) Two dimensional fit of crossfeed ( $B^0 \bar{B}^0$ ) events in  $M_{bc}$  and  $M(pK\pi)$ .

757 The procedure adopted to model the continuum background is the same used for the  
 758 charged correlated  $B \rightarrow \Lambda_c$  decays. To obtain the shape that can describe the continuum  
 759 background  $M_{bc}$  distribution, the continuum suppression is not applied on the off-resonance  
 760 continuum sample in order to acquire more statistics. It is then scaled and corrected for  
 761 the *SignalProbability* correlated effects. The scaling and bin-correction procedure was  
 762 carried out on a sample of five streams of on- and off-resonance MC. From a ratio plot,  
 763 like the one in Fig. 73a, showing the continuum on-resonance distribution in  $M_{bc}$  and the  
 764 scaled continuum on-resonance distribution without the continuum suppression applied,  
 765 the bin-correction is obtained to correct the off-resonance data in the scaling procedure.

766 The validity of this procedure is first tested on the sixth independent MC sample: Fig.  
 767 73b shows the scaled and bin-corrected off-resonance continuum histogram compared with  
 768 the continuum on-resonance distribution of the independent stream. Compared to the  
 769 charged correlated decays one can notice larger statistical fluctuations but the overall  
 770 result looks still fairly reasonable. In order to obtain the PDF describing the distribution  
 771 the histogram is fitted (see Fig. 74a), i.e. with a Novosibirsk function.

772 Since in the  $\Lambda_c$  invariant mass one doesn't expect correlation effects, one can fit directly the  
 773 properly scaled distribution with a first order polynomial (see Fig. 74b) It is possible then  
 774 to check the validity of the whole procedure on the on-resonance Monte Carlo independent  
 775 stream (Fig. 75)

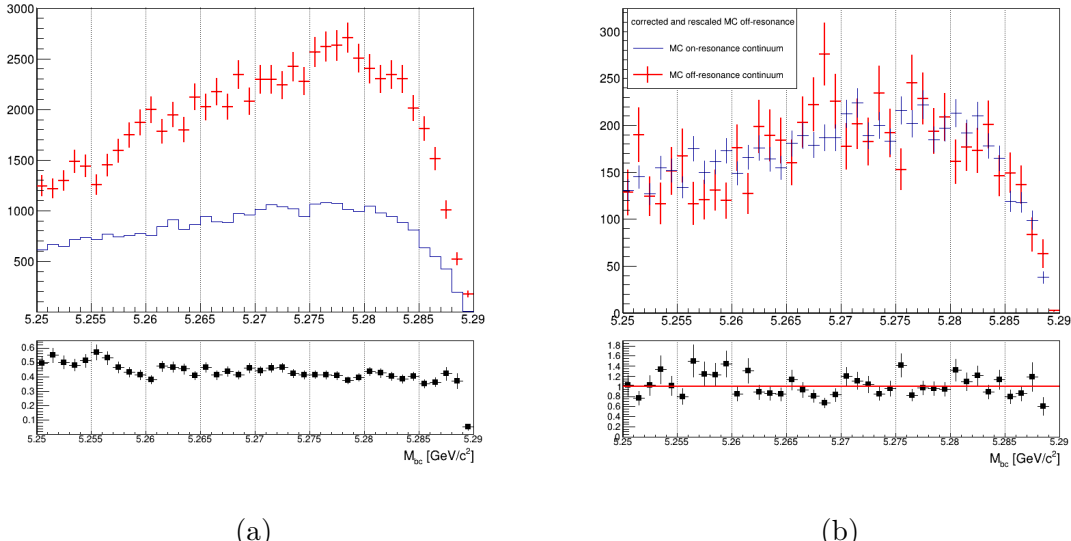


Figure (73) On the left:  $M_{bc}$  distributions of the MC off-resonance sample without continuum suppression and the MC continuum sample with applied continuum suppression (5 streams). On the right:  $M_{bc}$  distributions of the corrected scaled MC off-resonance and on-resonance MC continuum (independent stream).

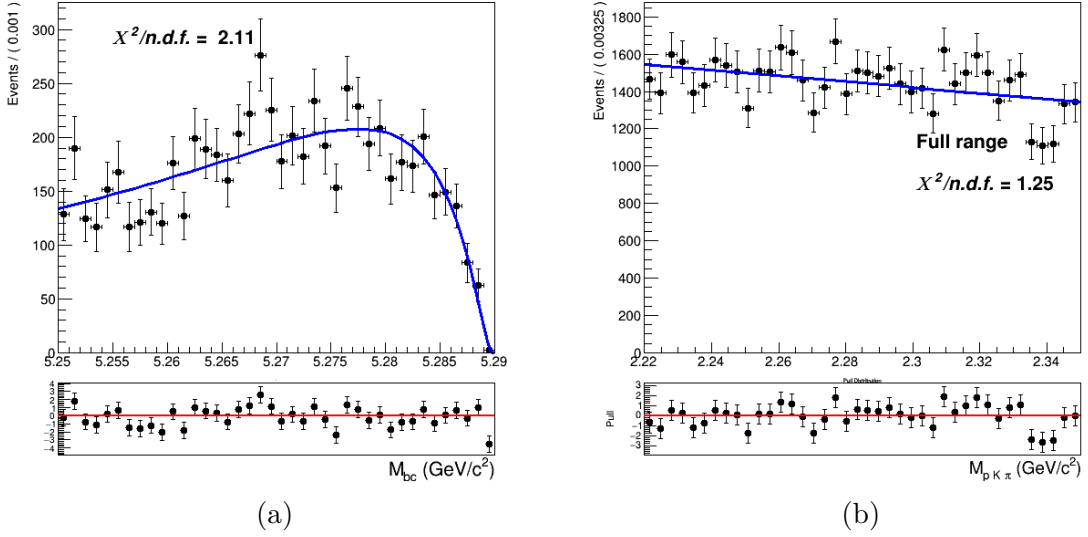


Figure (74) On the left: fit of the  $M_{bc}$  distribution MC (scaled and corrected) off-resonance continuum (one stream). On the right: fit of the  $\Lambda_c$  invariant mass distribution of five stream scaled off-resonance continuum.

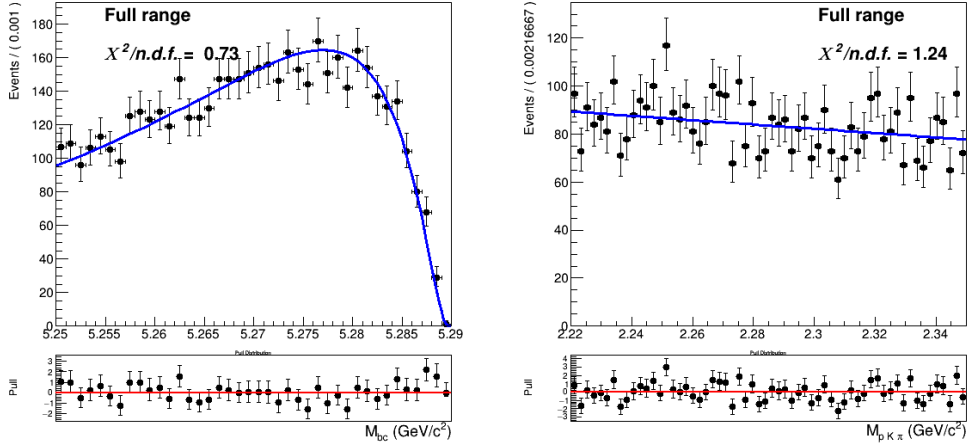


Figure (75) Continuum  $M_{bc}$  and  $M(pK\pi)$  distributions overlaid by the PDFs obtained in fits shown in Figures 74a - 74b

## 776 6.2 Two dimensional fit

777 After obtaining the PDFs describing the various signal/background components using five  
 778 streams statistics, the fit model is tested with six fits on the six independent Monte Carlo  
 779 streams. The conditions for these six two dimensional fits are again the same used for the  
 780 charged correlated decays (see Sec. 4.2). Exemplary, the distributions of stream 0 overlaid

by the fitted PDF are depicted in Fig. 76 (see Appendix .3 for the projections in signal and sideband regions). In Table 1 the signal yields of the fits (**Reconstructed Signal**) to the two dimensional distributions for the six streams of  $B^- \rightarrow \bar{\Lambda}_c^-$  flavor-anticorrelated decays are listed and compared to the expected yields of reconstructed signal, and fitted and truth-matched total signal events are also compared, together with their deviations.

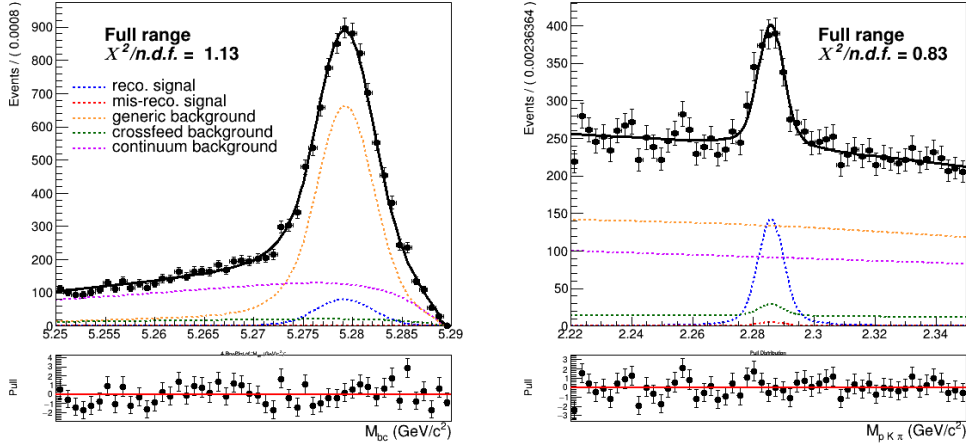


Figure (76) Two dimensional fit on stream 0 Monte Carlo simulated data.

	Reconstructed Signal		Total Signal			fit - MC truth
	fit	expected	fit	MC truth	fit - MC truth	
stream 0	$729 \pm 63$	$660 \pm 21$	$810 \pm 63$	765	45	5.9 %
stream 1	$729 \pm 61$	$698 \pm 29$	$791 \pm 61$	785	6	0.8%
stream 2	$760 \pm 66$	$718 \pm 29$	$800 \pm 65$	797	3	0.4%
stream 3	$719 \pm 68$	$702 \pm 29$	$764 \pm 65$	802	-38	-4.7%
stream 4	$830 \pm 71$	$710 \pm 29$	$810 \pm 71$	804	6	0.7%
stream 5	$640 \pm 54$	$675 \pm 29$	$699 \pm 59$	765	-66	-8.6%
sum	4407	4163	4674	4718	-44	-0.9%

Table (12) Comparison of fitted and expected signal yields, fitted and truth-matched total signal for six streams of Belle generic MC when fitting the two dimensional distributions of  $M_{bc}$  and  $M(pK\pi)$ .

Except for stream 4 all the fits show values of reconstructed signal within the  $1\sigma$  uncertainties in agreement with the expected ones, but as already encountered in Sec. 4.2 a tendency of overestimation can be seen also in these fits, confirmed by the fit shown in Fig 78. Again this small, but not negligible, bias has to be taken into account while fitting the data.

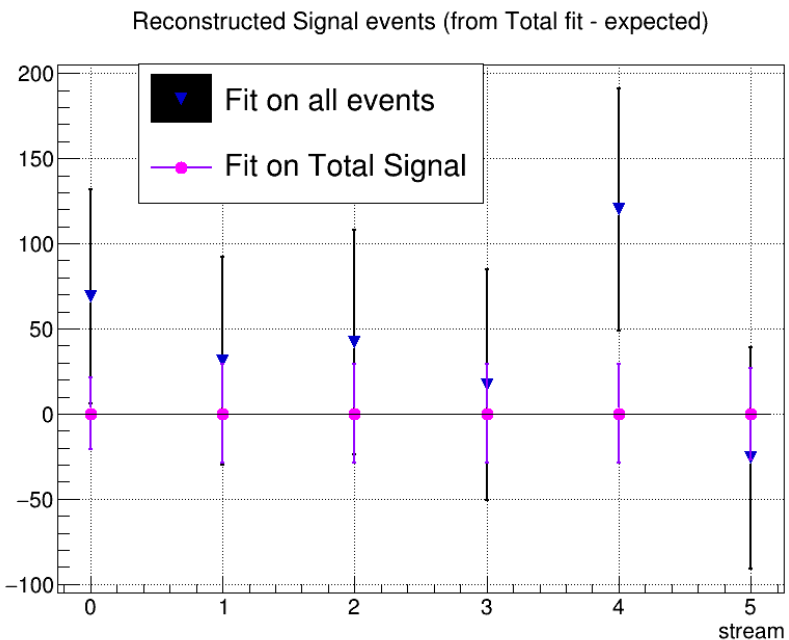


Figure (77) Differences between results from the fits and "expected" values for signal yields as reported in the first columns on Table 12 .

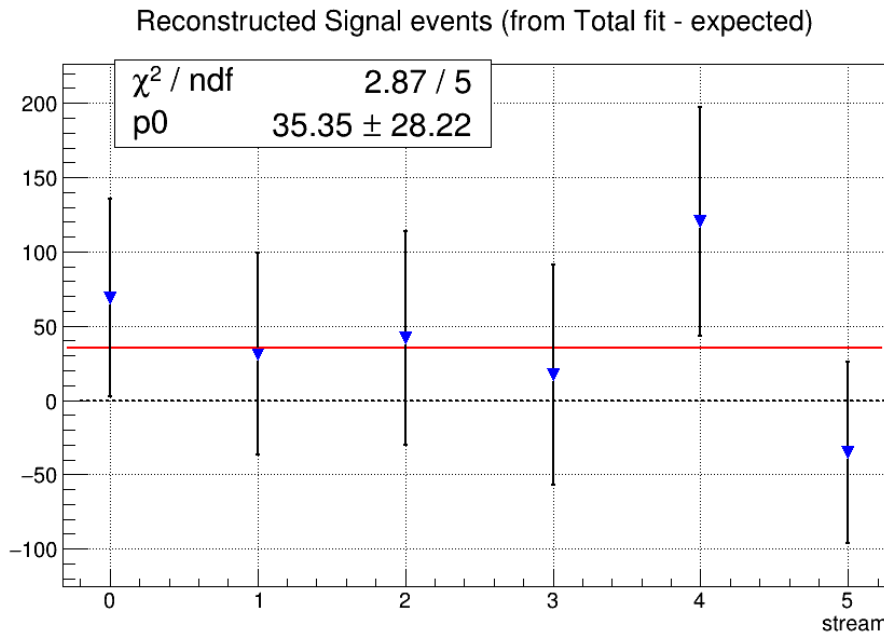


Figure (78)

<sup>791</sup> Also the behaviour for different signal-to-background ratio was investigated using five  
<sup>792</sup> independent streams. The amount of total signal is varied between 50% and 150% of the

nominal values. The amount of background varies according to poissonian fluctuations,  
 as it is taken from the five independent streams. The plot in Fig. 79 shows the values  
 of reconstructed signal obtained in the total fits versus those expected by the fits on  
 total signal events. The performed linear fit suggests a compatibility with a 1:1 relation,  
 although the points are located above the bisector line (dotted blue line). Therefore also for  
 this decay channel one doesn't expect any systematics due to different signal-to-background  
 ratio.

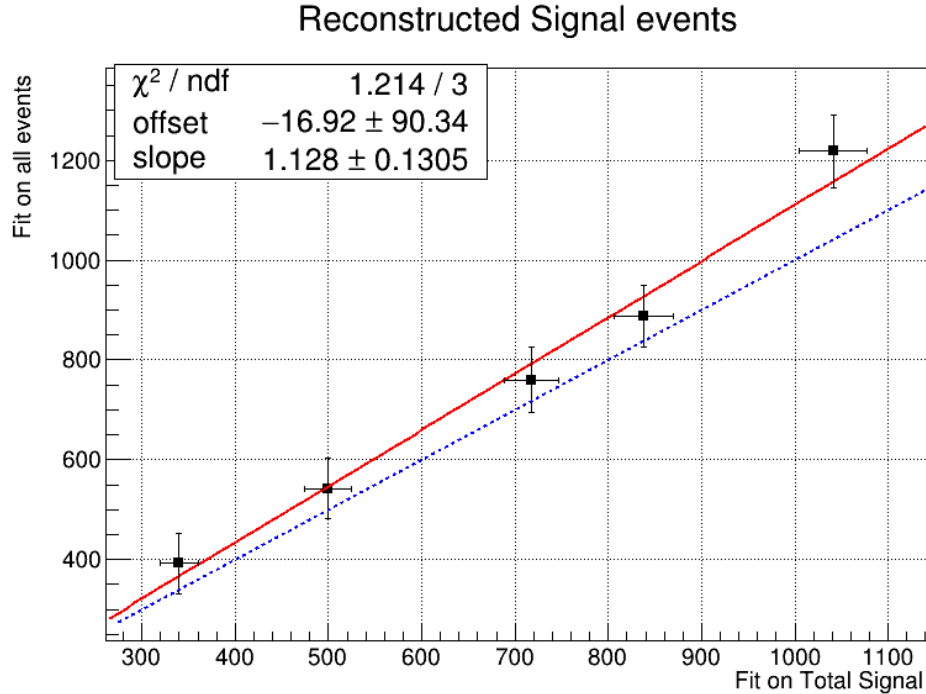


Figure (79) Linearity test: on the x-axis the obtained reconstructed signal yields from fits on different amounts of total signal; on y-axis the yields of reconstructed signal obtained fitting all events. The values are fitted with a red continuous line, whereas the blue dotted line corresponds to a 1:1 linear dependence.

Toy MC pseudo-experiments were performed as well (see Appendix), which also don't  
 show evidence of any bias on the signal yields.

### 802 6.3 Probability Density Functions (PDFs) for the $B_{tag}$

803 The  $M_{bc}$  distribution of the tagged  $B$  mesons is fitted with a Crystal Ball as for the  
 804 "peaking" component and the "flat" component is fitted with a Argus function (Fig. 80a).  
 805 The crossfeed background, consisting of neutral  $B$  mesons tagged as charged  $B$ , is fitted  
 806 instead with a sum of a Novosibirsk and an asymmetric Gaussian PDF (Fig. 80b).

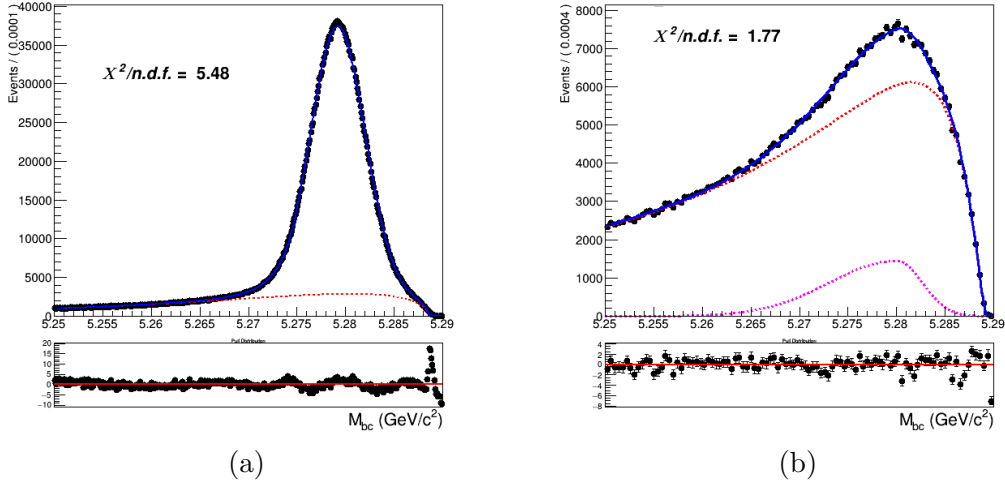


Figure (80) On the left: fitted distribution of tagged charged  $B$  mesons, reconstructed signal events (magenta) are described by a Crystal Ball whereas the misreconstructed signal events (red) are described by an Argus function. On the right: Crossfeed distribution fitted with a sum of Novosibirsk (red) and asymmetric Gaussian PDF (magenta)

807 As for the continuum background, same procedure as the one in the case of charged  
 808 flavor-correlated decays is adopted:

- 809 • first the off-resonance sample is scaled accordingly with all the included cuts.
- 810 • the ratio between the scaled off-resonance and the on-resonance in MC is calculated  
 811 in each bin (see Fig. 81a)
- 812 • the bin-correction is applied on an independent stream and the scaled and bin-  
 813 corrected  $M_{bc}$  distribution is compared with the on-resonance distribution as shown  
 814 in Fig. 81b

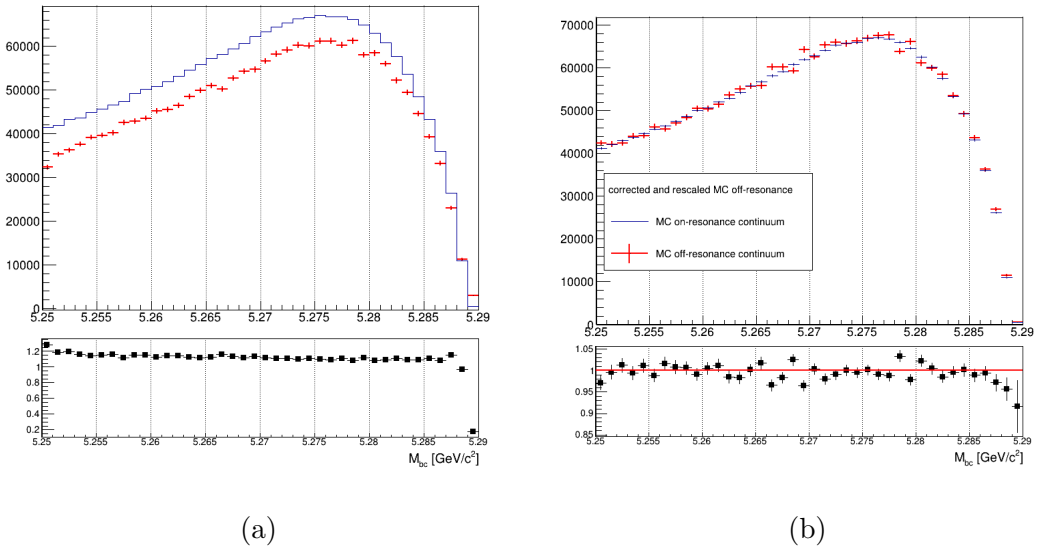


Figure (81) On the left:  $M_{bc}$  distributions of the MC off-resonance sample and the MC continuum sample with applied continuum suppression. On the right:  $M_{bc}$  distributions of the corrected scaled MC off-resonance and on-resonance MC continuum.

815    **6.4       $B_{tag}$  fit**

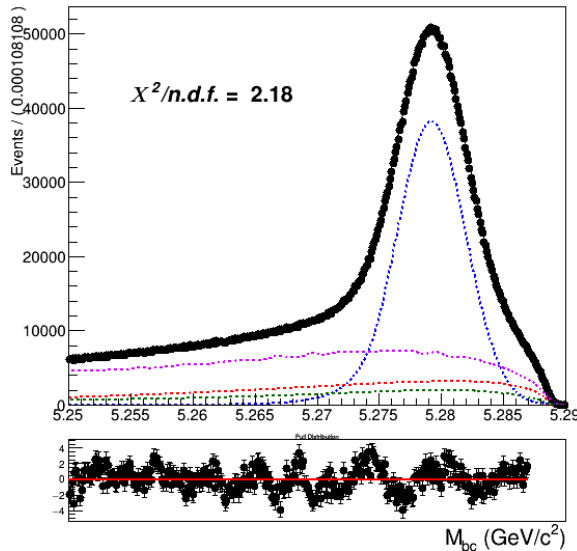


Figure (82) Total fit of tagged  $B$  mesons on Monte Carlo simulated data.

816    An independent Monte Carlo stream was used to test the total fit model on tagged  $B$   
 817    meson candidates. As in the 2D fit, the parameter for the width,  $\sigma_{CB}$ , of the Crystal Ball is  
 818    floated and the ratio between expected crossfeed background events and misreconstructed  
 819    signal events is fixed from the MC. The Argus function describing the misreconstructed  
 820    signal is also not fully constrained: the parameter describing the tail is free. As in the  
 821    previous  $B_{tag}$  fits, the range for the fit is restricted to values between 5.250 and 5.287  
 822     $\text{GeV}/c^2$ . Yields for the reconstructed and misreconstructed signal are obtained from the  
 823    fit:

824

NrecSig	$2.5099 \cdot 10^6 \pm 4408$
NmisSig	$7.82307 \cdot 10^5 \pm 2936$

826    The Total Signal (the sum NrecSig+NmisSig) is  $3292168 \pm 2423$  (to be compared with  
 827    3299629 from the Monte Carlo), which means a  $\sim 3\sigma$  underestimation. As in the case of  
 828    charged flavor-correlated decays, this can produce some systematic effect which needs to  
 829    be taken into account. In fact, a slight underestimation of the Total Signal is found also  
 830    in the result of the toy Monte Carlo study<sup>7</sup>: Fig. 83 shows the results for the Total Signal  
 831    events and one can notice a mean value for the pulls consistently below zero.

<sup>7</sup>as usual performed with  $3 \times 10^3$  pseudo-datasets

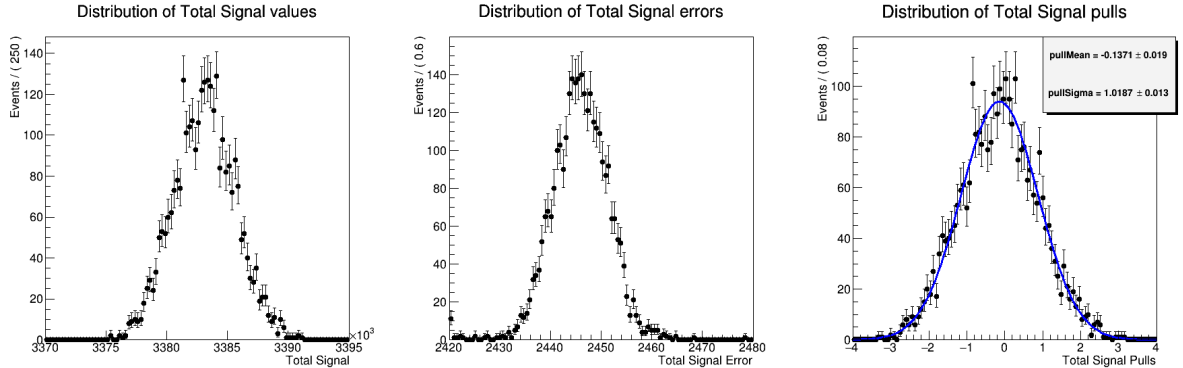


Figure (83) Toy MC fits of pseudo-data showing the Total Signal yield (left), Total Signal yield errors (center) and the pull distribution of the Total Signal (right).

## 832    6.5 $\Lambda_c$ and FEI efficiency

833    The efficiency in reconstructing the  $\Lambda_c$  baryon after correctly tagging the charged  $B$  meson,  
834    is as usual estimated as the ratio:

$$\frac{N_{recSig}(B_{tag}, \Lambda_c)}{N_{recSig}(B_{tag}^{sig})} \quad (10)$$

835    where  $N_{recSig}(B_{tag}, \Lambda_c)$  are the yields of reconstructed signal from the two dimensional fits  
836    (reported in Table 12 ) and  $N_{recSig}(B_{tag}^{sig})$  are the yields of correctly reconstructed signal in  
837    a fit of  $B$  mesons tagged in events where one of the two mesons decayed hadronically and  
838    inclusively into a  $\Lambda_c$  baryon (see Fig 45). This ratio was calculated upon six streams of  
839    Monte Carlo simulated data.

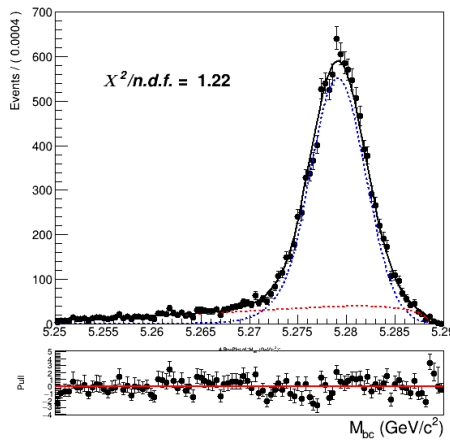


Figure (84) Fit of tagged  $B$  mesons in the "signal events" sample

840 From this and the results listed in Sec. 6.2 the efficiency to reconstruct  $\Lambda_c$  is obtained :

841

$$\epsilon_{\Lambda_c} = \frac{N_{recSig}(B_{tag}, \Lambda_c)}{N_{recSig}(B_{tag})} = 40.95 \pm 1.77\%$$

843 The yields from the fit shown in Fig. 84) are then used to calculate the FEI tag-side  
 844 efficiency for signal events. The yields from the fit of charged  $B_{tag}$  shown in Fig. 80a can  
 845 be used to calculate the hadronic tag-side efficiency in the generic  $B^+B^-$  events case.

846 The ratio between the two efficiencies is calculated:  $\frac{\epsilon_{FEI,sig}^+}{\epsilon_{FEI}^+} = 0.973 \pm 0.009$

847

## 848 6.6 Studies of Systematic Effects

849 The systematic uncertainties are estimated the same way as in the case of charged flavor-  
 850 correlated decays (see Sec. 4.7 and the following Sections). In Table 13 the systematic  
 851 uncertainties of the various considered sources are summarized. Their individual calculation  
 852 is outlined in the subsequent subsections (the uncertainties on the PID efficiency corrections  
 853 are the same already discussed in Sec. 4.12)

source	%
Continuum modeling	0.04
Crossfeed fraction	0.01
$\epsilon_{FEI,sig}^+/\epsilon_{FEI}^+$	0.01
$\epsilon_{\Lambda_c}$	0.05
Fit bias	0.05
PID	0.02
Total	0.08

Table (13) Systematic uncertainties in the determination of the  $B^- \rightarrow \bar{\Lambda}_c^- X$  branching fractions in %.

## 854 6.7 Continuum background modeling

855 Exemplary, fits used to estimate the impact of these uncertainties deriving from statistical  
 856 uncertainties are shown here in Figures 85 - 86. Mean deviation values are then obtained  
 857 for both the two-dimensional fit and the  $B_{tag}$  fit.

858

Fit	$-\sigma$	$+\sigma$	$\pm\bar{\sigma}$
2D	21	22	22
$B_{tag}$	5800	5800	5800

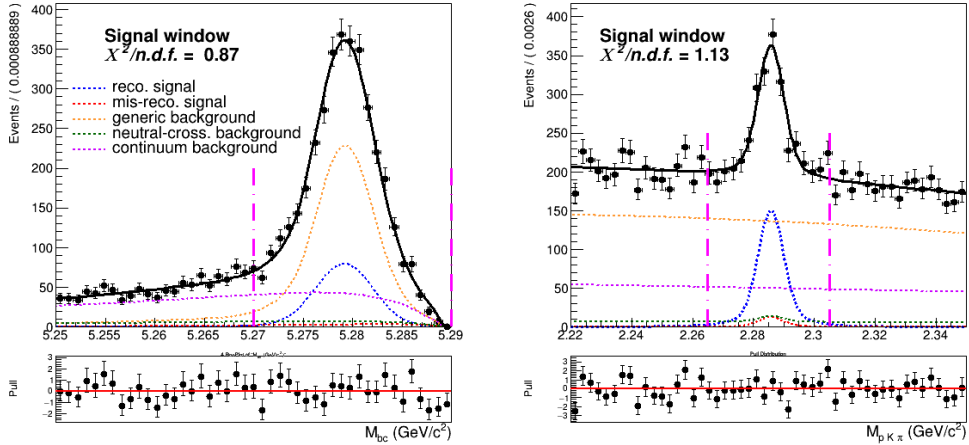


Figure (85) Signal window projections of a two dimensional fit on Monte Carlo simulated data where the shaping parameters were varied of their uncertainties.

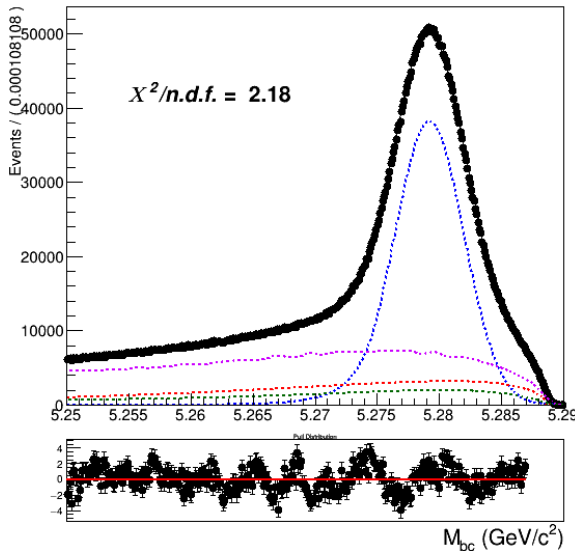


Figure (86) Fit of tagged  $B$  meson candidates on Monte Carlo simulated data where the shaping parameters were varied of their uncertainties.

The estimated systematic uncertainty on Br value from this source is 0.04%.

The continuum suppression cut is found to reject about 68% of the continuum background in data, whereas it rejects 64% of the continuum background in MC (66.5% in on-resonance MC). This means that in data one can expect about 1.4% less continuum background events. The statistical uncertainty on this fraction of events can be also be taken into account as systematics. But again, as already seen in the case of charged flavor-correlated decays, the statistical uncertainty on the on-resonance continuum background

866 events in MC originates a much larger systematic uncertainty: the relative systematic  
 867 uncertainty deriving from the different impact on data of the continuum suppression would  
 868 account for just 0.004% on the BR value (one order of magnitude smaller than systematics  
 869 deriving from the statistical uncertainties). This second source is again consequently  
 870 neglected.

## 871 **6.8 Crossfeed background modeling**

872 This source of systematic uncertainty is again estimated performing the fits varying the  
 873 parameters of the Crossfeed PDFs by their uncertainties (see the table below for the  
 874 deviations in terms of signal yields). The resulting absolute systematic uncertainty is  
 875 about 0.003% on the BR value, which is negligible compared to the other systematic  
 876 effectes.

Fit	$-\sigma$	$+\sigma$	$\pm\bar{\sigma}$
2D	2	1	2
$B_{tag}$	1500	1100	1300

Table (14) Offsets on the signal yields obtained varying the parameters of crossfeed background PDFs within their uncertainties in the two dimensional and  $B_{tag}$  fit and mean deviations reported in the last column.

## 877 **6.9 Crossfeed ratio**

878 As already done for the charged flavor-correlated decays, the systematic uncertainty on  
 879 the crossfeed/misreconstructed events' ratio is studied considering a maximal discrepancy  
 880 of this value up to 20% between Monte Carlo and data (the procedure adopted is the same  
 881 as illustrated in Sec. 4.9).

Fit	$-\sigma$	$+\sigma$	$\pm\bar{\sigma}$
2D	8	3	6
$B_{tag}$	5800	800	3300

Table (15) Offsets on the signal yields obtained varying of  $\pm 20\%$  the crossfeed/misreconstructed ratio in the two dimensional and  $B_{tag}$  fit and mean deviations reported in the last column.

882 The estimated systematic uncertainty on Br value from this source is 0.01%.

883 **6.10 Efficiencies**

884 The ratio between the two FEI efficiencies is:  $\frac{\epsilon_{FEI,sig}^+}{\epsilon_{FEI}^+} = 0.973 \pm 0.009$

885 The uncertainty on this value originates a systematic uncertainty of 0.01% on the Br  
 886 value. The  $\Lambda_c$  reconstruction efficiency is determined to be  $\epsilon_{\Lambda_c} = 40.95 \pm 1.77\%$ . When  
 887 propagating its uncertainty, a systematic error of 0.07% on the Br value is calculated.

888 **6.11 Fit biases**

889 The small bias on the reconstructed signal seen in the two-dimensional fit model produces  
 890 a not negligible systematic uncertainty on the branching fraction. The discrepancy in the  
 891 amount of the total signal estimated by the  $B_{tag}$  fit needs to be included as well in the  
 892 systematic effects. Propagating the two sources of systematics in the branching fraction  
 893 calculation results in an additional 0.05% uncertainty on the branching fraction value.

894 **6.12 Measured  $B^+ \rightarrow \Lambda_c^+$  inclusive Branching Fraction**

895 Using the results from the two dimensional fit reported in Table 12 with all the needed  
 896 factors known, it's possible to examine the agreement between the the branching ratio  
 897 value used in MC generation and the measured ones. In Table 16 one can first of all notice  
 898 the slight shift of the branching fraction value obtained with the fits, but it is still agreeing  
 899 within  $1\sigma$  statistical uncertainty with the MC set value.

	total fit	signal fit	BELLE MC VALUE
stream 0	$(1.32 \pm 0.12)\%$	$(1.19 \pm 0.04)\%$	$(1.233 \pm 0.007)\%$
stream 1	$(1.32 \pm 0.11)\%$	$(1.26 \pm 0.05)\%$	$(1.218 \pm 0.007)\%$
stream 2	$(1.37 \pm 0.12)\%$	$(1.29 \pm 0.05)\%$	$(1.218 \pm 0.007)\%$
stream 3	$(1.30 \pm 0.12)\%$	$(1.26 \pm 0.05)\%$	$(1.215 \pm 0.007)\%$
stream 4	$(1.32 \pm 0.13)\%$	$(1.26 \pm 0.05)\%$	$(1.218 \pm 0.007)\%$
stream 5	$(1.16 \pm 0.10)\%$	$(1.22 \pm 0.05)\%$	$(1.217 \pm 0.007)\%$
average	$(1.30 \pm 0.05)\%$	$(1.25 \pm 0.02)\%$	$(1.220 \pm 0.003)\%$

Table (16) Measured branching fraction values obtained using the results listed in Table 12 for the six different streams (only statistical uncertainties are displayed) and its average.

900 As in the charged flavor-correlated decays the precision obtained on Monte Carlo simulated  
 901 data is improved by factors compared to the branching fraction measured by BaBar  
 902 experiment (see [?]).

903 Appendices



904 .1  $B^- \rightarrow \Lambda_c^+$  decays: additional plots

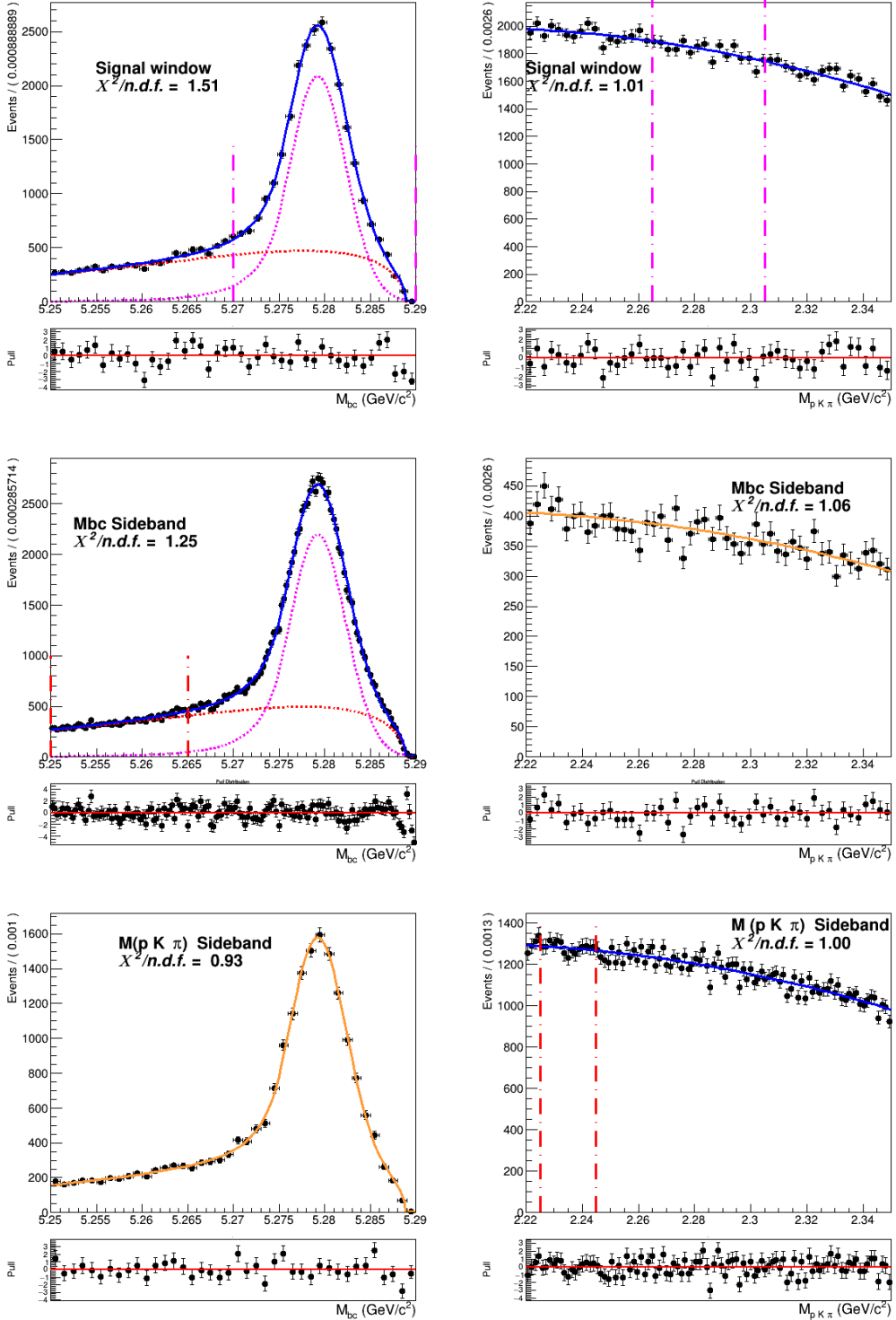


Figure (87) Signal region and sidebands of the two dimensional fit of generic background shown in Fig. 13

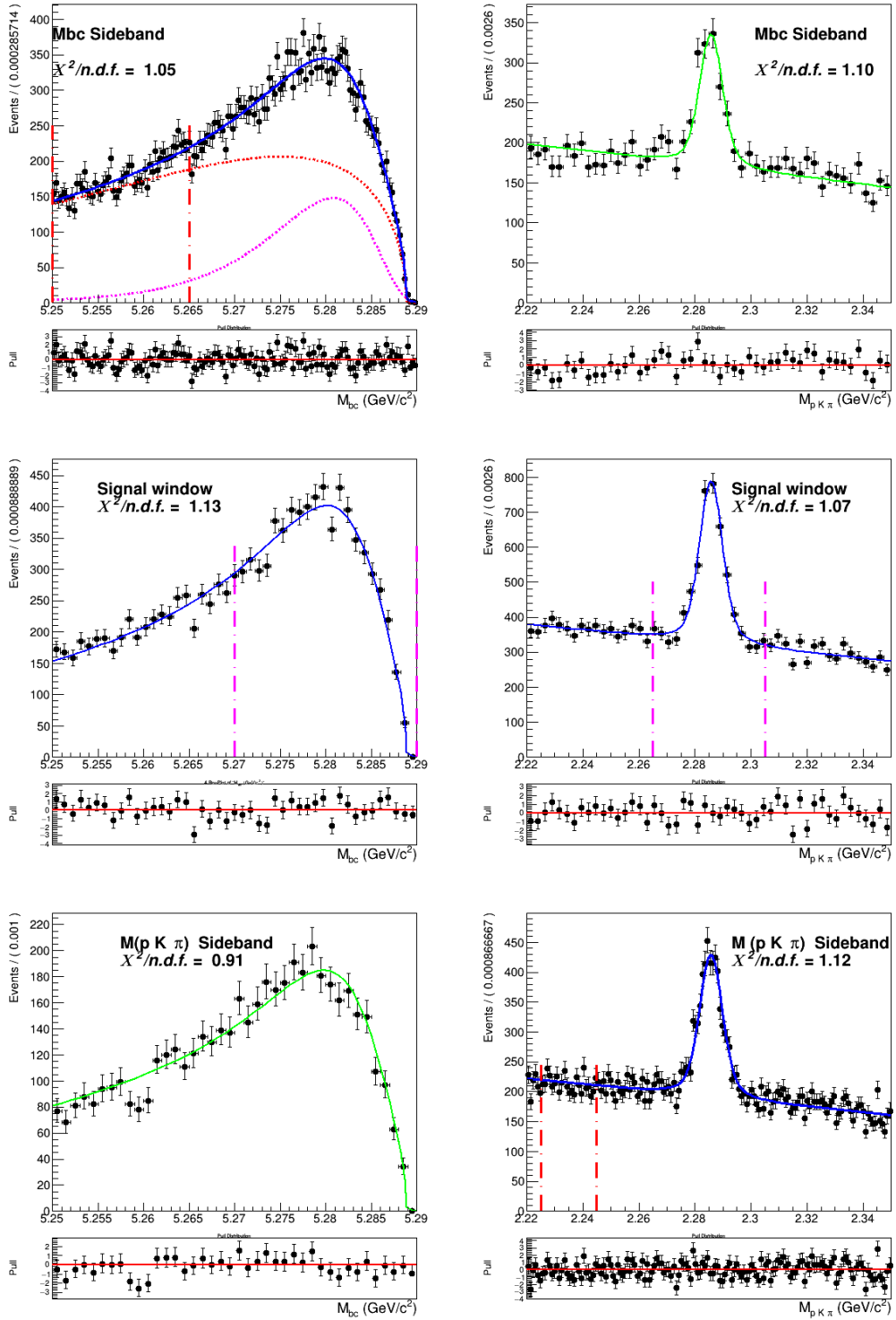


Figure (88) Signal region and sidebands of the two dimensional fit of crossfeed background after parametrization

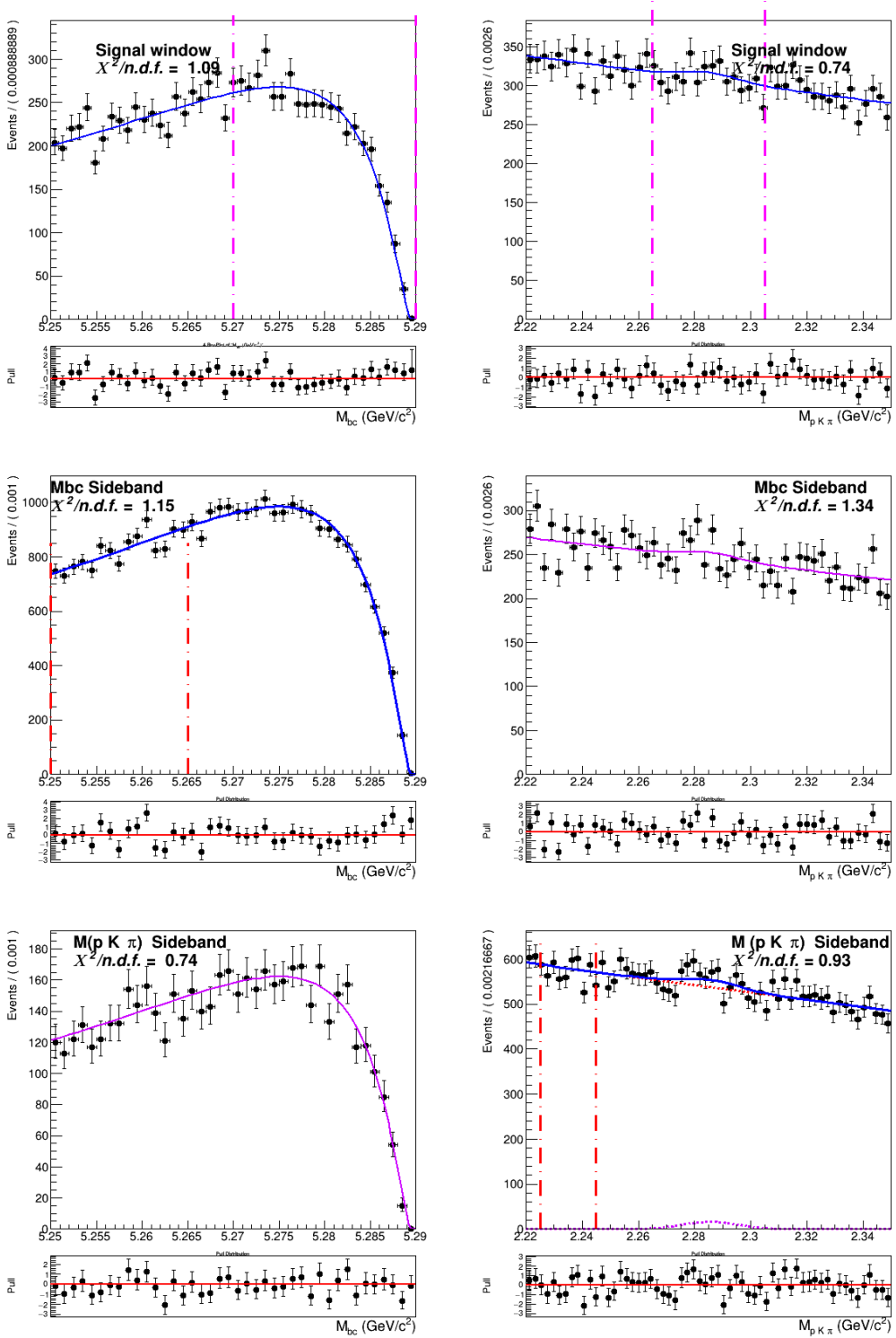


Figure (89) Signal region and sidebands of the two dimensional fit of continuum background shown in Fig. 33

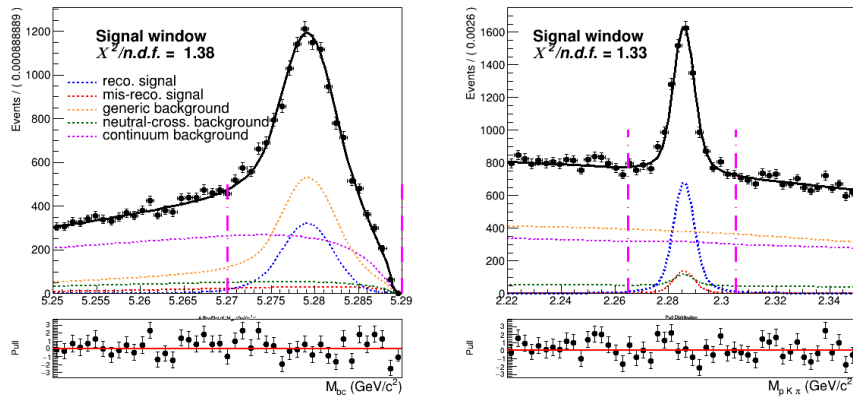


Figure (90) Signal region ( $2.22 < M(pK\pi) < 2.35 \text{ GeV}/c^2$  and  $5.27 < M_{bc} < 5.29 \text{ GeV}/c^2$ ) projections pf the dimensional fit on stream 0 Monte Carlo simulated data.

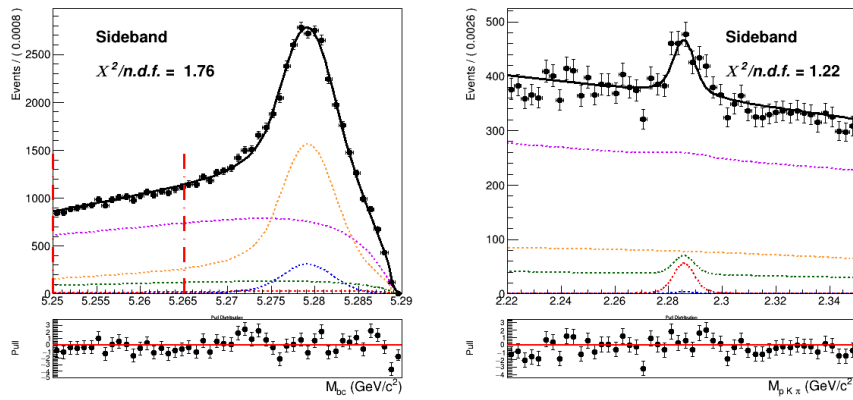


Figure (91) Sideband region of  $5.25 < M_{bc} < 5.265 \text{ GeV}/c^2$  projection of the two dimensional fit on stream 0 Monte Carlo simulated data.

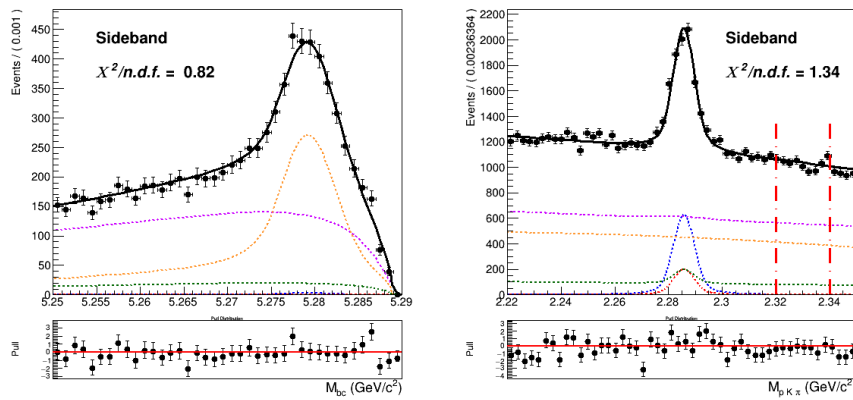


Figure (92) Sideband region of  $2.22 < M(pK\pi) < 2.35 \text{ GeV}/c^2$  projection of the two dimensional fit on stream 0 Monte Carlo simulated data.

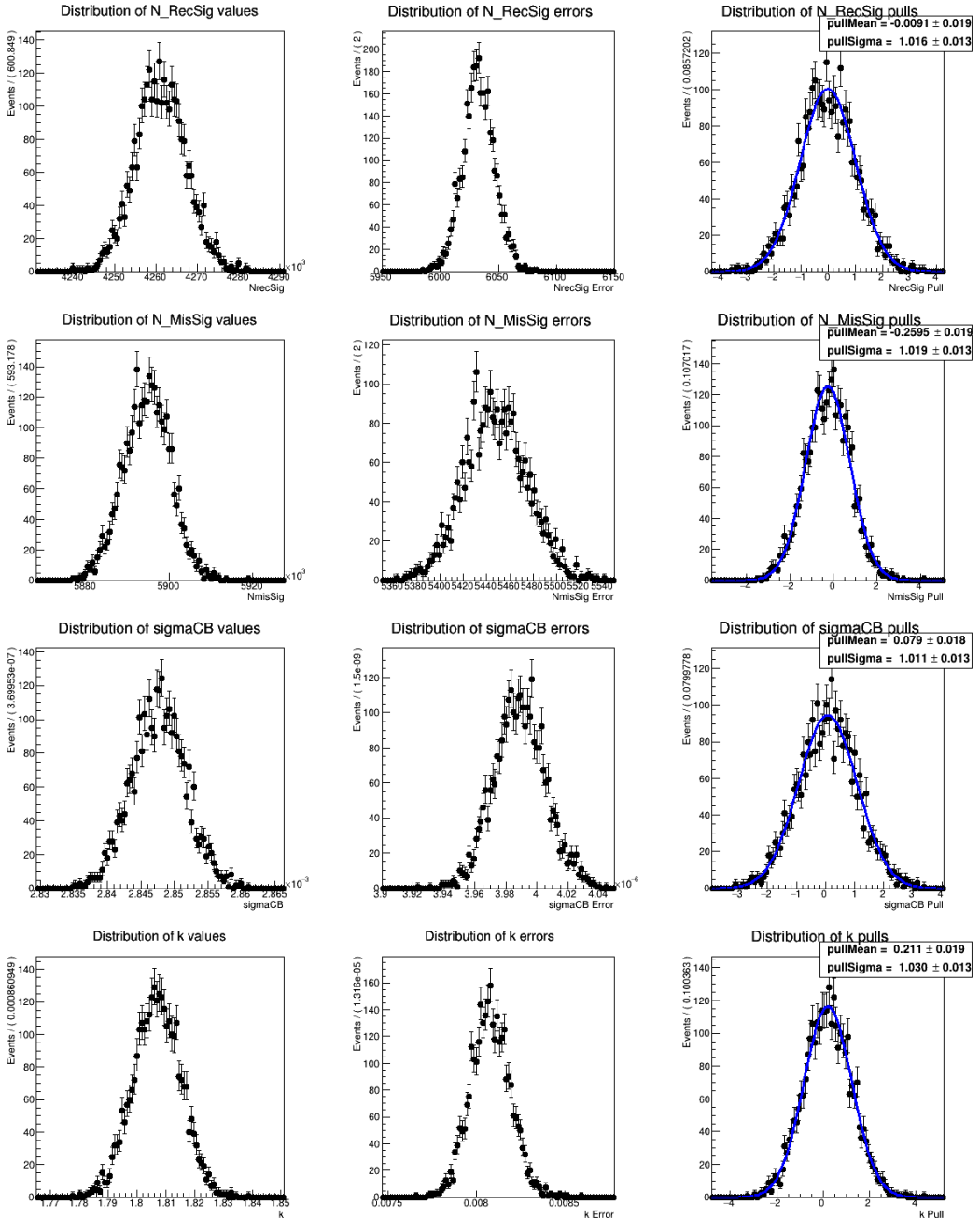


Figure (93) Toy MC study for the  $B_{\text{tag}}$  fit model described in Sec. 4.4

905 .2  $B^- \rightarrow D^0$  decays: additional plots

906 Figures 94-96 show the projections of signal regions and sidebands in  $M_{bc}$  and in the  $D^0$   
 907 invariant mass of the two dimensional fit on stream 0.

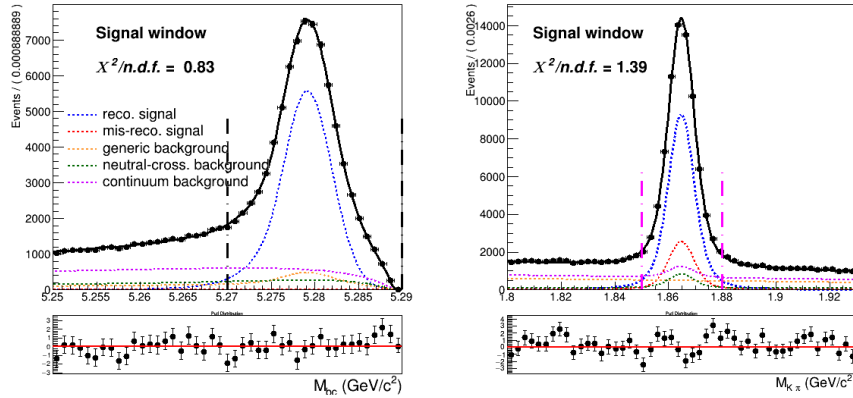


Figure (94) Signal region ( $1.85 < M(\pi K) < 1.88 \text{ GeV}/c^2$  and  $5.27 < M_{bc} < 5.29 \text{ GeV}/c^2$ ) projections of the two dimensional fit on stream0 (Fig. 55).

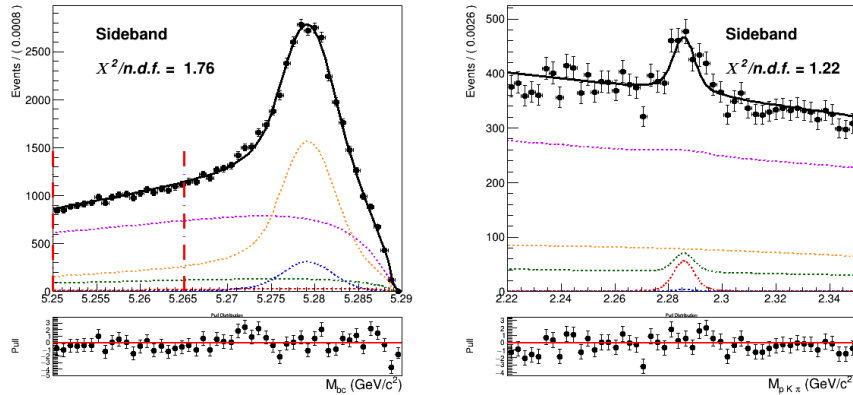


Figure (95) Sideband region of  $5.25 < M_{bc} < 5.265 \text{ GeV}/c^2$  projection in  $M(\pi K)$  of the two dimensional fit on stream 0.

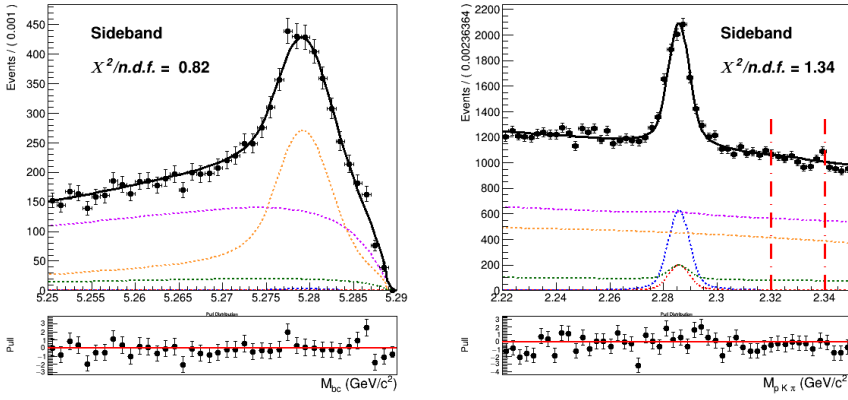


Figure (96) Sideband region of  $1.8 < M(\pi K) < 1.84 \text{ GeV}/c^2$  projection in  $M_{bc}$  of the two dimensional fit on stream 0.

908 Figs. 97 to 99 show the projections in  $M_{bc}$  and in the  $D^0$  invariant mass of the two  
909 dimensional fit on data.

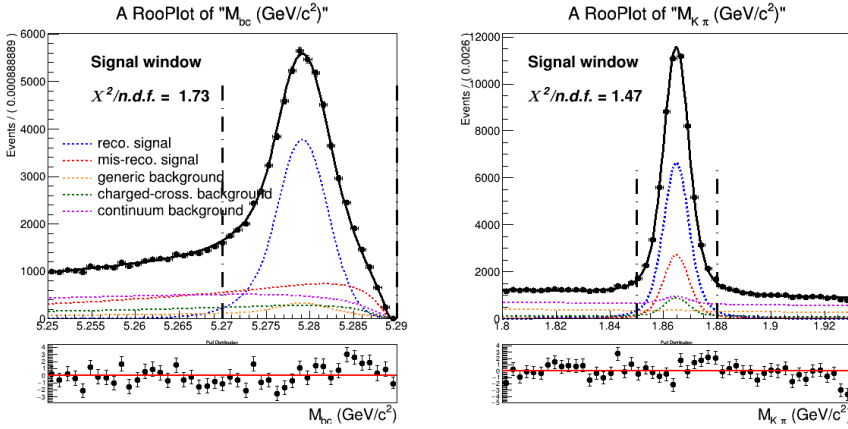


Figure (97) Signal region ( $1.85 < M(\pi K) < 1.88 \text{ GeV}/c^2$  and  $5.27 < M_{bc} < 5.29 \text{ GeV}/c^2$ ) projections of the two dimensional fit on data described in Sec. 5.6

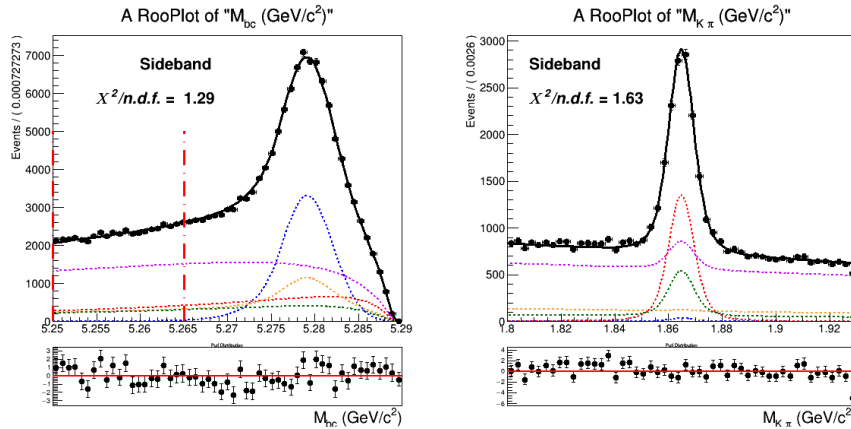


Figure (98) Sideband region of  $5.25 < M_{bc} < 5.265$  GeV/c<sup>2</sup> projection in  $M(\pi K)$  of the two dimensional fit on data

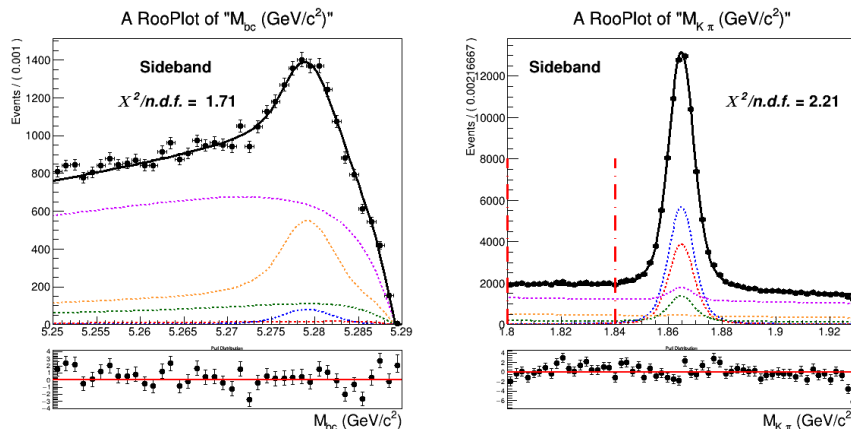


Figure (99) Sideband region of  $1.8 < M(\pi K) < 1.84$  GeV/c<sup>2</sup> projection in  $M_{bc}$  of the two dimensional fit on data.



910 .3  $B^- \rightarrow \bar{\Lambda}_c^-$  decays: additional plots

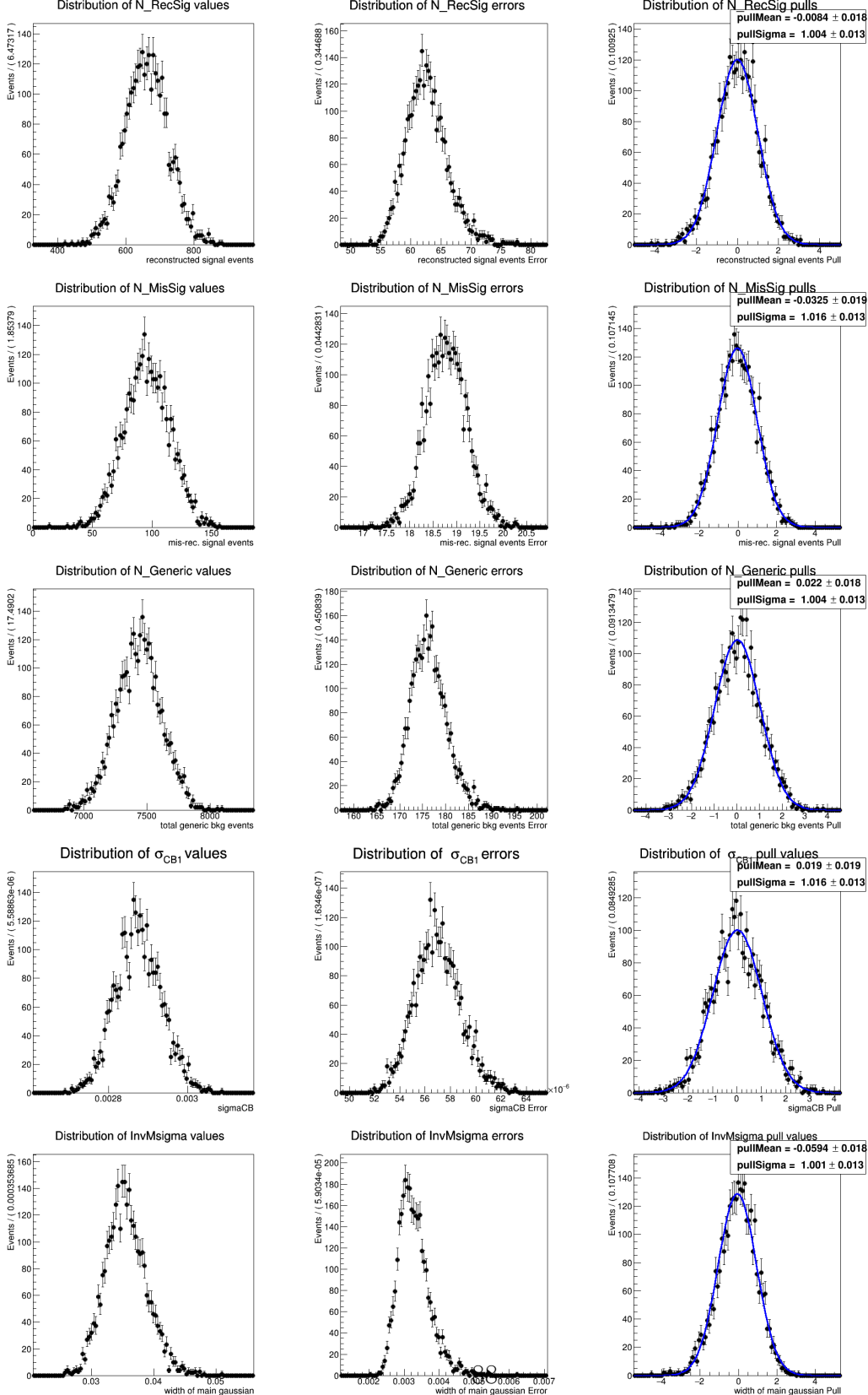


Figure (100) Toy MC study for the two dimensional fit model described in Sec. 6.2

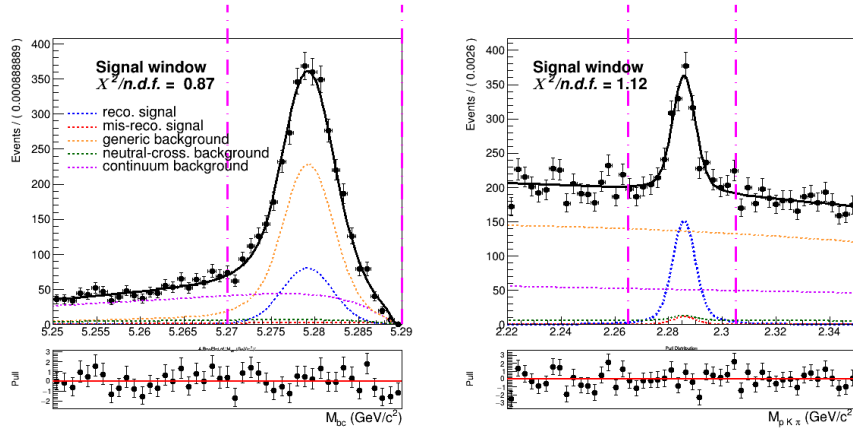


Figure (101) Signal region ( $2.22 < M(pK\pi) < 2.35 \text{ GeV}/c^2$  and  $5.27 < M_{bc} < 5.29 \text{ GeV}/c^2$ ) projections of the dimensional fit on stream 0 Monte Carlo simulated data.

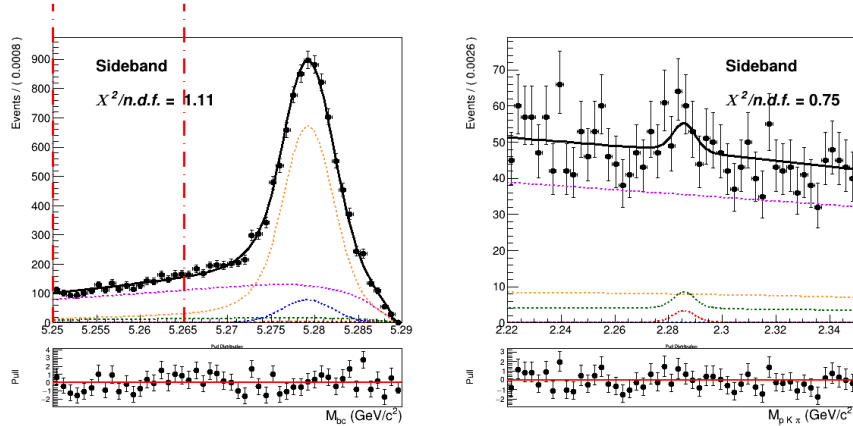


Figure (102) Sideband of  $5.25 < M_{bc} < 5.265 \text{ GeV}/c^2$  projection of the two dimensional fit on stream 0 Monte Carlo simulated data.

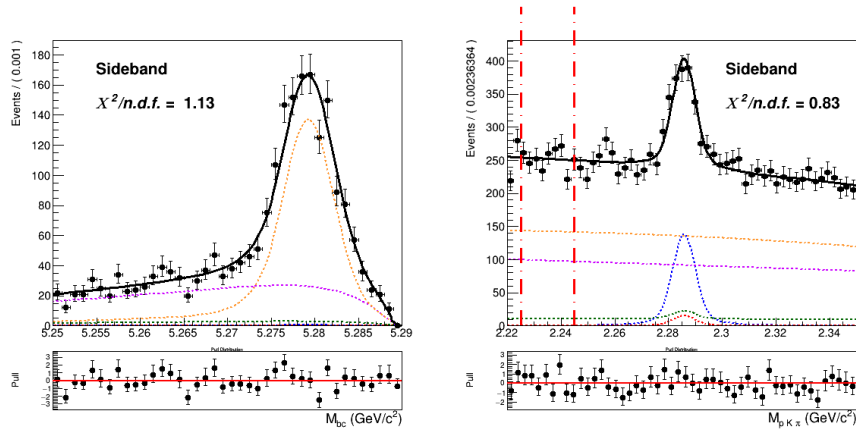


Figure (103) Sideband region of  $2.22 < M(pK\pi) < 2.35 \text{ GeV}/c^2$  projection of the two dimensional fit on stream 0 Monte Carlo simulated data.

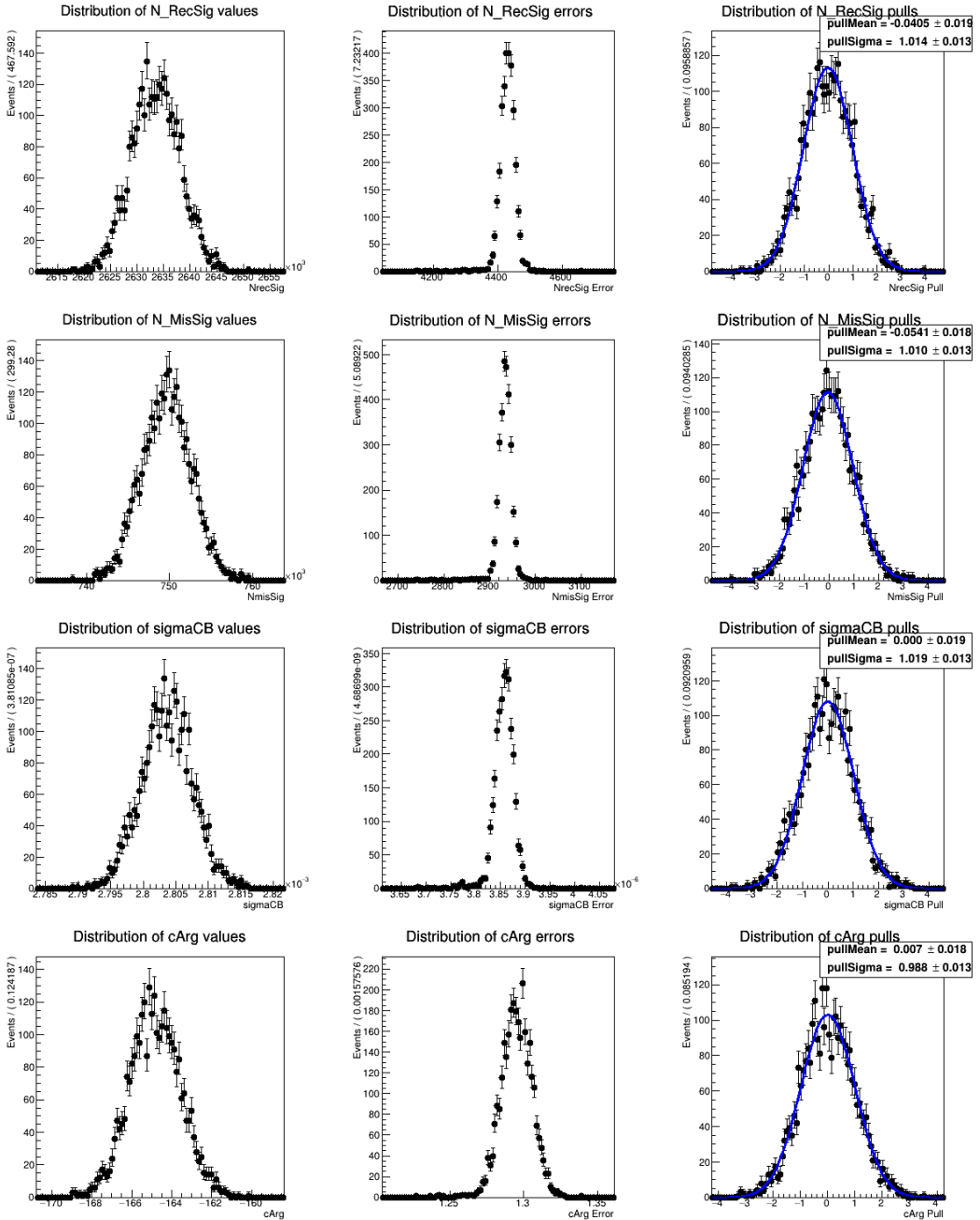


Figure (104) Toy MC study for the  $B_{tag}$  fit model described in Sec. 6.4

- 911 **References**
- 912 [1] B. Aubert et al., BaBar, *Study of inclusive  $B^-$  and  $\bar{B}^0$  decays to flavor-tagged  $D$ ,  $D_s$*   
913 *and  $\Lambda_c^+$* , Phys. Rev. D **75** (2007) 072002, [arXiv:hep-ex/0606026](https://arxiv.org/abs/hep-ex/0606026).
- 914 [2] I. Grach, I. Narodetskii, S. Simula, and K. Ter-Martirosyan, *Exclusive and inclusive*  
915 *weak decays of the  $B$ -meson*, Nuclear Physics B **502** (1997) no. 1-2, 227–248.
- 916 [3] M. Gelb, *Search for the Rare Decay  $B^+ \rightarrow \ell^+ \nu_\ell \gamma$  with the Full Event Interpretation at*  
917 *the Belle Experiment*. PhD thesis, Karlsruhe Institute of Technology (KIT), 2018.
- 918 [4] J. Schwab, *Calibration of the Full Event Interpretation for the Belle and the Belle II*  
919 *Experiment*, Master's thesis, Karlsruhe Institute of Technology (KIT), 2017.
- 920 [5] K.-J. Tien and M.-Z. Wang, *Proton identification efficiency study*, BELLE NOTE 1279.
- 921 [6] S. Nishida, *Study of Kaon and Pion Identification Using Inclusive  $D^*$  Sample*, BELLE  
922 NOTE 779.